

**This is a self-archived version of an original article. This version may differ from the original in pagination and typographic details.**

**Author(s):** Shapiguzov, Alexey; Vainonen, Julia P.; Hunter, Kerri; Tossavainen, Helena; Tiwari, Arjun; Järvi, Sari; Hellman, Maarit; Aarabi, Fayeze; Alseekh, Saleh; Wybouw, Brecht; Kelen, Katrien Van Der; Nikkanen, Lauri; Krasensky-Wrzaczek, Julia; Sipari, Nina; Keinänen, Markku; Tyystjärvi, Esa; Rintamäki, Eevi; De Rybel, Bert; Salojärvi, Jarkko; van Breusegem, Frank; Fernie, Alisdair R.; Brosché, Mikael;

**Title:** Arabidopsis RCD1 coordinates chloroplast and mitochondrial functions through interaction with ANAC transcription factors

**Year:** 2019

**Version:** Accepted version (Final draft)

**Copyright:** © The Authors. 2019.

**Rights:** CC BY 4.0

**Rights url:** <https://creativecommons.org/licenses/by/4.0/>

**Please cite the original version:**

Shapiguzov, A., Vainonen, J. P., Hunter, K., Tossavainen, H., Tiwari, A., Järvi, S., Hellman, M., Aarabi, F., Alseekh, S., Wybouw, B., Kelen, K. V. D., Nikkanen, L., Krasensky-Wrzaczek, J., Sipari, N., Keinänen, M., Tyystjärvi, E., Rintamäki, E., De Rybel, B., Salojärvi, J., . . . Kangasjärvi, J. (2019). Arabidopsis RCD1 coordinates chloroplast and mitochondrial functions through interaction with ANAC transcription factors. *eLife*, 2019(8), Article e43284. <https://doi.org/10.7554/elife.43284>

1 **Arabidopsis RCD1 Coordinates Chloroplast and Mitochondrial Functions through**  
 2 **Interaction with ANAC Transcription Factors**

3

4 Short title: RCD1 and organellar redox status

5 Alexey Shapiguzov<sup>1,2\*</sup>, Julia P. Vainonen<sup>1\*</sup>, Kerri Hunter<sup>1\*\*</sup>, Helena Tossavainen<sup>3,4\*\*</sup>,  
 6 Arjun Tiwari<sup>5\*\*</sup>, Sari Järvi<sup>5\*\*</sup>, Maarit Hellman<sup>4</sup>, Fayeze Aarabi<sup>6</sup>, Saleh Alseekh<sup>6,7</sup>,  
 7 Brecht Wybouw<sup>8,9</sup>, Katrien Van Der Kelen<sup>8,9,10</sup>, Lauri Nikkanen<sup>5</sup>, Julia Krasensky-  
 8 Wrzaczek<sup>1</sup>, Nina Sipari<sup>11</sup>, Markku Keinänen<sup>12</sup>, Esa Tyystjärvi<sup>5</sup>, Eevi Rintamäki<sup>5</sup>, Bert  
 9 De Rybel<sup>8,9</sup>, Jarkko Salojärvi<sup>1,13</sup>, Frank Van Breusegem<sup>8,9</sup>, Alisdair R. Fernie<sup>6,7</sup>, Mikael  
 10 Brosché<sup>1,14</sup>, Perttu Permi<sup>3,4,15</sup>, Eva-Mari Aro<sup>5</sup>, Michael Wrzaczek<sup>1</sup>, and Jaakko  
 11 Kangasjärvi<sup>1</sup>.

12 \* These authors contributed equally to the manuscript.

13 \*\* These authors contributed equally to the manuscript.

14 **Author affiliations**

15 <sup>1</sup>. Organismal and Evolutionary Biology Research Programme, Faculty of Biological and  
 16 Environmental Sciences, and Viikki Plant Science Center, University of Helsinki, FI-  
 17 00014 Helsinki, Finland.

18 <sup>2</sup>. Permanent address: Institute of Plant Physiology, Russian Academy of Sciences,  
 19 Botanicheskaya Street, 35, 127276 Moscow, Russia.

20 <sup>3</sup>. Program in Structural Biology and Biophysics, Institute of Biotechnology, University of  
 21 Helsinki, FI-00014 Helsinki, Finland.

22 <sup>4</sup>. Department of Chemistry, Nanoscience Center, University of Jyväskylä, FI-40014  
 23 Jyväskylä, Finland.

24 <sup>5</sup>. Department of Biochemistry / Molecular Plant Biology, University of Turku, FI-20014  
 25 Turku, Finland.

26 <sup>6</sup>. Max-Planck Institute for Molecular Plant Physiology, D-14476 Potsdam-Golm,  
 27 Germany.

28 <sup>7</sup>. Center of Plant System Biology and Biotechnology, 4000 Plovdiv, Bulgaria.

29 <sup>8</sup>. Department of Plant Biotechnology and Bioinformatics, Ghent University, 9052 Ghent,  
 30 Belgium.

31 <sup>9</sup>. VIB Center for Plant Systems Biology, 9052 Ghent, Belgium.

32 <sup>10</sup>. Current address: Sciensano. Rue Juliette Wytsmanstraat 14, 1050 Brussels,  
33 Belgium.

34 <sup>11</sup>. Viikki Metabolomics Unit, Organismal and Evolutionary Biology Research  
35 Programme, Faculty of Biological and Environmental Sciences, University of Helsinki,  
36 FI-00014 Helsinki, Finland.

37 <sup>12</sup>. Department of Environmental and Biological Sciences, University of Eastern Finland,  
38 FI-80101 Joensuu, Finland.

39 <sup>13</sup>. Current address: School of Biological Sciences, Nanyang Technological University,  
40 60 Nanyang Drive, Singapore 637551, Singapore.

41 <sup>14</sup>. Institute of Technology, University of Tartu, 50411 Tartu, Estonia.

42 <sup>15</sup>. Department of Biological and Environmental Science, Nanoscience Center,  
43 University of Jyväskylä, FI-40014 Jyväskylä, Finland.

44 The author responsible for distribution of materials integral to the findings presented in  
45 this article is: Jaakko Kangasjärvi (jaakko.kangasjarvi@helsinki.fi), University of  
46 Helsinki.

47 **Corresponding author email: jaakko.kangasjarvi@helsinki.fi**

48 **Abstract**

49 Reactive oxygen species (ROS)-dependent signaling pathways from chloroplasts and  
50 mitochondria merge at the nuclear protein RADICAL-INDUCED CELL DEATH1 (RCD1).  
51 RCD1 interacts *in vivo* and suppresses the activity of the transcription factors ANAC013  
52 and ANAC017, which mediate a ROS-related retrograde signal originating from  
53 mitochondrial complex III. Inactivation of *RCD1* leads to increased expression of  
54 mitochondrial dysfunction stimulon (MDS) genes regulated by ANAC013 and ANAC017.  
55 Accumulating MDS gene products, including alternative oxidases (AOXs), affect redox  
56 status of the chloroplasts, leading to changes in chloroplast ROS processing and  
57 increased protection of photosynthetic apparatus. ROS alter the abundance, thiol redox  
58 state and oligomerization of the RCD1 protein *in vivo*, providing feedback control on its  
59 function. RCD1-dependent regulation is linked to chloroplast signaling by 3'-  
60 phosphoadenosine 5'-phosphate (PAP). Thus, RCD1 integrates organellar signaling  
61 from chloroplasts and mitochondria to establish transcriptional control over the  
62 metabolic processes in both organelles.

## 63 Introduction

64 Cells of photosynthesizing eukaryotes are unique in harboring two types of energy  
65 organelles, the chloroplasts and the mitochondria, which interact at an operational level  
66 by the exchange of metabolites, energy and reducing power (*Noguchi and Yoshida,*  
67 *2008; Cardol et al., 2009; Bailleul et al., 2015*). Reducing power flows between the  
68 organelles through several pathways, including photorespiration (*Watanabe et al.,*  
69 *2016*), malate shuttles (*Scheibe, 2004; Zhao et al., 2018*) and transport of  
70 photoassimilate-derived carbon rich metabolites from chloroplasts to mitochondria. At  
71 the signaling level, the so-called retrograde signaling pathways originating from the  
72 organelles influence the expression of nuclear genes (*de Souza et al., 2016; Leister,*  
73 *2017; Waszczak et al., 2018*). These pathways provide feedback communication  
74 between the organelles and the gene expression apparatus in the nucleus to adjust  
75 expression of genes encoding organelle components in accordance with changes in the  
76 developmental stage or environmental conditions.

77 Reactive oxygen species (ROS), inevitable by-products of aerobic energy metabolism,  
78 play pivotal roles in plant organellar signaling from both chloroplasts and mitochondria  
79 (*Dietz et al., 2016; Noctor et al., 2017; Waszczak et al., 2018*). Superoxide anion radical  
80 ( $O_2^{\cdot-}$ ) is formed in the organelles by the transfer of electrons from the organellar  
81 electron transfer chains (ETCs) to molecular oxygen ( $O_2$ ). In illuminated chloroplasts,  
82 superoxide anion formed from  $O_2$  reduction by Photosystem I (PSI) is converted to  
83 hydrogen peroxide ( $H_2O_2$ ) which is further reduced to water by chloroplastic  $H_2O_2$ -  
84 scavenging systems during the water-water cycle (*Asada, 2006; Awad et al., 2015*).  
85 Chloroplastic ROS production can be enhanced by application of methyl viologen (MV),  
86 a chemical that catalyzes shuttling of electrons from PSI to  $O_2$  (*Farrington et al., 1973*).  
87 The immediate product of this reaction,  $O_2^{\cdot-}$ , is not likely to directly mediate organellar  
88 signaling; however,  $H_2O_2$  is involved in many retrograde signaling pathways (*Leister,*  
89 *2017; Mullineaux et al., 2018; Waszczak et al., 2018*). Organellar  $H_2O_2$  has been  
90 suggested to translocate directly to the nucleus (*Caplan et al., 2015; Exposito-*  
91 *Rodriguez et al., 2017*), where it can oxidize thiol groups of specific proteins, thereby  
92 converting the ROS signal into thiol redox signals (*Møller and Kristensen, 2004; Nietzel*  
93 *et al., 2017*). One recently discovered process affected by chloroplastic  $H_2O_2$  is the  
94 metabolism of 3'-phosphoadenosine 5'-phosphate (PAP). PAP is a toxic by-product of  
95 sulfate metabolism produced when cytoplasmic sulfotransferases (SOTs, e.g., SOT12)

96 transfer a sulfuryl group from PAP-sulfate (PAPS) to various target compounds (*Klein*  
97 *and Papenbrock, 2004*). PAP is transported to chloroplasts where it is detoxified by  
98 dephosphorylation to adenosine monophosphate in a reaction catalyzed by the  
99 adenosine bisphosphate phosphatase 1, SAL1 (*Quintero et al., 1996; Chan et al.,*  
100 *2016*). It has been proposed that oxidation of SAL1 thiols directly or indirectly  
101 dependent on chloroplastic H<sub>2</sub>O<sub>2</sub> inactivates the enzyme, and accumulating PAP may  
102 act as a retrograde signal (*Estavillo et al., 2011; Chan et al., 2016; Crisp et al., 2018*).

103 ROS are also produced in the mitochondria, for example by complex III at the outer side  
104 of the inner mitochondrial membrane (*Cvetkovska et al., 2013; Ng et al., 2014; Huang et*  
105 *al., 2016; Wang et al., 2018*). Blocking electron transfer through complex III by  
106 application of the inhibitors antimycin A (AA) or myxothiazol (myx) enhances electron  
107 leakage and thus induces the retrograde signal. Two known mediators of this signal are  
108 the transcription factors ANAC013 (*De Clercq et al., 2013*) and ANAC017 (*Ng et al.,*  
109 *2013b; Van Aken et al., 2016b*) that are both bound to the endoplasmic reticulum (ER)  
110 by a transmembrane domain. Mitochondria-derived signals lead to proteolytic cleavage  
111 of this domain. The proteins are released from the ER and translocated to the nucleus  
112 where they activate the mitochondrial dysfunction stimulon (MDS) genes (*De Clercq et*  
113 *al., 2013; Van Aken et al., 2016a*). MDS genes include the mitochondrial alternative  
114 oxidases (AOXs), *SOT12*, and *ANAC013* itself, which provides positive feedback  
115 regulation and thus enhancement of the signal.

116 Whereas multiple retrograde signaling pathways have been described in detail (*de*  
117 *Souza et al., 2016; Leister, 2017; Waszczak et al., 2018*), it is still largely unknown how  
118 the numerous chloroplast- and mitochondria-derived signals are integrated and  
119 processed by the nuclear gene expression system. Nuclear cyclin-dependent kinase E  
120 is implicated in the expression of both chloroplastic (*LHCB2.4*) and mitochondrial  
121 (*AOX1a*) components in response to perturbations of chloroplast ETC (*Blanco et al.,*  
122 *2014*), mitochondrial ETC, or H<sub>2</sub>O<sub>2</sub> treatment (*Ng et al., 2013a*). The transcription factor  
123 *ABI4* is also suggested to respond to retrograde signals from both organelles (*Giraud et*  
124 *al., 2009; Blanco et al., 2014*), although its significance in chloroplast signaling has  
125 recently been disputed (*Kacprzak et al., 2019*). Mitochondrial signaling *via* ANAC017  
126 was recently suggested to converge with chloroplast PAP signaling based on similarities  
127 in their transcriptomic profiles (*Van Aken and Pogson, 2017*). However, the mechanistic  
128 details underlying this convergence remain currently unknown.

129 Arabidopsis RADICAL-INDUCED CELL DEATH1 (RCD1) is a nuclear protein containing  
130 a WWE, a PARP-like [poly (ADP-ribose) polymerase-like], and a C-terminal RST  
131 domain (RCD1-SRO1-TAF4) (Overmyer *et al.*, 2000; Ahlfors *et al.*, 2004; Jaspers *et al.*,  
132 2009; Jaspers *et al.*, 2010a). In yeast two-hybrid studies RCD1 interacted with several  
133 transcription factors (Jaspers *et al.*, 2009) including ANAC013, DREB2A (Vainonen *et al.*,  
134 2012), and Rap2.4a (Hiltscher *et al.*, 2014) via the RST domain (Jaspers *et al.*,  
135 2010b), and with the sodium transporter SOS1 (Katiyar-Agarwal *et al.*, 2006). In  
136 agreement with the numerous potential interaction partners of RCD1, the *rcd1* mutant  
137 demonstrates pleiotropic phenotypes in diverse stress and developmental responses  
138 (Jaspers *et al.*, 2009). It has been identified in screens for sensitivity to ozone  
139 (Overmyer *et al.*, 2000), tolerance to MV (Fujibe *et al.*, 2004) and redox imbalance in  
140 the chloroplasts (Heiber *et al.*, 2007; Hiltscher *et al.*, 2014). RCD1 was found to  
141 complement the deficiency of the redox sensor YAP1 in yeast (Belles-Boix *et al.*, 2000).  
142 Under standard growth conditions, the *rcd1* mutant displays differential expression of  
143 over 400 genes, including those encoding mitochondrial AOXs (Jaspers *et al.*, 2009;  
144 Brosché *et al.*, 2014) and the chloroplast 2-Cys peroxiredoxin (2-CP) (Heiber *et al.*,  
145 2007; Hiltscher *et al.*, 2014).

146 Here we have addressed the role of RCD1 in the integration of ROS signals emitted by  
147 both mitochondria and chloroplasts. Abundance, redox status and oligomerization state  
148 of the nuclear-localized RCD1 protein changed in response to ROS generated in the  
149 chloroplasts. Furthermore, RCD1 directly interacted *in vivo* with ANAC013 and  
150 ANAC017 and appeared to function as a negative regulator of both transcription factors.  
151 The RST domain, mediating RCD1 interaction with ANAC transcription factors, was  
152 required for plant sensitivity to chloroplastic ROS. We demonstrate that RCD1 is a  
153 molecular component that integrates organellar signal input from both chloroplasts and  
154 mitochondria to exert its influence on nuclear gene expression.

## 155 Results

### 156 The response to chloroplastic ROS is compromised in *rcd1*

157 Methyl viologen (MV) enhances ROS generation in illuminated chloroplasts by  
158 catalyzing the transfer of electrons from Photosystem I (PSI) to molecular oxygen. This  
159 triggers a chain of reactions that ultimately inhibit Photosystem II (PSII) (*Farrington et*  
160 *al.*, 1973; *Nishiyama et al.*, 2011). To reveal the significance of nuclear protein RCD1 in  
161 these reactions, rosettes of Arabidopsis were pre-treated with MV in darkness. Without  
162 exposure to light, the plants displayed unchanged PSII photochemical yield (Fv/Fm).  
163 Illumination resulted in a decrease of Fv/Fm in wild type (Col-0), but not in the *rcd1*  
164 mutant (*Figure 1A*), suggesting increased tolerance of *rcd1* to chloroplastic ROS  
165 production. Analysis of several independent *rcd1* complementation lines expressing  
166 different levels of HA-tagged RCD1 revealed that tolerance to MV inversely correlated  
167 with the amount of expressed RCD1 (*Figure 1 – figure supplements 1, 2*). This suggests  
168 that RCD1 protein quantitatively lowered the resistance of the photosynthetic apparatus  
169 to ROS.

170 Treatment with MV leads to formation of superoxide that is enzymatically dismutated to  
171 the more long-lived H<sub>2</sub>O<sub>2</sub>. Chloroplastic production of H<sub>2</sub>O<sub>2</sub> in the presence of MV was  
172 assessed by staining plants with 3,3'-diaminobenzidine (DAB) in light. Higher production  
173 rate of H<sub>2</sub>O<sub>2</sub> was evident in MV pre-treated rosettes of both Col-0 and *rcd1*. Longer  
174 illumination led to a time-dependent increase in the DAB staining intensity in Col-0, but  
175 not in *rcd1* (*Figure 1 – figure supplement 3*). In several MV-tolerant mutants, the  
176 resistance is based on restricted access of MV to chloroplasts (*Hawkes, 2014*).  
177 However, in *rcd1* MV pre-treatment led to an initial increase in H<sub>2</sub>O<sub>2</sub> production rate  
178 similar to that in the wild type (*Figure 1 – figure supplement 3*), suggesting that  
179 resistance of *rcd1* was not due to lowered delivery of MV to PSI. To test this directly, the  
180 kinetics of PSI oxidation was assessed by *in vivo* spectroscopy using DUAL-PAM. As  
181 expected, pre-treatment of leaves with MV led to accelerated oxidation of PSI. This  
182 effect was identical in Col-0 and *rcd1*, indicating unrestricted access of MV to PSI in the  
183 *rcd1* mutant (*Figure 1B*).

184 The MV toxicity was not associated with the changed stoichiometry of photosystems  
185 (*Figure 1 – figure supplement 4A*). However, in Col-0 it coincided with progressive  
186 destabilization of PSII complex with its light-harvesting antennae (LHCII) and



187 accumulation of PSII monomer (*Figure 1 – figure supplement 4B*). No signs of PSI  
188 inhibition were evident either in DUAL-PAM (*Figure 1B*) or in PSI immunoblotting  
189 assays (*Figure 1 – figure supplement 4B*) in either genotype. The fact that production of  
190 ROS affected PSII, but not PSI where these ROS are formed, suggests that PSII  
191 inhibition results from a regulated mechanism rather than uncontrolled oxidation by  
192 ROS, and that this mechanism requires the activity of RCD1.

193 Previous studies have described *rcd1* as a mutant with altered ROS metabolism and  
194 redox status of the chloroplasts, although the underlying mechanisms are unknown  
195 (*Fujibe et al., 2004; Heiber et al., 2007; Hiltcher et al., 2014; Cui et al., 2019*). No  
196 significant changes were detected in *rcd1* in transcript levels of chloroplast-related  
197 genes (*Brosché et al., 2014*). Analyses of the low molecular weight antioxidant  
198 compounds ascorbate and glutathione did not explain the tolerance of *rcd1* to  
199 chloroplastic ROS either (*Heiber et al., 2007; Hiltcher et al., 2014*). To understand the  
200 molecular basis of the RCD1-dependent redox alterations, the levels of chloroplast  
201 proteins related to photosynthesis and ROS scavenging were analyzed by  
202 immunoblotting. None of these showed significantly altered abundance in *rcd1*  
203 compared to Col-0 (*Figure 1 – figure supplement 5A*). Furthermore, no difference was  
204 detected between the genotypes in abundance and subcellular distribution of the  
205 nucleotide redox couples  $\text{NAD}^+/\text{NADH}$  and  $\text{NADP}^+/\text{NADPH}$  (*Figure 1 – figure*  
206 *supplement 5B, C*). Finally, the redox status of chloroplast thiol redox enzymes was  
207 addressed. The chloroplast stroma-localized 2-Cys peroxiredoxin (2-CP) is an abundant  
208 enzyme (*König et al., 2002; Peltier et al., 2006; Liebthal et al., 2018*) that was recently  
209 found to link chloroplast thiol redox system to ROS (*Ojeda et al., 2018; Vaseghi et al.,*  
210 *2018; Yoshida et al., 2018*). The level of the 2-CP protein was unchanged in *rcd1*  
211 (*Figure 1 – figure supplement 5A*). However, when protein extracts were subjected to  
212 thiol bond-specific labeling (*Nikkanen et al., 2016*) as described in *Figure 1C*, most 2-  
213 CP was reduced in *rcd1* both in darkness and in light, while in Col-0 the larger fraction  
214 of 2-CP was present as oxidized forms. Thus, RCD1 is likely involved in the regulation  
215 of the redox status of chloroplastic thiol enzymes.

216 Taken together, the results hinted that the mechanisms by which RCD1 regulates  
217 chloroplastic redox status are independent of the photosynthetic ETC, or steady-state  
218 levels and distribution of nucleotide electron carriers. However, they appear to be  
219 associated with changed thiol redox state of chloroplast enzymes.

## 220 RCD1 protein is sensitive to ROS

221 It was next tested whether the nuclear RCD1 protein could itself be sensitive to ROS,  
222 thus accounting for the observed alterations. For that, an RCD1-HA complementation  
223 line was used (line “a” in *Figure 1 – figure supplement 1*). No changes were detected in  
224 RCD1-HA abundance during 5 hours amid the standard growth light period, or during 5-  
225 hour high light treatment. On the other hand, both MV and H<sub>2</sub>O<sub>2</sub> treatments led to a  
226 gradual decrease in RCD1 abundance (*Figure 2A*). When plant extracts from these  
227 experiments were separated in non-reducing SDS-PAGE, the RCD1-HA signal resolved  
228 into species of different molecular weights (*Figure 2B*). Under standard growth  
229 conditions or high light, most RCD1-HA formed a reduced monomer. In contrast,  
230 treatment with MV under light or H<sub>2</sub>O<sub>2</sub> resulted in fast conversion of RCD1-HA  
231 monomers into high-molecular-weight aggregates (*Figure 2B*). Importantly, MV-induced  
232 redox changes in RCD1-HA only occurred in light, but not in darkness, suggesting that  
233 the changes were mediated by increased chloroplastic ROS production (*Figure 2B* and  
234 *Figure 4 – figure supplement 2B*). To test whether oligomerization of RCD1 was thiol-  
235 regulated, a variant of RCD1-HA was generated where seven cysteines in the linkers  
236 between the RCD1 domains were substituted by alanines (RCD1Δ7Cys; *Figure 2 –*  
237 *figure supplement 1A*). The treatments of *rcd1*: RCD1Δ7Cys-HA plants with MV or H<sub>2</sub>O<sub>2</sub>  
238 led to significantly less aggregation of RCD1Δ7Cys-HA compared to RCD1-HA. In  
239 addition, the levels of RCD1Δ7Cys-HA were insensitive to MV or H<sub>2</sub>O<sub>2</sub> (*Figure 2 – figure*  
240 *supplement 1B*). In three independent complementation lines the RCD1Δ7Cys-HA  
241 variant accumulated to higher levels compared to RCD1-HA (*Figure 2 – figure*  
242 *supplement 1C*). This suggests the involvement of the tested RCD1 cysteine residues in  
243 the regulation of the protein oligomerization and stability *in vivo*. However, the tolerance  
244 of the RCD1Δ7Cys-HA lines to chloroplastic ROS and the expression of the selected  
245 RCD1-regulated genes in response to MV treatment were comparable to that of the  
246 RCD1-HA lines or Col-0 (*Figure 2 – figure supplement 1C, D*). These results suggest  
247 that the RCD1 protein is sensitive to chloroplastic ROS. However, the changes in RCD1  
248 abundance and redox state did not explain the RCD1-dependent redox alternations  
249 observed in the chloroplasts.

## 250 **Mitochondrial respiration is altered in *rcd1***

251 In further search for the mechanisms of RCD1-dependent redox alternations in the  
252 chloroplast (*Figure 1*), analysis of cell energy metabolism was performed by feeding  
253 uniformly labeled [U-<sup>14</sup>C] glucose) to leaf discs from light- and dark-adapted Col-0 and  
254 *rcd1* plants. Distribution of radioactive label between emitted <sup>14</sup>CO<sub>2</sub> and fractionated  
255 plant material was analyzed. This revealed significantly more active carbohydrate  
256 metabolism in *rcd1* (*Figure 3 – source data 1*). The redistribution of radiolabel to  
257 sucrose, starch and cell wall was elevated in *rcd1* as were the corresponding deduced  
258 fluxes (*Figure 3*), suggesting that *rcd1* displayed a higher respiration rate indicative of  
259 mitochondrial defects.

260 Indeed, earlier transcriptomic studies in *rcd1* have revealed increased expression of  
261 genes encoding mitochondrial functions, including mitochondrial alternative oxidases  
262 (AOXs) (*Jaspers et al., 2009; Brosché et al., 2014*). Immunoblotting of protein extracts  
263 from isolated mitochondria with an antibody recognizing all five isoforms of Arabidopsis  
264 AOX confirmed the increased abundance of AOX in *rcd1* (*Figure 4A*). The most  
265 abundant AOX isoform in Arabidopsis is AOX1a. Accordingly, only a weak signal was  
266 detected in the *aox1a* mutant. However, in the *rcd1 aox1a* double mutant AOXs other  
267 than AOX1a were evident, thus the absence of RCD1 led to an increased abundance of  
268 several AOX isoforms.

269 To test whether the high abundance of AOXs in *rcd1* correlated with their increased  
270 activity, seedling respiration was assayed *in vivo*. Mitochondrial AOXs form an  
271 alternative respiratory pathway to the KCN-sensitive electron transfer through complex  
272 III and cytochrome C (*Figure 4B*). Thus, after recording the initial rate of O<sub>2</sub> uptake,  
273 KCN was added to inhibit cytochrome-dependent respiration. In Col-0 seedlings KCN  
274 led to approximately 80 % decrease in O<sub>2</sub> uptake, *versus* only about 20 % in *rcd1*,  
275 revealing elevated AOX capacity of the mutant (*Figure 4C*). The elevated AOX capacity  
276 of *rcd1* was similar to that of an *AOX1a*-OE overexpressor line (*Umbach et al., 2005*). In  
277 the *rcd1 aox1a* double mutant the AOX capacity was comparable to Col-0 or *aox1a*  
278 (*Figure 4C*). Thus, elevated AOX respiration of *rcd1* seedlings was dependent on the  
279 AOX1a isoform. Importantly, however, metabolism of *rcd1 aox1a* was only slightly  
280 different from *rcd1* under light and indistinguishable from *rcd1* in the darkness (*Figure 3*  
281 – *source data 1*). This again indicated that the studied phenotypes of *rcd1* are

282 associated with the induction of more than one AOX isoform. Taken together, the  
283 results suggested that inactivation of *RCD1* led to increased expression and activity of  
284 AOX isoforms, which could contribute to the observed changes in energy metabolism of  
285 *rcd1* (Figure 3).

### 286 **Mitochondrial AOXs affect ROS processing in the chloroplasts**

287 Inhibition of complex III by antimycin A (AA) or myxothiazol (myx) activates  
288 mitochondrial retrograde signaling (Figure 4B). It leads to nuclear transcriptional  
289 reprogramming including induction of AOX genes (Clifton *et al.*, 2006). Accordingly,  
290 overnight treatment with either of these chemicals significantly increased the abundance  
291 of AOXs in Col-0, *rcd1* and *rcd1 aox1a* (Figure 4 – figure supplement 1). Thus,  
292 sensitivity of *rcd1* to the complex III retrograde signal was not compromised, rather  
293 continuously augmented. In addition, no major effect was observed on RCD1-HA  
294 protein level or redox state in the RCD1-HA line treated with AA or myx, suggesting that  
295 RCD1 acts as a modulator, not as a mediator, of the mitochondrial retrograde signal  
296 (Figure 4 – figure supplement 2).

297 To assess whether increased AOX abundance affected chloroplast functions, PSII  
298 inhibition was assayed in the presence of MV in AA- or myx-pre-treated leaf discs. Pre-  
299 treatment of Col-0 with either AA or myx increased the resistance of PSII to inhibition by  
300 chloroplastic ROS (Figure 4D), thus mimicking the *rcd1* phenotype. In addition to  
301 complex III, AA has been reported to inhibit plastid cyclic electron flow dependent on  
302 PGR5 (PROTON GRADIENT REGULATION 5). Thus, *pgr5* mutant was tested for its  
303 tolerance to chloroplastic ROS after AA pre-treatment. AA made *pgr5* more MV-tolerant  
304 similarly to the wild type, indicating that PGR5 is not involved in the observed gain in  
305 ROS tolerance (Figure 4 – figure supplement 3A).

306 Mitochondrial complex III signaling induces expression of several genes other than  
307 AOX. To test whether accumulation of AOXs contributed to PSII protection from  
308 chloroplastic ROS or merely correlated with it, the AOX inhibitor salicylhydroxamic acid  
309 (SHAM) was used. Treatment of plants with SHAM alone resulted in very mild PSII  
310 inhibition, which was similar in *rcd1* and Col-0 (Figure 4 – figure supplement 3B).  
311 However, pre-treatment with SHAM made both *rcd1* and Col-0 plants significantly more  
312 sensitive to chloroplastic ROS generated by MV (Figure 4E), thereby partially abolishing  
313 MV tolerance of the *rcd1* mutant. Involvement of the plastid terminal oxidase PTOX (*Fu*

314 *et al.*, 2012) in this effect was excluded by using the *ptox* mutant (*Figure 4 – figure*  
315 *supplement 3C*). Noteworthy, analyses of *AOX1a*-OE, *aox1a* and *rcd1 aox1a* lines  
316 demonstrated that *AOX1a* isoform was neither sufficient nor necessary for chloroplast  
317 ROS tolerance (*Figure 4 – figure supplement 4*). Taken together, these results indicated  
318 that mitochondrial AOXs contributed to resistance of PSII to chloroplastic ROS. We  
319 hypothesize that AOX isoforms other than *AOX1a* are implicated in this process.

### 320 **Evidence for altered electron transfer between chloroplasts and mitochondria in** 321 ***rcd1***

322 The pathway linking mitochondrial AOXs with chloroplastic ROS processing is likely to  
323 involve electron transfer between the two organelles. Chlorophyll fluorescence under  
324 light (*F<sub>s</sub>*; *Figure 1 – figure supplement 2*) inversely correlates with the rate of electron  
325 transfer from PSII to plastoquinone and thus can be used as a proxy of the reduction  
326 state of the chloroplast ETC. After combined treatment with SHAM and MV (as in *Figure*  
327 *4E*), *F<sub>s</sub>* increased in *rcd1*, but not in Col-0 (*Figure 5A*). This hinted that a pathway in  
328 *rcd1* linked the chloroplast ETC to the activity of mitochondrial AOXs, with the latter  
329 functioning as an electron sink. When the AOX activity was inhibited by SHAM, electron  
330 flow along this pathway was blocked. This led to accumulation of electrons in the  
331 chloroplast ETC and hence to the observed rise in *F<sub>s</sub>*. As a parallel approach, dynamics  
332 of PSII photochemical quenching was evaluated in MV-pre-treated Col-0 and *rcd1*. In  
333 both lines, this parameter dropped within the first 20 min upon exposure to light and  
334 then started to recover. Recovery was more pronounced and more suppressed by  
335 SHAM in *rcd1* (*Figure 5 – figure supplement 1*). These experiments suggest that  
336 exposure of MV-pretreated plants to light triggered an adjustment of electron flows,  
337 which was compromised by SHAM. This was in line with the involvement of AOXs in  
338 photosynthetic electron transfer and chloroplast ROS maintenance.

339 One of the mediators of electron transfer between the organelles is the malate shuttle  
340 (*Scheibe, 2004; Zhao et al., 2018*). Thus, malate concentrations were measured in total  
341 extracts from Col-0 and *rcd1* seedlings. Illumination of seedlings pre-treated with MV led  
342 to dramatic decrease in malate concentration in Col-0, but not in *rcd1* (*Figure 5B*).  
343 Noteworthy, under standard light-adapted growth conditions, the concentration and the  
344 subcellular distribution of malate was unchanged in *rcd1* (*Figure 5 – figure supplement*

345 2). These observations suggest that exposure to light of MV-pre-treated plants resulted  
346 in rearrangements of electron flows that were different in Col-0 and *rcd1*.

347 Next, the activity of another component of the malate shuttle, the NADPH-dependent  
348 malate dehydrogenase (NADPH-MDH), was measured. Chloroplast NADPH-MDH is a  
349 redox-regulated enzyme activated by reduction of thiol bridges. Thus, the initial NADPH-  
350 MDH activity may reflect the *in vivo* thiol redox state of the cellular compartment from  
351 which it has been isolated. After measuring this parameter, thiol reductant was added to  
352 the extracts to reveal the total NADPH-MDH activity. Both values were higher in *rcd1*  
353 than in Col-0 (*Figure 5C*). To determine the contribution of *in vivo* thiol redox state, the  
354 initial NADPH-MDH activity was divided by the total activity. This value, the activation  
355 state, was also increased in *rcd1* (*Figure 5C*).

356 Taken together, our results suggested that mitochondria contributed to ROS processing  
357 in the chloroplasts *via* a mechanism involving mitochondrial AOXs and possibly the  
358 malate shuttle. These processes appeared to be dynamically regulated in response to  
359 chloroplastic ROS production, and RCD1 was involved in this regulation.

### 360 **Retrograde signaling from both chloroplasts and mitochondria is altered in *rcd1***

361 Our results demonstrated that absence of RCD1 caused physiological alterations in  
362 both chloroplasts and mitochondria. As RCD1 is a nuclear-localized transcriptional co-  
363 regulator (*Jaspers et al., 2009; Jaspers et al., 2010a*), its involvement in retrograde  
364 signaling pathways from both organelles was assessed. Transcriptional changes  
365 observed in *rcd1* (*Jaspers et al., 2009; Brosché et al., 2014*) were compared to gene  
366 expression datasets obtained after perturbations in energy organelles. This revealed a  
367 striking similarity of genes differentially regulated in *rcd1* to those affected by disturbed  
368 organellar function (*Figure 6 – figure supplement 1*). Analyzed perturbations included  
369 disruptions of mitochondrial genome stability (*msh1 recA3*), organelle translation  
370 (*mterf6, prors1*), activity of mitochondrial complex I (*ndufs4*, rotenone), complex III (AA),  
371 and ATP synthase function (oligomycin), as well as treatments and mutants related to  
372 chloroplastic ROS production (high light, MV, H<sub>2</sub>O<sub>2</sub>, *alx8/ fry1*, norflurazon).

373 In particular, a significant overlap was observed between genes mis-regulated in *rcd1*  
374 and the mitochondrial dysfunction stimulon (MDS) genes (*De Clercq et al., 2013*)  
375 (*Figure 6A*). Consistently, *AOX1a* was among the genes induced by the majority of the

376 treatments. To address the role of RCD1 protein in the induction of other MDS genes,  
377 mRNA steady state levels for some of them was assayed 3 hours after AA treatment  
378 (*Figure 6 – figure supplement 2*). As expected, expression of all these genes was  
379 elevated in *rcd1* under control conditions. Treatment with AA induced accumulation of  
380 MDS transcripts to similar levels in Col-0, *rcd1*, and in *rcd1*: RCD1-HA lines that  
381 expressed low levels of RCD1. For one marker gene, *UPOX* (*UP-REGULATED BY*  
382 *OXIDATIVE STRESS*), AA induction was impaired in the lines expressing high levels of  
383 RCD1-HA or RCD1 $\Delta$ 7Cys-HA (*Figure 6 – figure supplement 2*).

384 In addition to MDS, the list of genes mis-regulated in *rcd1* overlapped with those  
385 affected by 3'-phosphoadenosine 5'-phosphate (PAP) signaling (*Estavillo et al., 2011*;  
386 *Van Aken and Pogson, 2017*) (*Figure 6A*). Given that PAP signaling is suppressed by  
387 the activity of SAL1, expression of PAP-regulated genes was increased in the mutants  
388 deficient in SAL1 (*alx8* and *fry1*, *Figure 6A* and *Figure 6 – figure supplement 1*). One of  
389 the MDS genes with increased expression in *rcd1* encoded the sulfotransferase SOT12,  
390 an enzyme generating PAP. Accordingly, immunoblotting of total protein extracts with  
391  $\alpha$ SOT12 antibody demonstrated elevated SOT12 protein abundance in *rcd1* (*Figure*  
392 *6B*). To address the functional interaction of RCD1 with PAP signaling, *rcd1-4* was  
393 crossed with *alx8* (also known as *sal1-8*). The resulting *rcd1 sal1* mutant was severely  
394 affected in development (*Figure 6C*). The effect of PAP signaling on the tolerance of  
395 PSII to chloroplastic ROS production was tested. The single *sal1* mutant was more  
396 tolerant to MV than Col-0, while under high MV concentration *rcd1 sal1* was even more  
397 MV-tolerant than *rcd1* (*Figure 6 – figure supplement 3*). Together with transcriptomic  
398 similarities between *rcd1* and *sal1* mutants, these results further supported an overlap  
399 and/ or synergy of PAP and RCD1 signaling pathways.

#### 400 **RCD1 interacts with ANAC transcription factors *in vivo***

401 Expression of the MDS genes is regulated by the transcription factors ANAC013 and  
402 ANAC017 (*De Clercq et al., 2013*). The ANAC-responsive *cis*-element (*De Clercq et al.,*  
403 *2013*) was significantly enriched in promoter regions of *rcd1* mis-regulated genes  
404 (*Figure 6 – figure supplement 1*). This suggested a functional connection between  
405 RCD1 and transcriptional regulation of the MDS genes by ANAC013/ ANAC017. In an  
406 earlier study, ANAC013 was identified among many transcription factors interacting with  
407 RCD1 in the yeast two-hybrid system (*Jaspers et al., 2009*). This prompted us to

408 investigate further the connection between RCD1 and ANAC013 and the *in vivo*  
409 relevance of this interaction.

410 Association of RCD1 with ANAC transcription factors *in vivo* was tested in two  
411 independent pull-down experiments. To identify interaction partners of ANAC013, an  
412 Arabidopsis line expressing ANAC013-GFP (*De Clercq et al., 2013*) was used.  
413 ANAC013-GFP was purified with  $\alpha$ GFP beads, and associated proteins were identified  
414 by mass spectrometry in three replicates. RCD1 and its closest homolog SRO1, as well  
415 as ANAC017, were identified as ANAC013 interacting proteins (see Table 1 for a list of  
416 selected nuclear-localized interaction partners of ANAC013, and *Figure 7 – source data*  
417 *1* for the full list of identified proteins and mapped peptides). These data confirmed that  
418 ANAC013, RCD1 and ANAC017 are components of the same protein complex *in vivo*.  
419 In a reciprocal pull-down assay using transgenic Arabidopsis line expressing RCD1  
420 tagged with triple Venus YFP under the control of *UBIQUITIN10* promoter, RCD1-  
421 3xVenus and interacting proteins were immunoprecipitated using  $\alpha$ GFP (Table 1; *Figure*  
422 *7 – source data 2*). ANAC017 was found among RCD1 interactors.

423 To test whether RCD1 directly interacts with ANAC013/ ANAC017 *in vivo*, the complex  
424 was reconstituted in the human embryonic kidney cell (HEK293T) heterologous  
425 expression system (details in *Figure 7 – figure supplement 1*). Together with the results  
426 of *in vivo* pull-down assays, these experiments strongly supported the formation of a  
427 complex between RCD1 and ANAC013/ ANAC017 transcription factors.

### 428 **Structural and functional consequences of RCD1-ANAC interaction**

429 RCD1 interacts with many transcription factors belonging to different families (*Jaspers*  
430 *et al., 2009; Jaspers et al., 2010a; Vainonen et al., 2012; Bugge et al., 2018*) via its RST  
431 domain. The strikingly diverse set of RCD1 interacting partners may be partially  
432 explained by disordered flexible regions present in the transcription factors (*Kragelund*  
433 *et al., 2012; O'Shea et al., 2017; Bugge et al., 2018*). To address structural details of  
434 this interaction, the C-terminal domain of RCD1 (residues 468-589) including the RST  
435 domain (RST<sub>RCD1</sub>; 510-568) was purified and labeled with <sup>13</sup>C and <sup>15</sup>N for NMR  
436 spectroscopic study (*Tossavainen et al., 2017*) (details in *Figure 7 – figure supplement*  
437 *2* and *Figure 7 – source data 3*). ANAC013 was shown to interact with RCD1 in yeast  
438 two-hybrid assays (*Jaspers et al., 2009; O'Shea et al., 2017*). Thus, ANAC013<sup>235-284</sup>  
439 peptide was selected to address the specificity of the interaction of the RST domain with



440 ANAC transcription factors using NMR (details in *Figure 7 – figure supplement 3A, B*).  
441 Binding of RCD1<sup>468-589</sup> to ANAC013<sup>235-284</sup> caused profound changes in the HSQC  
442 spectrum of RCD1<sup>468-589</sup> (*Figure 7A* and *Figure 7 – figure supplement 3C*). These data  
443 supported a strong and specific binary interaction between the RCD1 RST domain and  
444 the ANAC013 transcription factor.

445 To evaluate the physiological significance of this interaction, stable *rcd1*  
446 complementation lines expressing an HA-tagged RCD1 variant lacking the C-terminus  
447 (amino acids 462-589) were generated. The *rcd1*: RCD1 $\Delta$ RST-HA lines were  
448 characterized by increased accumulation of AOXs in comparison with the *rcd1*: RCD1-  
449 HA lines (*Figure 7B*). They also had *rcd1*-like tolerance of PSII to chloroplastic ROS  
450 (*Figure 7C*).

451 Physiological outcomes of the interaction between RCD1 and ANAC transcription  
452 factors were further tested by reverse genetics. ANAC017 regulates the expression of  
453 ANAC013 in the mitochondrial retrograde signaling cascade (*Van Aken et al., 2016a*).  
454 Since ANAC017 precedes ANAC013 in the regulatory pathway and because no  
455 *anac013* knockout mutant is available, only the *rcd1-1 anac017* double mutant was  
456 generated. In the double mutant curly leaf habitus of *rcd1* was partially suppressed  
457 (*Figure 8A*). The *rcd1-1 anac017* mutant was more sensitive to chloroplastic ROS than  
458 the parental *rcd1* line (*Figure 8B*). The double mutant was characterized by lower  
459 abundance of AOX isoforms (*Figure 8C*), dramatically decreased expression of MDS  
460 genes (*Figure 8 – figure supplement 1*) and lower AOX respiration capacity (*Figure 8D*)  
461 compared to *rcd1*. Thus, gene expression, developmental, chloroplast- and  
462 mitochondria-related phenotypes of *rcd1* were partially mediated by ANAC017. These  
463 observations suggested that the *in vivo* interaction of RCD1 with ANAC transcription  
464 factors, mediated by the RCD1 C-terminal RST domain, is necessary for regulation of  
465 mitochondrial respiration and chloroplast ROS processing.

## 466 Discussion

### 467 *RCD1 integrates chloroplast and mitochondrial signaling pathways*

468 Plant chloroplasts and mitochondria work together to supply the cell with energy and  
469 metabolites. In these organelles, ROS are formed as by-products of the electron  
470 transfer chains (photosynthetic in chloroplasts and respiratory in mitochondria). ROS  
471 serve as versatile signaling molecules regulating many aspects of plant physiology such  
472 as development, stress signaling, systemic responses, and programmed cell death  
473 (PCD) (*Dietz et al., 2016; Noctor et al., 2017; Waszczak et al., 2018*). This  
474 communication network also affects gene expression in the nucleus where numerous  
475 signals are perceived and integrated. However, the molecular mechanisms of the  
476 coordinated action of the two energy organelles in response to environmental cues are  
477 only poorly understood. Evidence accumulated in this and earlier studies revealed the  
478 nuclear protein RCD1 as a regulator of energy organelle communication with the  
479 nuclear gene expression apparatus.

480 The *rcd1* mutant displays alterations in both chloroplasts and mitochondria (*Fujibe et al.,*  
481 *2004; Heiber et al., 2007; Jaspers et al., 2009; Brosché et al., 2014; Hiltcher et al.,*  
482 *2014*), and transcriptomic outcomes of RCD1 inactivation share similarities with those  
483 triggered by disrupted functions of both organelles (*Figure 6*). The results here suggest  
484 that RCD1 forms inhibitory complexes with components of mitochondrial retrograde  
485 signaling *in vivo*. Chloroplastic ROS appear to exhibit a direct influence on redox state  
486 and stability of RCD1 in the nucleus. These properties position RCD1 within a  
487 regulatory system encompassing mitochondrial complex III signaling through ANAC013/  
488 ANAC017 transcription factors and chloroplastic signaling by H<sub>2</sub>O<sub>2</sub>. The existence of  
489 such an inter-organellar regulatory system, integrating mitochondrial ANAC013 and  
490 ANAC017-mediated signaling (*De Clercq et al., 2013; Ng et al., 2013b*) with the PAP-  
491 mediated chloroplastic signaling (*Estavillo et al., 2011; Chan et al., 2016; Crisp et al.,*  
492 *2018*) has been previously proposed on the basis of transcriptomic analyses (*Van Aken*  
493 *and Pogson, 2017*). However, the underlying molecular mechanisms remained  
494 unknown. Based on our results we propose that RCD1 may function at the intersection  
495 of mitochondrial and chloroplast signaling pathways and act as a nuclear integrator of  
496 both PAP and ANAC013 and ANAC017-mediated retrograde signals.

497 RCD1 has been proposed to act as a transcriptional co-regulator because of its  
498 interaction with many transcription factors in yeast-two-hybrid analyses (*Jaspers et al.*,  
499 2009). The *in vivo* interaction of RCD1 with ANAC013 and ANAC017 revealed in this  
500 study (Table 1, *Figures 7, 8*) suggests that RCD1 modulates expression of the MDS, a  
501 set of ANAC013/ ANAC017-activated nuclear genes mostly encoding mitochondrial  
502 components (*De Clercq et al.*, 2013). ANAC013 itself is an MDS gene, thus  
503 mitochondrial signaling through ANAC013/ ANAC017 establishes a self-amplifying loop.  
504 Transcriptomic and physiological data support the role of RCD1 as a negative regulator  
505 of these transcription factors (*Figures 6-8*). Thus, RCD1 is likely involved in the negative  
506 regulation of the ANAC013/ ANAC017 self-amplifying loop and in downregulating the  
507 expression of MDS genes after their induction.

508 Induction of genes in response to stress is commonly associated with rapid inactivation  
509 of a negative co-regulator. Accordingly, the RCD1 protein was sensitive to treatments  
510 triggering or mimicking chloroplastic ROS production. MV and H<sub>2</sub>O<sub>2</sub> treatment of plants  
511 resulted in rapid oligomerization of RCD1 (*Figure 2*). Involvement of chloroplasts is  
512 indicated by the fact that MV treatment led to redox changes of RCD1-HA only in light  
513 (*Figure 2B* and *Figure 4 – figure supplement 2B*). In addition, little change was observed  
514 with the mitochondrial complex III inhibitors AA or myx (*Figure 4 – figure supplement*  
515 *2A, B*). Together with the fact that MDS induction was not compromised in the *rcd1*  
516 mutant (*Figure 4 – figure supplement 1* and *Figure 6 – figure supplement 2*), this  
517 suggests that RCD1 may primarily function as a redox sensor of chloroplastic, rather  
518 than mitochondrial, ROS/ redox signaling. In addition to fast redox changes, the overall  
519 level of RCD1 gradually decreased during prolonged (5 hours) stress treatments. This  
520 suggests several independent modes of RCD1 regulation at the protein level.

521 The complicated post-translational regulation of RCD1 is reminiscent of another  
522 prominent transcriptional co-regulator protein NONEXPRESSER OF PR GENES 1  
523 (NPR1). NPR1 exists as a high molecular weight oligomer stabilized by intermolecular  
524 disulfide bonds between conserved cysteine residues. Accumulation of salicylic acid  
525 and cellular redox changes lead to the reduction of cysteines and release of NPR1  
526 monomers that translocate to the nucleus and activate expression of defense genes  
527 (*Kinkema et al.*, 2000; *Mou et al.*, 2003; *Withers and Dong*, 2016). Similar to NPR1,  
528 RCD1 has a bipartite nuclear localization signal and, in addition, a putative nuclear  
529 export signal between the WWE and PARP-like domains. Like NPR1, RCD1 has

530 several conserved cysteine residues. Interestingly, mutation of seven interdomain  
531 cysteines in RCD1 largely eliminated the fast *in vivo* effect of chloroplastic ROS on  
532 redox state and stability of RCD1; however, it did not significantly alter the plant  
533 response to MV (*Figure 2* and *Figure 2 – figure supplement 1C, D*). This suggests that  
534 redox-dependent oligomerization of RCD1 may serve to fine-tune its activity.

#### 535 *MDS genes are involved in interactions between the organelles*

536 How the RCD1-dependent induction of MDS genes contributes to the energetic and  
537 signaling landscape of the plant cell remains to be investigated. Our results suggest that  
538 one component of this adaptation is the activity of mitochondrial alternative oxidases,  
539 which are part of the MDS regulon. Consequently, AOX proteins accumulate at higher  
540 amounts in *rcd1* (*Figure 4*). Pretreatment of wild type plants with complex III inhibitors  
541 AA or myx led to elevated AOX abundance coinciding with increased tolerance to  
542 chloroplastic ROS. Moreover, the AOX inhibitor SHAM made plants more sensitive to  
543 MV, indicating the direct involvement of AOX activity in the chloroplastic ROS  
544 processing. It thus appears that AOXs in the mitochondria form an electron sink that  
545 indirectly contributes to the oxidization of the electron acceptor side of PSI. In the *rcd1*  
546 mutant, this mechanism may be continuously active. The described inter-organellar  
547 electron transfer may decrease production of ROS by PSI (asterisk in *Figure 9*).  
548 Furthermore, chloroplastic ROS are considered the main electron sink for oxidation of  
549 chloroplast thiol enzymes (*Ojeda et al., 2018; Vaseghi et al., 2018; Yoshida et al.,*  
550 *2018*). Thus, the redox status of these enzymes could depend on the proposed inter-  
551 organellar pathway. This is in line with higher reduction of the chloroplast enzymes 2-  
552 CP and NADPH-MDH observed in *rcd1* (*Figure 1C* and *Figure 5C*).

553 The malate shuttle was recently shown to mediate a chloroplast-to-mitochondria  
554 electron transfer pathway that caused ROS production by complex III and evoked  
555 mitochondrial retrograde signaling (*Wu et al., 2015; Zhao et al., 2018*). Altered levels of  
556 malate and increased activity of NADPH-dependent malate dehydrogenase in *rcd1*  
557 (*Figure 5*) suggest that in this mutant the malate shuttle could act as an inter-organellar  
558 electron carrier.

559 Another MDS gene with more abundant mRNA levels in the *rcd1* mutant encodes  
560 sulfotransferase SOT12, an enzyme involved in PAP metabolism (*Klein and*  
561 *Papenbrock, 2004*). Accordingly, SOT12 protein level was significantly increased in the

562 *rcd1* mutant (Figure 6B). Accumulation of SOT12 and similarities between transcript  
563 profiles of RCD1- and PAP-regulated genes suggest that PAP signaling is likely to be  
564 constitutively active in the *rcd1* mutant. Unbalancing this signaling by elimination of  
565 SAL1 leads to severe developmental defects, as evidenced by the stunted phenotype of  
566 the *rcd1 sal1* double mutant. Thus, the RCD1 and the PAP signaling pathways appear  
567 to be overlapping and somewhat complementary, but the exact molecular mechanisms  
568 remain to be explored.

#### 569 *RCD1 regulates stress responses and cell fate*

570 The MDS genes represent only a fraction of genes showing differential regulation in  
571 *rcd1* (Figure 6 – figure supplement 1). This likely reflects the fact that RCD1 interacts  
572 with many other protein partners in addition to ANACs. The C-terminal RST domain of  
573 RCD1 was shown to interact with transcription factors belonging to DREB, PIF, ANAC,  
574 Rap2.4 and other families (Jaspers *et al.*, 2009; Vainonen *et al.*, 2012; Hiltcher *et al.*,  
575 2014; Bugge *et al.*, 2018). Analyses of various transcription factors interacting with  
576 RCD1 revealed little structural similarity between their RCD1-interacting sequences  
577 (O'Shea *et al.*, 2017). The flexible structure of the C-terminal domain of RCD1 probably  
578 determines the specificity and ability of RCD1 to interact with those different  
579 transcription factors. This makes RCD1 a hub in the crosstalk of organellar signaling  
580 with hormonal, photoreceptor, immune and other pathways and a likely mechanism by  
581 which these pathways are integrated and co-regulated.

582 The changing environment requires plants to readjust continuously their energy  
583 metabolism and ROS processing. On the one hand, this happens because of abiotic  
584 stress factors such as changing light intensity or temperature. For example, a sunlight  
585 fleck on a shade-adapted leaf can instantly alter excitation pressure on photosystems  
586 by two orders of magnitude (Allahverdiyeva *et al.*, 2015). On the other hand,  
587 chloroplasts and mitochondria are implicated in plant immune reactions to pathogens,  
588 contributing to decisive checkpoints including PCD (Shapiguzov *et al.*, 2012; Petrov *et al.*,  
589 2015; Wu *et al.*, 2015; Van Aken and Pogson, 2017; Zhao *et al.*, 2018). In both  
590 scenarios, perturbations of organellar ETCs may be associated with increased  
591 production of ROS. However, the physiological outcomes of the two situations can be  
592 opposite: acclimation in one case and cell death in the other. The existence of  
593 molecular mechanisms that unambiguously differentiate one type of response from the

594 other has been previously suggested (*Trotta et al., 2014; Sowden et al., 2017; Van*  
595 *Aken and Pogson, 2017*). The ANAC017 transcription factor and MDS genes, as well as  
596 PAP signaling, were proposed as organelle-related components counteracting PCD  
597 during abiotic stress (*Van Aken and Pogson, 2017*). This suggests that RCD1 is  
598 involved in the regulation of the cell fate checkpoint. Accordingly, the *rcd1* mutant is  
599 resistant to a number of abiotic stress treatments (*Ahlfors et al., 2004; Fujibe et al.,*  
600 *2004; Jaspers et al., 2009*).

601 Interestingly, in contrast to its resistance to abiotic stress, *rcd1* is more sensitive to  
602 treatments related to biotic stress. The *rcd1* mutant was originally identified in a forward  
603 genetic screen for sensitivity to ozone (*Overmyer et al., 2000*). Ozone decomposes in  
604 the plant cell wall to ROS mimicking formation of ROS by respiratory burst oxidases  
605 (RBOHs) in the course of plant immune reactions (*Joo et al., 2005; Vainonen and*  
606 *Kangasjarvi, 2015*). The opposing roles of RCD1 in the cell fate may be related to its  
607 interaction with diverse transcription factor partners and/ or different regulation of its  
608 stability and abundance. For example, transcriptomic analyses showed that under  
609 standard growth conditions, a cluster of genes associated with defense against  
610 pathogens had decreased expression in *rcd1* (*Brosché et al., 2014*), and no ANAC013/  
611 ANAC017 *cis*-element motif is associated with these genes (*Figure 6 – figure*  
612 *supplement 1*). In agreement with its role in biotic stress, RCD1 is a target for a fungal  
613 effector protein that prevents the activation of plant immunity (*Wirthmueller et al., 2018*).

614 Another possible factor determining varying roles of RCD1 in the cell fate is differential  
615 regulation of RCD1 protein function by ROS/ redox signals emitted by different  
616 subcellular compartments. The sensitivity of RCD1 to chloroplastic ROS (*Figure 2*) can  
617 be interpreted as negative regulation of the pro-PCD component. We hypothesize that  
618 this inactivation can occur in environmental situations that require physiological  
619 adaptation rather than PCD. For example, an abrupt increase in light intensity can  
620 cause excessive electron flow in photosynthetic ETC and overproduction of reducing  
621 power. The resulting deficiency of PSI electron acceptors can lead to changes in  
622 chloroplastic ROS production, which *via* retrograde signaling might influence RCD1  
623 stability and/ or redox status, inhibiting its activity and thus affecting adjustments in  
624 nuclear gene expression (*Figure 9*). Among other processes, RCD1-mediated  
625 suppression of ANAC013/ ANAC017 transcription factors is released, allowing the  
626 induction of the MDS regulon. The consequent expression of AOXs together with

627 increased chloroplast-to-mitochondrial electron transfer is likely to provide electron sink  
628 for photosynthesis, which could suppress chloroplast ROS production and contribute to  
629 the plant's survival under a changing environment (*Figure 9*).

**Key Resources Table**

| <b>Reagent type (species) or resource</b>              | <b>Designation</b>          | <b>Source or reference</b> | <b>Identifiers</b> | <b>Additional information</b>      |
|--|-----------------------------|----------------------------|--------------------|------------------------------------|
| genetic reagent ( <i>Arabidopsis thaliana</i> , Col-0) | <i>rcd1-4</i>               | NASC stock center          | GK-229D11          | homozygous mutant plant line       |
| genetic reagent ( <i>Arabidopsis thaliana</i> , Col-0) | <i>rcd1-1</i>               | PMID: 11041881             |                    | homozygous mutant plant line       |
| genetic reagent ( <i>Arabidopsis thaliana</i> , Col-0) | <i>aox1a</i>                | PMID: 16299171             |                    | homozygous mutant plant line       |
| genetic reagent ( <i>Arabidopsis thaliana</i> , Col-0) | AOX1a-OE                    | PMID: 16299171             |                    | homozygous mutant plant line       |
| genetic reagent ( <i>Arabidopsis thaliana</i> , Col-0) | <i>ptox</i>                 | PMID: 7920709              |                    | homozygous mutant plant line       |
| genetic reagent ( <i>Arabidopsis thaliana</i> , Col-0) | <i>anac017</i>              | NASC stock center          | SALK_022174        | homozygous mutant plant line       |
| genetic reagent ( <i>Arabidopsis thaliana</i> , Col-0) | <i>sal1-8</i>               | PMID: 19170934             |                    | homozygous mutant plant line       |
| genetic reagent ( <i>Arabidopsis thaliana</i> , Col-0) | <i>rcd1 aox1a</i>           | PMID: 24550736             |                    | homozygous mutant plant line       |
| genetic reagent ( <i>Arabidopsis thaliana</i> , Col-0) | <i>rcd1-1 anac017</i>       | this paper                 |                    | homozygous mutant plant line       |
| genetic reagent ( <i>Arabidopsis thaliana</i> , Col-0) | <i>rcd1-4 sal1-8</i>        | this paper                 |                    | homozygous mutant plant line       |
| genetic reagent ( <i>Arabidopsis thaliana</i> , Col-0) | <i>rcd1-4: RCD1-HA</i>      | this paper                 |                    | set of complementation plant lines |
| genetic reagent ( <i>Arabidopsis thaliana</i> , Col-0) | <i>rcd1-4: RCD1-3xVenus</i> | this paper                 |                    | set of complementation plant lines |
| genetic reagent ( <i>Arabidopsis thaliana</i> , Col-0) | <i>rcd1-4: RCD1Δ7Cys-HA</i> | this paper                 |                    | set of complementation plant lines |
| genetic reagent ( <i>Arabidopsis thaliana</i> , Col-0) | <i>rcd1-4: RCD1ΔRS T-HA</i> | this paper                 |                    | set of complementation plant lines |
| genetic reagent ( <i>Arabidopsis</i>                   | ANAC013-GFP                 | PMID: 24045019             |                    | transgenic plant line              |



|   |                  |                            |                     |   |
|---|------------------|----------------------------|---------------------|---|
| <i>thaliana</i> , Col-0)  |                  |                            |                     |   |
| genetic reagent<br>( <i>Arabidopsis thaliana</i> , <i>gl1</i> ) | <i>pgr5</i>      | PMID: 12176323             |                     | homozygous mutant plant line              |
| cell line ( <i>Homo sapiens</i> )                               | HEK293T          | ATCC                       | ATCC CRL-3216       | human embryonic kidney cell line          |
| gene ( <i>Homo sapiens</i> )                                    | HA-RCD1          | this paper                 |                     | construct for expression in HEK293T cells |
| gene ( <i>Homo sapiens</i> )                                    | ANAC013-myc      | this paper                 |                     | construct for expression in HEK293T cells |
| gene ( <i>Homo sapiens</i> )                                    | ANAC017-myc      | this paper                 |                     | construct for expression in HEK293T cells |
| antibody  | $\alpha$ HA      | Roche                      | Roche 1 867 423 001 | 1 : 2 000 for immunoblotting              |
| antibody  | $\alpha$ GFP     | Milteny Biotech            |                     |   |
| antibody  | $\alpha$ RCD1    | this paper                 |                     | 1 : 500 for immunoblotting                |
| antibody  | $\alpha$ SOT12   | Dr. Saijaliisa Kangasjärvi | Agrisera AS16 3943  | 1 : 500 for immunoblotting                |
| peptide, recombinant protein                                    | ANAC013 peptides | Genecust                   |                     | Synthetic peptides                        |

630

631

## 632 **Materials and methods**

### 633 ***Plants and mutants***

634 *Arabidopsis thaliana* adult plants were grown on soil (peat : vermiculite = 1:1) in white  
635 luminescent light (220-250  $\mu\text{mol m}^{-2} \text{s}^{-1}$ ) at a 12-hour photoperiod. Seedlings were  
636 grown for 14 days on 1 x MS basal medium (Sigma-Aldrich) with 0.5 % Phytigel  
637 (Sigma-Aldrich) without added sucrose in white luminescent light (150-180  $\mu\text{mol m}^{-2} \text{s}^{-1}$ )  
638 at a 12-hour photoperiod. *Arabidopsis rcd1-4* mutant (GK-229D11), *rcd1-1* (Overmyer *et al.*,  
639 *2000*), *aox1a* (SAIL\_030\_D08), *AOX1a-OE* (Umbach *et al.*, 2005), *plox* (Wetzelsch *et al.*,  
640 *1994*), *anac017* (SALK\_022174), and *sal1-8* (Wilson *et al.*, 2009) mutants are of  
641 Col-0 background; *pgr5* mutant is of *gl1* background (Munekage *et al.*, 2002).  
642 ANAC013-GFP line is described in (De Clercq *et al.*, 2013), RCD1-HA line labeled “a” in  
643 *Figure 1 – figure supplement 1* is described in (Jaspers *et al.*, 2009), *rcd1 aox1a* double  
644 mutant – in (Brosché *et al.*, 2014). RCD1-3xVenus, RCD1 $\Delta$ 7Cys-HA, RCD1 $\Delta$ RST-HA  
645 lines are described in *Cloning*.

### 646 ***Cloning***

647 *rcd1* complementation line expressing RCD1 tagged with triple HA epitope on the C-  
648 terminus was described previously (Jaspers *et al.*, 2009). In this line the genomic  
649 sequence of RCD1 was expressed under the control of the *RCD1* native promoter  
650 (3505 bp upstream the start codon). The RCD1 $\Delta$ 7Cys-HA construct was generated in  
651 the same way as RCD1-HA. The cysteine residues were mutated to alanines by  
652 sequential PCR-based mutagenesis of the genomic sequence of *RCD1* in the  
653 pDONR/Zeo vector followed by end-joining with In-Fusion (Clontech). The RCD1 $\Delta$ RST-  
654 HA variant was generated in the same vector by removal with a PCR reaction of the  
655 region corresponding to amino acid residues 462-589. The resulting construct was  
656 transferred to the pGWB13 binary vector by a Gateway reaction. To generate the  
657 RCD1-3xVenus construct, RCD1 cDNA was fused to the *UBIQUITIN10* promoter region  
658 and to the C-terminal triple Venus YFP tag in a MultiSite Gateway reaction as described  
659 in (Siligato *et al.*, 2016). The vectors were introduced in the *rcd1-4* mutant by floral  
660 dipping. Homozygous single insertion *Arabidopsis* lines were obtained. They were  
661 defined as the lines demonstrating 1:3 segregation of marker antibiotic resistance in T2  
662 generation and 100 % resistance to the marker antibiotic in T3 generation.  
663 For HEK293T cell experiments codon-optimized N-terminal 3xHA-fusion of RCD1 and  
664 C-terminal 3xmyc-fusion of ANAC013 were cloned into pcDNA3.1(+). Full-length

665 ANAC017 was cloned pcDNA3.1(-) in the Xho I/ Hind III sites, the double myc tag was  
666 introduced in the reverse primer sequence. The primer sequences used for the study  
667 are presented in Supplementary file 1.

#### 668 **Generation of the $\alpha$ RCD1 antibody**

669  $\alpha$ RCD1 specific antibody was raised in rabbit using denatured RCD1-6His protein as  
670 the antigen for immunization (Storkbio, Estonia). The final serum was purified using  
671 denatured RCD1-6His immobilized on nitrocellulose membrane, aliquoted and stored at  
672  $-80\text{ }^{\circ}\text{C}$ . For immunoblotting, 200  $\mu\text{g}$  of total protein were loaded per well, the antibody  
673 was used in dilution 1 : 500.

#### 674 **Inhibitor treatments**

675 For PSII inhibition studies, leaf discs were let floating on Milli-Q water solution  
676 supplemented with 0.05 % Tween 20 (Sigma-Aldrich). Final concentration of AA and  
677 myx was 2.5  $\mu\text{M}$  each, of SHAM – 2 mM. For transcriptomic experiments, plant rosettes  
678 were sprayed with water solution of 50  $\mu\text{M}$  AA complemented with 0.01 % Silwet Gold  
679 (Nordisk Alkali). Stock solutions of these chemicals were prepared in DMSO, equal  
680 volumes of DMSO were added to control samples. Pre-treatment with chemicals was  
681 carried out in the darkness, overnight for MV, AA and myx, 1 hour for SHAM. After  
682 spraying plants with 50  $\mu\text{M}$  AA they were incubated in growth light for 3 hours. For  
683 chemical treatment in seedlings grown on MS plates, 5 mL of Milli-Q water with or  
684 without 50  $\mu\text{M}$  MV were poured in 9-cm plates at the end of the light period. The  
685 seedlings were kept in the darkness overnight, and light treatment was performed on  
686 the following morning. For  $\text{H}_2\text{O}_2$  treatment, the seedlings were incubated in 5 mL of  
687 Milli-Q water with or without 100 mM  $\text{H}_2\text{O}_2$  in light.

#### 688 **DAB staining**

689 Plant rosettes were stained with 3,3'-diaminobenzidine (DAB) essentially as described  
690 in (Daudi *et al.*, 2012) [Daudi, A. and O'Brien, J. A. (2012). Detection of Hydrogen  
691 Peroxide by DAB Staining in Arabidopsis Leaves. Bio-protocol 2(18): e263. DOI:  
692 10.21769/BioProtoc.263.]. After vacuum infiltration of DAB-staining solution in the  
693 darkness, rosettes were exposed to light ( $180\text{ }\mu\text{mol m}^{-2}\text{ s}^{-1}$ ) for 20 min to induce  
694 production of chloroplastic ROS and then immediately transferred to the bleaching  
695 solution.

696 ***Spectroscopic measurements of photosynthesis***

697 Chlorophyll fluorescence was measured by MAXI Imaging PAM (Walz, Germany). PSII  
 698 inhibition protocol consisted of repetitive 1-hour periods of blue actinic light (450 nm, 80  
 699  $\mu\text{mol m}^{-2} \text{s}^{-1}$ ) each followed by a 20-min dark adaptation, then  $F_o$  and  $F_m$  measurement.  
 700 PSII photochemical yield was calculated as  $F_v/F_m = (F_m - F_o)/F_m$  (Figure 1 – figure  
 701 supplement 2). To plot raw chlorophyll fluorescence kinetics under light ( $F_s$ ) against  
 702 time, the reads were normalized to dark-adapted  $F_o$ . For the measurements of  
 703 photochemical quenching,  $F_m'$  was measured with saturating pulses triggered against  
 704 the background of activating light (450 nm, 80  $\mu\text{mol m}^{-2} \text{s}^{-1}$ ), and the following formulae  
 705 were used:  $qP = (F_m' - F_s)/(F_m' - F_o')$ , where  $F_o' \approx F_o / (((F_m - F_o) / F_m) + (F_o / F_m'))$   
 706 (Oxborough and Baker, 1997). The assays were performed in 96-well plates. In each  
 707 assay, leaf discs from at least 4 individual plants were analyzed. Each assay was  
 708 reproduced at least three times.

709 PSI (P700) oxidation was measured by DUAL-PAM-100 (Walz, Germany) as described  
 710 (Tiwari et al., 2016). Leaves were pre-treated in 1  $\mu\text{M}$  MV for 4 hours, then shifted to  
 711 light (160  $\mu\text{mol m}^{-2} \text{s}^{-1}$ ) for indicated time. Oxidation of P700 was induced by PSI-  
 712 specific far red light (FR, 720 nm). To determine fully oxidized P700 ( $P_m$ ), a saturating  
 713 pulse of actinic light was applied under continuous background of FR, followed by  
 714 switching off both the actinic and FR light. The kinetics of  $P700^+$  reduction by  
 715 intersystem electron transfer pool and re-oxidation by FR was determined by using a  
 716 multiple turnover saturating flash of PSII light (635 nm) in the background of continuous  
 717 FR.

718 ***Isolation, separation and detection of proteins and protein complexes***

719 Thylakoids were isolated as described in (Järvi et al., 2016). Chlorophyll content was  
 720 determined according to (Porra et al., 1989) and protein content according to (Lowry et  
 721 al., 1951). For immunoblotting of total plant extracts, the plant material was frozen  
 722 immediately after treatments in liquid nitrogen and ground. Total proteins were extracted  
 723 in SDS extraction buffer [50 mM Tris-HCl (pH 7.8), 2 % SDS, 1 x protease inhibitor  
 724 cocktail (Sigma-Aldrich), 2 mg/ mL NaF] for 20 min at 37 °C and centrifuged at 18 000 x  
 725 g for 10 min. Supernatants were normalized for protein concentration and resolved by  
 726 SDS-PAGE. For separation of proteins, SDS-PAGE (10-12 % polyacrylamide) was used  
 727 (Laemmli, 1970). For thylakoid proteins, the gel was complemented with 6 M urea. To  
 728 separate thylakoid membrane protein complexes, isolated thylakoids were solubilized

729 with *n*-dodecyl  $\beta$ -D-maltoside (Sigma-Aldrich) and separated in BN-PAGE (5-12.5 %  
730 polyacrylamide) as described by (Järvi *et al.*, 2016). After electrophoresis, proteins were  
731 electroblotted to PVDF membrane and immunoblotted with specific antibodies.  $\alpha$ SOT12  
732 antibodies have Agrisera reference number AS16 3943. For quantification of  
733 immunoblotting signal, ImageJ software was used (<https://imagej.nih.gov/ij/>).

#### 734 ***Analysis of protein thiol redox state by mobility shift assays***

735 Thiol redox state of 2-CPs in detached Col-0 and *rcd1* leaves adapted to darkness or  
736 light (3 hours of 160  $\mu\text{mol m}^{-2} \text{s}^{-1}$ ), was determined by alkylating free thiols in TCA-  
737 precipitated proteins with 50 mM N-ethylmaleimide in the buffer containing 8 M urea,  
738 100 mM Tris-HCl (pH 7.5), 1 mM EDTA, 2% SDS, and 1/10 of protease inhibitor cocktail  
739 (Thermo Scientific), reducing *in vivo* disulfides with 100 mM DTT and then alkylating the  
740 newly reduced thiols with 10 mM methoxypolyethylene glycol maleimide of molecular  
741 weight 5 kDa (Sigma-Aldrich), as described in (Nikkanen *et al.*, 2016). Proteins were  
742 then separated by SDS-PAGE and immunoblotted with a 2-CP-specific antibody.

#### 743 ***Non-aqueous fractionation (NAF)***

744 Leaves of Arabidopsis plants were harvested in the middle of the light period and snap-  
745 frozen in liquid nitrogen. Four grams of fresh weight of frozen plant material was ground  
746 to a fine powder using a mixer mill (Retsch), transferred to Falcon tubes and freeze-  
747 dried at 0.02 bar for 5 days in a lyophilizer, which had been pre-cooled to  $-40^\circ\text{C}$ . The  
748 NAF-fractionation procedure was performed as described in (Krueger *et al.*, 2011;  
749 Arrivault *et al.*, 2014; Krueger *et al.*, 2014) except that the gradient volume, composed  
750 of the solvents tetrachloroethylene ( $\text{C}_2\text{Cl}_4$ )/ heptane ( $\text{C}_7\text{H}_{16}$ ), was reduced from 30 mL to  
751 25 mL but with the same linear density. Leaf powder was resuspended in 20 mL  $\text{C}_2\text{Cl}_4$ /  
752  $\text{C}_7\text{H}_{16}$  mixture 66:34 (v/v; density  $\rho = 1.3 \text{ g cm}^{-3}$ ), and sonicated for 2 min, with  $6 \times 10$   
753 cycles at 65 % power. The sonicated suspension was filtered through a nylon net (20  
754  $\mu\text{m}$  pore size). The net was washed with 30 mL of heptane. The suspension was  
755 centrifuged for 10 min at  $3\ 200 \times g$  at  $4^\circ\text{C}$  and the pellet was resuspended in 5 mL  
756  $\text{C}_2\text{Cl}_4$ /  $\text{C}_7\text{H}_{16}$  mixture 66:34. The gradient was formed in 38 mL polyallomer  
757 centrifugation tube using a peristaltic gradient pump (BioRad) generating a linear  
758 gradient from 70 % solvent A ( $\text{C}_2\text{Cl}_4$ /  $\text{C}_7\text{H}_{16}$  mixture 66:34) to 100 % solvent B (100 %  
759  $\text{C}_2\text{Cl}_4$ ) with a flow rate of  $1.15 \text{ mL min}^{-1}$ , resulting in a density gradient from  $1.43 \text{ g cm}^{-3}$   
760 to  $1.62 \text{ g cm}^{-3}$ . Five mL suspension containing the sample was loaded on top of the  
761 gradient and centrifuged for 55 min at  $5\ 000 \times g$  at  $4^\circ\text{C}$  using a swing-out rotor with

762 acceleration and deceleration of 3:3 (brakes off). Each of the compartment-enriched  
763 fractions (F1 to F8) were transferred carefully from the top of the gradient into a 50-mL  
764 Falcon tube, filled up with heptane to a volume of 20 mL and centrifuged at 3 200 x g for  
765 10 min. The pellet was resuspended in 6 mL of heptane and subsequently divided into 6  
766 aliquots of equal volume (950 µL). The pellets had been dried in a vacuum concentrator  
767 without heating and stored at -80 °C until further use. Subcellular compartmentation of  
768 markers or the metabolites of our interest was calculated by BestFit method as  
769 described in (*Krueger et al., 2011; Krueger et al., 2014*). Percentage values (% of the  
770 total found in all fractions) of markers and metabolites have been used to make the  
771 linear regressions for subcellular compartments using BestFit.

### 772 ***Marker measurements for non-aqueous fractionation***

773 Before enzyme and metabolite measurements, dried pellets were homogenized in the  
774 corresponding extraction buffer by the addition of one steel ball (2-mm diameter) to  
775 each sample and shaking at 25 Hz for 1 min in a mixer mill. Enzyme extracts were  
776 prepared as described in (*Gibon et al., 2004*) with some modifications. The extraction  
777 buffer contained 50 mM HEPES-KOH (pH 7.5), 10 mM MgCl<sub>2</sub>, 1 mM EDTA, 1 mM  
778 EGTA, 1 mM benzamidine, 1 mM ε-aminocaproic acid, 0.25 % (w/v) BSA, 20 µM  
779 leupeptin, 0.5 mM DTT, 1 mM phenylmethylsulfonyl fluoride (PMSF), 1 % (v/v) Triton X-  
780 100, 20 % glycerol. The extract was centrifuged (14 000 rpm at 4 °C for 10 min) and the  
781 supernatant was used directly for the enzymatic assays. The activities of adenosine  
782 diphosphate glucose pyrophosphorylase (AGPase) and phosphoenolpyruvate  
783 carboxylase (PEPC) were determined as described in (*Gibon et al., 2004*) but without  
784 using the robot-based platform. Chlorophyll was extracted twice with 80 % (v/v) and  
785 once with 50 % (v/v) hot ethanol/ 10 mM HEPES (pH 7.0) followed by 30-min incubation  
786 at 80 °C and determined as described in (*Cross et al., 2006*). Nitrate was measured by  
787 the enzymatic reaction as described in (*Cross et al., 2006*).

### 788 ***Incubation of Arabidopsis leaf discs with [U-<sup>14</sup>C] glucose***

789 For the light experiment, leaf discs were incubated in light in 5 mL 10 mM MES-KOH  
790 (pH 6.5), containing 1.85 MBq/ mmol [U-<sup>14</sup>C] glucose (Hartmann Analytic) in a final  
791 concentration of 2 mM. In the dark experiment, leaf discs were incubated under green  
792 light for 150 min. Leaf discs were placed in a sieve, washed several times in double-  
793 distilled water, frozen in liquid nitrogen, and stored at -80 °C until further analysis. All

794 incubations were performed in sealed flasks under green light and shaken at 100 rpm.  
795 The evolved  $^{14}\text{CO}_2$  was collected in 0.5 mL of 10 % (w/v) KOH.

#### 796 ***Fractionation of $^{14}\text{C}$ -labeled tissue extracts and measurement of metabolic fluxes***

797 Extraction and fractionation were performed according to (Obata *et al.*, 2017). Frozen  
798 leaf discs were extracted with 80 % (v/v) ethanol at 80 °C (1 mL per sample) and re-  
799 extracted in two subsequent steps with 50 % (v/v) ethanol (1 mL per sample for each  
800 step), and the combined supernatants were dried under an air stream at 35 °C and  
801 resuspended in 1 mL of water (Ferne *et al.*, 2001). The soluble fraction was  
802 subsequently separated into neutral, anionic, and basic fractions by ion-exchange  
803 chromatography; the neutral fraction (2.5 mL) was freeze-dried, resuspended in 100  $\mu\text{L}$   
804 of water, and further analyzed by enzymatic digestion followed by a second ion-  
805 exchange chromatography step (Carrari *et al.*, 2006). To measure phosphate esters,  
806 samples (250  $\mu\text{L}$ ) of the soluble fraction were incubated in 50  $\mu\text{L}$  of 10 mM MES-KOH  
807 (pH 6.0), with or without 1 unit of potato acid phosphatase (grade II; Boehringer  
808 Mannheim) for 3 hours at 37 °C, boiled for 2 min, and analyzed by ion-exchange  
809 chromatography (Ferne *et al.*, 2001). The insoluble material left after ethanol extraction  
810 was homogenized, resuspended in 1 mL of water, and counted for starch (Ferne *et al.*,  
811 2001). Fluxes were calculated as described following the assumptions detailed by  
812 Geigenberger *et al* (Geigenberger *et al.*, 1997; Geigenberger *et al.*, 2000).  
813 Unfortunately, the discontinued commercial availability of the required positionally  
814 radiolabeled glucoses prevented us from analyzing fermentative fluxes more directly.

#### 815 ***Preparation of crude mitochondria***

816 Crude mitochondria were isolated from Arabidopsis rosette leaves as described in  
817 (Keech *et al.*, 2005).

#### 818 ***Measurements of AOX capacity in vivo***

819 Seedling respiration and AOX capacity were assessed by measuring  $\text{O}_2$  consumption in  
820 the darkness using a Clark electrode as described in (Schwarzländer *et al.*, 2009).

#### 821 ***Metabolite extraction***

822 Primary metabolites were analyzed with GC-MS according to (Roessner *et al.*, 2000).  
823 GC-MS analysis was executed from the plant extracts of eight biological replicates  
824 (pooled samples). Plant material was homogenized in a Qiagen TissueLyser II bead mill  
825 (Qiagen, Germany) with 1-1.5 mm Retsch glass beads. Soluble metabolites were

826 extracted from plant material in two steps, first with 1 mL of 100 % methanol (Merck)  
827 and second with 1 mL of 80 % (v/v) aqueous methanol. During the first extraction step,  
828 5  $\mu\text{L}$  of internal standard solution (0.2  $\text{mg mL}^{-1}$  of benzoic- $\text{d}_5$  acid, 0.1  $\text{mg mL}^{-1}$  of  
829 glycerol- $\text{d}_8$ , 0.2  $\text{mg mL}^{-1}$  of 4-methylumbelliferone in methanol) was added to each  
830 sample. During both extraction steps, the samples were vortexed for 30 min and  
831 centrifuged for 5 min at 13 000 rpm (13 500  $\times g$ ) at 4  $^\circ\text{C}$ . The supernatants were then  
832 combined for metabolite analysis. The extracts (2 mL) were dried in a vacuum  
833 concentrator (MiVac Duo, Genevac Ltd, Ipswich, UK), the vials were degassed with  
834 nitrogen and stored at -80  $^\circ\text{C}$  prior to derivatization and GC-MS analysis.

835 Dried extracts were re-suspended in 500  $\mu\text{L}$  of methanol. Aliquot of 200  $\mu\text{L}$  was  
836 transferred to a vial and dried in a vacuum. The samples were derivatized with 40  $\mu\text{L}$  of  
837 methoxyamine hydrochloride (MAHC, Sigma-Aldrich) (20  $\text{mg mL}^{-1}$ ) in pyridine (Sigma-  
838 Aldrich) for 90 min at 30  $^\circ\text{C}$  at 150 rpm, and with 80  $\mu\text{L}$  N-methyl-N-(trimethylsilyl)  
839 trifluoroacetamide with 1 % trimethylchlorosilane (MSTFA with 1 % TMCS, Thermo  
840 Scientific) for 120 min at 37  $^\circ\text{C}$  at 150 rpm. Alkane series (10  $\mu\text{L}$ , C10–C40, Supelco) in  
841 hexane (Sigma-Aldrich) and 100  $\mu\text{L}$  of hexane was added to each sample before GC-  
842 MS analysis.

#### 843 ***Metabolite analysis by gas chromatography-mass spectrometry***

844 The GC-MS system consisted of Agilent 7890A gas chromatograph with 7000 Triple  
845 quadrupole mass spectrometer and GC PAL autosampler and injector (CTC Analytics).  
846 Splitless injection (1  $\mu\text{L}$ ) was employed using a deactivated single tapered splitless liner  
847 with glass wool (Topaz, 4 mm ID, Restek). Helium flow in the column (Agilent HP-5MS  
848 Ultra Inert, length 30 m, 0.25 mm ID, 0.25  $\mu\text{m}$  film thickness combined with Agilent  
849 Ultimate Plus deactivated fused silica, length 5 m, 0.25 mm ID) was 1.2  $\text{mL min}^{-1}$  and  
850 purge flow at 0.60 min was 50  $\text{mL min}^{-1}$ . The injection temperature was set to 270  $^\circ\text{C}$ ,  
851 MS interface 180  $^\circ\text{C}$ , source 230  $^\circ\text{C}$  and quadrupole 150  $^\circ\text{C}$ . The oven temperature  
852 program was as follows: 2 min at 50  $^\circ\text{C}$ , followed by a 7  $^\circ\text{C min}^{-1}$  ramp to 260  $^\circ\text{C}$ , 15  $^\circ\text{C}$   
853  $\text{min}^{-1}$  ramp to 325  $^\circ\text{C}$ , 4 min at 325  $^\circ\text{C}$  and post-run at 50  $^\circ\text{C}$  for 4.5 min. Mass spectra  
854 were collected with a scan range of 55-550  $m/z$ .

855 Metabolite Detector (versions 2.06 beta and 2.2N) (Hiller *et al.*, 2009) and AMDIS  
856 (version 2.68, NIST) were used for deconvolution, component detection and  
857 quantification. Malate levels were calculated as the peak area of the metabolite



858 normalized with the peak area of the internal standard, glycerol-d<sub>8</sub>, and the fresh weight  
859 of the sample.

#### 860 **Measurements of NADPH-MDH activity**

861 From light-adapted plants grown for 5 weeks (100-120  $\mu\text{mol m}^{-2} \text{s}^{-1}$  at an 8-hour day  
862 photoperiod), total extracts were prepared as for non-aqueous fractionation in the  
863 extraction buffer supplemented with 250  $\mu\text{M}$  DTT. In microplates, 5  $\mu\text{L}$  of the extract  
864 (diluted x 500) were mixed with 20  $\mu\text{L}$  of activation buffer (0.1 M Tricine-KOH (pH 8.0),  
865 180 mM KCl, 0.5 % Triton X-100). Initial activity was measured immediately after, while  
866 total activity was measured after incubation for 2 hours at room temperature in presence  
867 of additional 150 mM DTT. Then assay mix was added consisting of 20  $\mu\text{L}$  of assay  
868 buffer [0.5 M Tricine-KOH (pH 8.0), 0.25 % Triton X-100, 0.5 mM EDTA], 9  $\mu\text{L}$  of water,  
869 and 1  $\mu\text{L}$  of 50 mM NADPH (prepared in 50 mM NaOH), after which 45  $\mu\text{L}$  of 2.5 mM  
870 oxaloacetate or water control was added. The reaction was mixed, and light absorbance  
871 at 340-nm wavelength was measured at 25 °C.

#### 872 **Analysis of *rcd1* misregulated genes in microarray experiments related to** 873 **chloroplast or mitochondrial dysfunction**

874 Genes with misregulated expression in *rcd1* were selected from our previous microarray  
875 datasets (Brosché *et al.*, 2014) with the cutoff, absolute value of logFC < 0.5. These  
876 genes were subsequently clustered with the *rcd1* gene expression dataset together with  
877 various Affymetrix datasets related to chloroplast or mitochondrial dysfunction from the  
878 public domain using bootstrapped Bayesian hierarchical clustering as described in  
879 (Wrzaczek *et al.*, 2010). Affymetrix raw data (.cel files) were normalized with Robust  
880 Multi-array Average normalization, and manually annotated to control and treatment  
881 conditions, or mutant *versus* wild type.

882 Affymetrix ATH1-121501 data were from the following sources: Gene Expression  
883 Omnibus <https://www.ncbi.nlm.nih.gov/geo/>, AA 3 hours (in figures labelled as  
884 experiment 1), GSE57140 (Ivanova *et al.*, 2014); AA and H<sub>2</sub>O<sub>2</sub>, 3 hour treatments (in  
885 figures labelled as experiment 2), GSE41136 (Ng *et al.*, 2013b); MV 3 hours,  
886 GSE41963 (Sharma *et al.*, 2013); *mterf6-1*, GSE75824 (Leister and Kleine, 2016);  
887 *prors1-2*, GSE54573 (Leister *et al.*, 2014); H<sub>2</sub>O<sub>2</sub> 30 min, GSE43551 (Gutiérrez *et al.*,  
888 2014); high light 1 hour (in figures labelled as experiment 1), GSE46107 (Van Aken *et al.*,  
889 2013); high light 30 min in cell culture, GSE22671 (González-Pérez *et al.*, 2011);  
890 high light 3 hours (in figures labelled as experiment 2), GSE7743 (Kleine *et al.*, 2007);

891 oligomycin 1 and 4 hours, GSE38965 (Geisler et al., 2012); norflurazon – 5 day-old  
 892 seedlings grown on plates with norflurazon, GSE12887 (Koussevitzky et al., 2007);  
 893 *msh1 recA3* double mutant, GSE19603 (Shedge et al., 2010). AtGenExpress oxidative  
 894 time series, MV 12 and 24 hours,  
 895 [http://www.arabidopsis.org/servlets/TairObject?type=expression\\_set&id=1007966941](http://www.arabidopsis.org/servlets/TairObject?type=expression_set&id=1007966941).  
 896 ArrayExpress, <https://www.ebi.ac.uk/arrayexpress/>: rotenone, 3 and 12 hours, E-MEXP-  
 897 1797 (Garmier et al., 2008); *alx8* and *fry1*, E-MEXP-1495 (Wilson et al., 2009); *ndufs4*,  
 898 E-MEXP-1967 (Meyer et al., 2009).

### 899 **Quantitative PCR**

900 Quantitative PCR was performed essentially as described in (Brosché et al., 2014). The  
 901 data were normalized with three reference genes, *PP2AA3*, *TIP41* and *YLS8*. Relative  
 902 expression of the genes *RCD1*, *AOX1a*, *UPOX*, *ANAC013*, *At5G24640* and *ZAT12* was  
 903 calculated in qBase+ 3.2 (Biogazelle, <https://www.qbaseplus.com/>). The primer  
 904 sequences and primer efficiencies are presented in Supplementary file 1.

### 905 **Identification of interacting proteins using IP/MS-MS**

906 Immunoprecipitation experiments were performed in three biological replicates as  
 907 described previously (De Rybel et al., 2013), using 3 g of rosette leaves from p35S:  
 908 ANAC013-GFP and 2.5 g of rosette leaves from pUBI10: RCD1-3xVenus transgenic  
 909 lines. Interacting proteins were isolated by applying total protein extracts to  $\alpha$ GFP-  
 910 coupled magnetic beads (Miltény Biotech). Three replicates of p35S: ANAC013-GFP or  
 911 pUBI10: RCD1-3xVenus were compared to three replicates of Col-0 controls. Tandem  
 912 mass spectrometry (MS) and statistical analysis using MaxQuant and Perseus software  
 913 was performed as described previously (Wendrich et al., 2017).

### 914 **HEK293T human embryonic kidney cell culture and transfection**

915 HEK293T cells were maintained at 37 °C and 5 % CO<sub>2</sub> in Dulbecco's Modified Eagle's  
 916 Medium F12-HAM, supplemented with 10 % fetal bovine serum, 15 mM HEPES, and 1  
 917 % penicillin/ streptomycin. Cells were transiently transfected using GeneJuice  
 918 (Novagen) according to the manufacturer's instructions.

919 For co-immunoprecipitation experiments, HEK293T cells were co-transfected with  
 920 plasmids encoding HA-RCD1 and ANAC013-myc or ANAC017-myc. Forty hours after  
 921 transfection, cells were lysed in TNE buffer [50 mM Tris-HCl (pH 7.4), 150 mM NaCl, 5

922 mM EDTA, 1 % Triton X-100, 1 x protease inhibitor cocktail, 50  $\mu$ M proteasome inhibitor  
923 MG132 (Sigma-Aldrich)]. After incubation for 2 hours at 4 °C, lysates were cleared by  
924 centrifugation at 18 000 x *g* for 10 min at 4 °C. For co-immunoprecipitation, cleared cell  
925 lysates were incubated with either  $\alpha$ HA or  $\alpha$ myc antibody immobilized on agarose  
926 beads overnight at 4 °C. Beads were washed six times with the lysis buffer. The bound  
927 proteins were dissolved in SDS sample buffer, resolved by SDS-PAGE, and  
928 immunoblotted with the specified antibodies.

### 929 ***Protein expression and purification***

930 The C-terminal domain of RCD1 for NMR study was expressed as GST-fusion protein in  
931 *E.coli* BL21 (DE3) Codon Plus strain and purified using GSH-Sepharose beads (GE  
932 Healthcare) according to the manufacturer's instruction. Cleavage of GST tag was  
933 performed with thrombin (GE Healthcare, 80 units per mL of beads) for 4 hours at room  
934 temperature and the C-terminal domain of RCD1 was eluted from the beads with PBS  
935 buffer (137 mM NaCl, 2.7 mM KCl, 10 mM Na<sub>2</sub>HPO<sub>4</sub>, 1.8 mM KH<sub>2</sub>PO<sub>4</sub>, pH 7.4). The  
936 protein was further purified by gel filtration with HiLoad 16/600 Superdex 75 column (GE  
937 Healthcare) equilibrated with 20 mM sodium phosphate buffer (pH 6.4), 50 mM NaCl at  
938 4 °C.

### 939 ***Peptide synthesis***

940 ANAC013 peptides of > 98 % purity for surface plasmon resonance and NMR analysis  
941 were purchased from Genecust, dissolved in water to 5 mM final concentration and  
942 stored at -80 °C before analyses.

### 943 ***Surface plasmon resonance***

944 The C-terminal domain of RCD1 was covalently coupled to a Biacore CM5 sensor chip  
945 *via* amino-groups. 500 nM of ANAC013 peptides were then profiled at a flow rate of 30  
946  $\mu$ L min<sup>-1</sup> for 300 s, followed by 600 s flow of running buffer. Analysis was performed at  
947 25 °C in the running buffer containing 10 mM HEPES (pH 7.4), 150 mM NaCl, 3 mM  
948 EDTA, 0.05 % surfactant P20 (Tween-20). After analysis in BiaEvaluation (Biacore)  
949 software, the normalized resonance units were plotted over time with the assumption of  
950 one-to-one binding.

### 951 ***NMR spectroscopy***

952 NMR sample production and chemical shift assignment have been described in  
953 (Tossavainen *et al.*, 2017). A Bruker Avance III HD 800 MHz spectrometer equipped

954 with a TCI  $^1\text{H}/^{13}\text{C}/^{15}\text{N}$  cryoprobe was used to acquire spectra for structure  
955 determination of RCD1<sup>468-589</sup>. Peaks were manually picked from three NOE spectra, a  
956  $^1\text{H}$ ,  $^{15}\text{N}$  NOESY-HSQC and  $^1\text{H}$ ,  $^{13}\text{C}$  NOESY-HSQC spectra for the aliphatic and  
957 aromatic  $^{13}\text{C}$  regions. CYANA 2.1 (*Lopez-Mendez and Guntert, 2006*) automatic NOE  
958 peak assignment – structure calculation routine was used to generate 300 structures  
959 from which 30 were further refined in explicit water with AMBER 16 (*Case et al., 2005*).  
960 Assignments of three NOE peaks were kept fixed using the KEEP subroutine in  
961 CYANA. These NOE peaks restrained distances between the side chains of W507 and  
962 M508 and adjacent helices 1 and 4, respectively. Fifteen lowest AMBER energy  
963 structures were chosen to represent of RCD1<sup>468-589</sup> structure in solution.  
964 Peptide binding experiment was carried out by preparing a sample containing of  
965 RCD1<sup>468-589</sup> and ANAC013<sup>235-284</sup> peptide in an approximately 1:2 concentration ratio,  
966 and recording a  $^1\text{H}$ ,  $^{15}\text{N}$  HSQC spectrum. Amide peak positions were compared with  
967 those of the free RCD1<sup>468-589</sup>.

968 **Acknowledgements**

969 We thank Dr. Olga Blokhina, Dr. Bernadette Gehl and Manuel Saornil for the help in  
970 studies of mitochondria, Katariina Vuorinen for genotyping *rcd1-1 anac017*, Richard  
971 Gossens for critical comments on the manuscript, Prof. F. J. Cejudo (Institute of Plant  
972 Biochemistry, University of Sevilla) for the  $\alpha$ 2-CP antibody, and Dr. Saijaliisa  
973 Kangasjärvi for the  $\alpha$ SOT12 antibody. We acknowledge CSC – IT Center for Science,  
974 Finland, for computational resources. This work was supported by the University of  
975 Helsinki (JK); the Academy of Finland Centre of Excellence programs (2006-11; JK and  
976 2014-19; JK, EMA) and Research Grant (Decision 250336; JK); Academy of Finland  
977 fellowships (Decisions 275632, 283139 and 312498; MW); Academy of Finland  
978 Research Grant (Decision 288235; PP); by The Research Foundation – Flanders  
979 (FWO; Odysseus II G0D0515N and Post-doc grant 12D1815N; BW and BDR);  
980 PlantaSYST project by the European Union’s Horizon 2020 research and innovation  
981 programme (SGA-CSA No 664621 and No 739582 under FPA No. 664620; SA and  
982 ARF); Deutsche Forschungsgemeinschaft (DFG TRR 175 The Green Hub – Central  
983 Coordinator of Acclimation in Plants; FA and ARF); the Research Foundation –  
984 Flanders (Excellence of Science project no 30829584; FVB).  
985

986 **Figure legends**

987 **Figure 1. RCD1 controls tolerance of photosynthetic apparatus to ROS.**

- 988 (A) MV treatment results in PSII inhibition under light, which is suppressed in the *rcd1*  
989 mutant. PSII Photochemical yield (Fv/Fm) was measured in rosettes pre-treated  
990 overnight in darkness with 1  $\mu\text{M}$  MV and then exposed to 3 hours of continuous light  
991 ( $80 \mu\text{mol m}^{-2} \text{s}^{-1}$ ). Representative false-color image of Fv/Fm is shown.
- 992 (B) MV access to electron-acceptor side of PSI is unaltered in *rcd1*. Treatment with MV  
993 led to similar changes in kinetics of PSI oxidation in Col-0 and *rcd1*. Oxidation of  
994 PSI reaction center (P700) was measured using DUAL-PAM. Leaves were first  
995 adapted to far-red light that is more efficiently used by PSI than PSII. In these  
996 conditions PSI is producing electrons at a faster rate than they are supplied by PSII,  
997 thus P700 is oxidized. Then a flash of orange light was provided that is efficiently  
998 absorbed by PSII (orange arrow). Electrons generated by PSII transiently reduced  
999 PSI, after which the kinetics of PSI re-oxidation was followed. Note the progressive  
1000 decrease in the effect of the orange flash occurring in Col-0 at later time points,  
1001 which suggests deterioration in PSII function. This was not observed in *rcd1*. Three  
1002 leaves from three individual plants were used for each measurement. The  
1003 experiment was repeated three times with similar results.
- 1004 (C) Redox state of the chloroplast enzyme 2-Cys peroxiredoxin (2-CP) assessed by  
1005 thiol bond-specific labeling in Col-0 (left) and *rcd1* (right). Total protein was isolated  
1006 from leaves incubated in darkness (D), or under light (L). Free sulfhydryls were  
1007 blocked with N-ethylmaleimide, then *in vivo* thiol bridges were reduced with DTT,  
1008 and finally the newly exposed sulfhydryls were labeled with methoxypolyethylene  
1009 glycol maleimide of molecular weight 5 kDa. The labeled protein extracts were  
1010 separated by SDS-PAGE and immunoblotted with  $\alpha$ 2-CP antibody. DTT (-) control  
1011 contained predominantly unlabeled form. Unlabeled reduced (red), singly and  
1012 doubly labeled oxidized forms and the putative dimer were annotated as in  
1013 (*Nikkanen et al., 2016*). Apparent molecular weight increment after the labeling of  
1014 one thiol bond appears on SDS-PAGE higher than 10 kDa because of steric  
1015 hindrance exerted on branched polymers during gel separation (*van Leeuwen et al.,*  
1016 *2017*). The experiment was repeated three times with similar results.

1017 **Figure 2. RCD1 protein is sensitive to chloroplastic ROS.**

1018 (A) The *rcd1*: RCD1-HA complementation line was used to assess RCD1-HA  
1019 abundance. It gradually decreased in response to chloroplastic ROS. Leaf discs  
1020 from plants expressing HA-tagged RCD1 were treated with 5-hour growth light ( $150$   
1021  $\mu\text{mol m}^{-2} \text{s}^{-1}$ ), high light ( $1\ 300 \mu\text{mol m}^{-2} \text{s}^{-1}$ ), MV ( $1 \mu\text{M}$ ) in light, or  $\text{H}_2\text{O}_2$  ( $100 \text{ mM}$ ).  
1022 The levels of RCD1-HA were monitored by immunoblotting with  $\alpha\text{HA}$  at indicated  
1023 time points. Rubisco large subunit (RbcL) detected by amido black staining is  
1024 shown as a control for equal protein loading. The “0” time point of the MV time  
1025 course represents dark-adapted leaf discs pre-treated with MV overnight. The  
1026 experiment was performed four times with similar results.

1027 (B) Chloroplastic ROS caused oligomerization of RCD1-HA. Total protein extracts from  
1028 the plants treated as in panel (A) were separated by non-reducing PAGE and  
1029 immunoblotted with  $\alpha\text{HA}$  antibody. Reduced (red) and oxidized (ox) forms of the  
1030 protein are labeled. To ascertain that all HA-tagged protein including that forming  
1031 high-molecular-weight aggregates has been detected by immunoblotting, the  
1032 transfer to a membrane was performed using the entire SDS-PAGE gel including  
1033 the stacking gel and the well pockets. The experiment was performed four times  
1034 with similar results.

1035

1036 **Figure 3. Altered energy metabolism of *rcd1*.** Deduced metabolic fluxes in light- and  
1037 dark- adapted Col-0 and *rcd1* rosettes were assessed by fractionation of the  
1038 extracts of leaves treated with [U-<sup>14</sup>C] glucose. Increased respiration flux and higher  
1039 amount of total metabolized glucose (*Figure 3 – source data 1*) in *rcd1* suggest a  
1040 more active glycolytic pathway. Higher cell wall metabolic flux in *rcd1* provided  
1041 indirect support of increased operation of the oxidative pentose phosphate pathway  
1042 which is required for generating pentoses used in cell wall biosynthesis (*Ap Rees,*  
1043 *1978*). Mean  $\pm$  SE are presented. Asterisks indicate values significantly different  
1044 from the wild type, \*\*P value < 0.01, \*P value < 0.05, Student's t-test. Source data  
1045 and statistics are presented in *Figure 3 – source data 2*.

1046



1047 **Figure 4. Mitochondrial AOXs affect energy metabolism of *rcd1* and alter**  
1048 **response to chloroplastic ROS.** Source data and statistics are presented in *Figure 4–*  
1049 *source data 1*.

1050 (A) Expression of AOXs is induced in *rcd1*. Abundance of AOX isoforms in  
1051 mitochondrial preparations was assessed by immunoblotting with  $\alpha$ AOX antibody  
1052 that recognizes AOX1a, -b, -c, -d, and AOX2 isoforms. 100 % corresponds to 15  $\mu$ g  
1053 of mitochondrial protein.

1054 (B) Two mitochondrial respiratory pathways (red arrows) and sites of action of  
1055 mitochondrial inhibitors. KCN inhibits complex IV (cytochrome c oxidase).  
1056 Salicylhydroxamic acid (SHAM) inhibits AOX activity. Antimycin A (AA) and  
1057 myxothiazol (myx) block electron transfer through complex III (ubiquinol-cytochrome  
1058 c oxidoreductase), creating ROS-related mitochondrial retrograde signal.

1059 (C) AOX capacity is significantly increased in *rcd1*. Oxygen uptake by seedlings was  
1060 measured in the darkness in presence of KCN and SHAM. Addition of KCN blocked  
1061 respiration through complex IV, thus revealing the capacity of the alternative  
1062 respiratory pathway through AOXs. Data is presented as mean  $\pm$  SD, asterisks  
1063 denote selected values that are significantly different (P value < 0.001, one-way  
1064 ANOVA with Bonferroni post hoc correction). Each measurement was performed on  
1065 10-15 pooled seedlings and repeated at least three times.

1066 (D) Inhibitors of mitochondrial complex III increase plant tolerance to chloroplastic ROS.  
1067 Effect of pre-treatment with 2.5  $\mu$ M AA or 2.5  $\mu$ M myx on PSII inhibition (Fv/Fm) by  
1068 MV. For each experiment, leaf discs from at least four individual rosettes were used.  
1069 The experiment was performed four times with similar results. Mean  $\pm$  SD are  
1070 shown. Asterisks indicate selected treatments that are significantly different (P value  
1071 < 0.001, Bonferroni post hoc correction). AOX abundance in the leaf discs treated in  
1072 the same way was quantified by immunoblotting (*Figure 4– figure supplement 1*).

1073 (E) AOX inhibitor SHAM decreases plant tolerance to chloroplastic ROS. 1-hour pre-  
1074 treatment with 2 mM SHAM inhibited tolerance to 1  $\mu$ M MV both in Col-0 and *rcd1*  
1075 as measured by Fv/Fm. SHAM stock solution was prepared in DMSO, thus pure  
1076 DMSO was added in the SHAM-minus controls. For each experiment, leaf discs  
1077 from at least four individual rosettes were used. The experiment was performed four  
1078 times with similar results. Mean  $\pm$  SD are shown. Asterisks indicate significant

1079 difference in the treatments of the same genotype at the selected time points (P  
1080 value < 0.001, Bonferroni post hoc correction).

1081

1082 **Figure 5. Altered electron transfer between the organelles in *rcd1*.**

1083 (A) Leaf discs were pre-treated with 1  $\mu\text{M}$  MV or MV plus 2 mM SHAM for 1 hour in the  
1084 darkness. Then light was turned on ( $80 \mu\text{mol m}^{-2} \text{s}^{-1}$ ) and chlorophyll fluorescence  
1085 under light (Fs) was recorded by Imaging PAM. Application of the two chemicals  
1086 together caused Fs rise in *rcd1*, but not Col-0, suggesting increase in the reduction  
1087 state of the chloroplast ETC in *rcd1*. For analysis of photochemical quenching see  
1088 *Figure 5 – figure supplement 1*.

1089 (B) Malate levels are significantly decreased in Col-0 but not in *rcd1* after MV treatment  
1090 in light. Malate level was measured in extracts from Col-0 and *rcd1* seedlings that  
1091 were pre-treated overnight with 50  $\mu\text{M}$  MV or water control and collected either  
1092 dark-adapted or after exposure to 4 hours of light. Mean  $\pm$  SE are shown. Asterisks  
1093 indicate values significantly different from those in the similarly treated wild type,  
1094 \*\*\*P value  $< 0.001$ , \*\*P value  $< 0.01$ , Student's t-test). For statistics, see *Figure 5 –*  
1095 *source data 1*.

1096 (C) NADPH-MDH activity is increased in *rcd1*. To measure the activity of chloroplastic  
1097 NADPH-MDH, plants were grown at  $100\text{--}120 \mu\text{mol m}^{-2} \text{s}^{-1}$  at an 8-hour day  
1098 photoperiod, leaves were collected in the middle of the day and freeze-dried. The  
1099 extracts were prepared in the buffer supplemented with 250  $\mu\text{M}$  thiol-reducing agent  
1100 DTT, and initial activity was measured (top left). The samples were then incubated  
1101 for 2 hours in the presence of additional 150 mM DTT, and total activity was  
1102 measured (top right). The activation state of NADPH-MDH (bottom) is presented as  
1103 the ratio of the initial and the total activity. Mean  $\pm$  SE are shown. Asterisks indicate  
1104 values significantly different from the wild type, \*\*P value  $< 0.01$ , \*P value  $< 0.05$ ,  
1105 Student's t-test. For statistics, see *Figure 5 – source data 1*.

1106

1107 **Figure 6. RCD1 is involved in mitochondrial dysfunction, chloroplast ROS and**  
1108 **PAP signaling pathways.**

1109 (A) Regulation of *rcd1* mis-expressed genes under perturbations of organellar functions  
1110 in the selected subset of genes. A complete list of *rcd1*-misexpressed genes is  
1111 presented in *Figure 6 – figure supplement 1*. Similar transcriptomic changes are  
1112 observed between the genes differentially regulated in *rcd1* and the genes affected  
1113 by disturbed chloroplastic or mitochondrial functions. Mitochondrial dysfunction  
1114 stimulon (MDS) genes regulated by ANAC013/ ANAC017 transcription factors, are  
1115 labeled green.

1116 (B) Sulfotransferase SOT12 encoded by an MDS gene accumulated in *rcd1* under  
1117 standard growth conditions, as revealed by immunoblotting with the specific  
1118 antibody.

1119 (C) Phenotype of the *rcd1 sal1* double mutant under standard growth conditions (12-  
1120 hour photoperiod with white luminescent light of 220-250  $\mu\text{mol m}^{-2} \text{s}^{-1}$ ).

1121

1122 **Figure 7. RST domain of RCD1 binds to ANAC transcription factors and is**  
1123 **necessary for RCD1 function *in vivo*.** Source data and statistics are presented in  
1124 *Figure 7 – source data 4.*

1125 (A) Biochemical interaction of ANAC013 with the RST domain of RCD1 *in vitro*.  
1126 Superimposed  $^1\text{H}$ ,  $^{15}\text{N}$  HSQC spectra of the C-terminal domain of RCD1 acquired in  
1127 absence (blue) and presence (red) of approximately two-fold excess of the  
1128 ANAC013<sup>235-284</sup> peptide. Interaction of RCD1<sup>468-589</sup> with ANAC013<sup>235-284</sup> caused  
1129 peptide-induced chemical shift changes in the  $^1\text{H}$ ,  $^{15}\text{N}$  correlation spectrum of  
1130 RCD1, which were mapped on the structure of the RST domain (inset). Inset:  
1131 RST<sub>RCD1</sub> structure with highlighted residues demonstrating the largest chemical shift  
1132 perturbations ( $\Delta\delta \geq 0.10$  ppm) between the free and bound forms (details in *Figure*  
1133 *7 – figure supplement 3C*), which probably corresponds to ANAC013-interaction  
1134 site.

1135 (B) Stable expression in *rcd1* of the HA-tagged RCD1 variant lacking its C-terminus  
1136 under the control of the native *RCD1* promoter does not complement *rcd1*  
1137 phenotypes. In the independent complementation lines RCD1 $\Delta$ RST-HA was  
1138 expressed at the levels comparable to those in the RCD1-HA lines (upper panel).  
1139 However, in *rcd1*: RCD1 $\Delta$ RST-HA lines abundance of AOXs (middle panel) was  
1140 similar to that in *rcd1*.

1141 (C) Tolerance of PSII to chloroplastic ROS was similar in the *rcd1*: RCD1 $\Delta$ RST-HA lines  
1142 and *rcd1*. For each PSII inhibition experiment, leaf discs from at least four individual  
1143 rosettes were used. The experiment was performed three times with similar results.  
1144 Mean  $\pm$  SD are shown.

1145

1146 **Figure 8. Developmental, chloroplast- and mitochondria-related phenotypes of**  
1147 ***rcd1* are partially mediated by ANAC017.** Source data and statistics are presented in  
1148 *Figure 8 – source data 1.*

1149 (A) Introducing *anac017* mutation in the *rcd1* background partially suppressed the curly  
1150 leaf phenotype of *rcd1*.

1151 (B) The *anac017* mutation partially suppressed tolerance of *rcd1* to chloroplastic ROS.  
1152 PSII inhibition by ROS was measured in *rcd1 anac017* double mutant by using 0.25  
1153  $\mu\text{M}$  or 1  $\mu\text{M}$  MV (left and right panel, accordingly). For each experiment, leaf discs  
1154 from at least four individual rosettes were used. The experiment was performed  
1155 three times with similar results. Mean  $\pm$  SD are shown. Asterisks denote values  
1156 significantly different from those in the similarly treated wild type at the last time  
1157 point of the assay (P value < 0.001, two-way ANOVA with Bonferroni post hoc  
1158 correction).

1159 (C) The *anac017* mutation partially suppressed mitochondrial phenotypes of *rcd1*. Total  
1160 AOX protein levels were lowered in *rcd1 anac017* double mutant as compared to  
1161 *rcd1* both after the overnight treatment with 2.5  $\mu\text{M}$  AA and in the untreated control.

1162 (D) Oxygen uptake by *rcd1 anac017* seedlings was measured in the darkness in  
1163 presence of mitochondrial respiration inhibitors as described in *Figure 4C*. The *rcd1*  
1164 *anac017* mutant demonstrated lower KCN-insensitive AOX respiration capacity than  
1165 *rcd1*. Each measurement was performed on 10-15 pooled seedlings and repeated  
1166 at least three times. Mean  $\pm$  SD are shown. Asterisks denote selected values that  
1167 are significantly different (P value < 0.001, one-way ANOVA with Bonferroni post  
1168 hoc correction).

1169

1170 **Figure 9. Hypothetical role of RCD1 in organelle signaling and energy**  
1171 **metabolism.** RCD1 is the direct suppressor of ANAC transcription factors that is  
1172 itself subject to redox regulation. Chloroplastic ROS likely affect RCD1 protein redox  
1173 state and abundance. Inactivation of RCD1 leads to induction of ANAC-controlled  
1174 MDS regulon. Expression of MDS genes is possibly feedback-regulated *via* the PAP  
1175 retrograde signaling (purple). Resulting activation of mitochondrial AOXs and other  
1176 MDS components is likely to affect electron flows (red) and ROS signaling in  
1177 mitochondria and in chloroplasts. Putative competition of AOX-directed electron  
1178 transfer with the formation of ROS at PSI is labeled with an asterisk.  
1179

1180 **Table 1. Overview of the immunoprecipitation results.** Selected proteins identified in  
 1181 ANAC013-GFP and RCD1-3xVenus pull-down assays. Ratio vs. Col-0 and the P-  
 1182 value were obtained by Perseus statistical analysis from the three repeats for each  
 1183 genotype used. Bold text indicates baits. The peptide coverage for selected proteins  
 1184 as well as full lists of identified proteins are presented in *Figure 7 – source datas 1*  
 1185 *and 2*.

1186

| <b>ANAC013-GFP pull-down</b>  |                               |                 |                  |                |            |
|-------------------------------|-------------------------------|-----------------|------------------|----------------|------------|
| Ratio ANAC013 vs. Col-0       | P-value                       | unique peptides | gene             | name           | stickiness |
| <b>50966</b>                  | <b>7.09 x 10<sup>-7</sup></b> | <b>29</b>       | <b>AT1G32870</b> | <b>ANAC013</b> |            |
| <b>22149</b>                  | <b>3.41 x 10<sup>-8</sup></b> | <b>25</b>       |                  | <b>GFP</b>     |            |
| 10097                         | 3.67 x 10 <sup>-6</sup>       | 37              | AT1G32230        | RCD1           | 1.00 %     |
| 110                           | 1.67 x 10 <sup>-6</sup>       | 8               | AT2G35510        | SRO1           | 1.00 %     |
| 74                            | 1.09 x 10 <sup>-9</sup>       | 4               | AT1G34190        | ANAC017        | 1.00 %     |
|                               |                               |                 |                  |                |            |
| <b>RCD1-3xVenus pull-down</b> |                               |                 |                  |                |            |
| Ratio RCD1 vs. Col-0          | p-value                       | unique peptides | gene             | name           | stickiness |
| <b>7593</b>                   | <b>0.000454</b>               | <b>35</b>       | <b>AT1G32230</b> | <b>RCD1</b>    |            |
| <b>1292</b>                   | <b>0.006746</b>               | <b>10</b>       |                  | <b>YFP</b>     |            |
| 108                           | 5.48 x 10 <sup>-8</sup>       | 2               | AT1G34190        | ANAC017        | 1.00 %     |

1187

1188



1189 **Supplementary Information**

1190 **Figure 1 – source data 1. Source data and statistics.**

1191 **Figure 2 – source data 1. Source data and statistics.**

1192 **Figure 3 – source data 1. Metabolic analyses.**

1193 Distribution of radioactive label was analyzed after feeding plants with <sup>14</sup>C-labeled  
1194 glucose. Metabolic fluxes in light- and dark-adapted Col-0, *rcd1*, *rcd1 aox1a*, and *aox1a*  
1195 plants were deduced.

1196 **Figure 3 – source data 2. Source data and statistics.**

1197 **Figure 4 – source data 1. Source data and statistics.**

1198 **Figure 5 – source data 1. Source data and statistics.**

1199 **Figure 6 – source data 1. Source data and statistics.**

1200 **Figure 7 – source data 1. *In vivo* interaction partners of ANAC013.**

1201 From Arabidopsis line expressing ANAC013-GFP, ANAC013-GFP and associated  
1202 proteins were purified with αGFP antibody and identified by mass spectrometry.  
1203 Identified proteins (Perseus analysis, ANAC013) and mapped peptides (peptide IDs)  
1204 are shown.

1205 **Figure 7 – source data 2. *In vivo* interaction partners of RCD1.**

1206 From Arabidopsis line expressing RCD1-3xVenus, RCD1-3xVenus and associated  
1207 proteins were purified with αGFP antibody and identified by mass spectrometry.  
1208 Identified proteins (Perseus analysis, RCD1) and mapped peptides (peptide IDs) are  
1209 shown.

1210 **Figure 7 – source data 3. NMR constraints and structural statistics for the**  
1211 **ensemble of the 15 lowest-energy structures of RCD1 RST.**

1212 **Figure 7 – source data 4. Source data and statistics.**

1213 **Figure 8 – source data 1. Source data and statistics.**

1214 **Supplementary file 1. Primers used in the study.**

1215

1216 **Figure 1 – figure supplement 1. Inverse correlation of RCD1 abundance with**  
1217 **tolerance to chloroplastic ROS.**

1218 (A) Several independent *rcd1* complementation lines were generated in which HA-  
1219 tagged RCD1 was reintroduced under the *RCD1* native promoter. Immunoblotting of  
1220 protein extracts from these lines with  $\alpha$ HA antibody revealed different levels of  
1221 RCD1-HA under standard light-adapted growth conditions. This was presumably  
1222 due to different transgene insertion sites in the genome. Line “a” was described in  
1223 (*Jaspers et al., 2009*). Rubisco large subunit (RbcL) detected by amido black  
1224 staining is shown as a control for equal protein loading.

1225 (B) An antibody was raised against the full-size RCD1 protein. This allowed comparing  
1226 abundance of RCD1 in independent *rcd1*: RCD1-HA complementation lines  
1227 described in the panel (A) versus Col-0 (two *rcd1*: RCD1-HA lines with the lowest  
1228 and two with the higher levels of RCD1-HA are shown). In the complementation  
1229 lines the RCD1 signal was detected at higher molecular weight due to the triple HA  
1230 tag. The *rcd1*: RCD1 $\Delta$ 7Cys-HA line will be addressed below.

1231 (C) Expression of *RCD1* gene was measured by real time quantitative PCR in Col-0 and  
1232 in four independent complementation lines described in the panel (A), two with the  
1233 lowest and two with the higher levels of RCD1-HA. Results in panels (B) and (C)  
1234 demonstrated that the levels of RCD1 protein and mRNA were about 10 times  
1235 higher in the high-expressing complementation lines than in Col-0. Relative  
1236 expression was calculated from three biological repeats and the data is scaled  
1237 relative to Col-0. Source data is presented in *Figure 6 – source data 1*.

1238 (D) Sensitivity of PSII to chloroplastic ROS in the *rcd1* complementation lines was  
1239 assessed using time-resolved analysis described in *Figure 1 – figure supplement 2*.  
1240 For that, leaf discs were pre-treated with 0.25  $\mu$ M MV overnight in the darkness.  
1241 PSII photochemical yield after two 1-hour light cycles was plotted against  
1242 abundance of RCD1-HA in the individual lines as determined in panel (A). Line “a”  
1243 was described in (*Jaspers et al., 2009*). Five individual plants were taken per each  
1244 line. The experiment was repeated three times with similar results. Source data and  
1245 statistics are presented in *Figure 1 – source data 1*.

1246

1247 **Figure 1 – figure supplement 2. The Imaging PAM protocol developed to monitor**  
1248 **kinetics of PSII inhibition by repetitive 1-hour light cycles.** Plants dark-adapted  
1249 for at least 20 min were first exposed to a saturating light pulse to measure  $F_m$ .  
1250 Then the blue actinic light (450 nm,  $80 \mu\text{mol m}^{-2} \text{s}^{-1}$ ) was turned on for 1 hour, over  
1251 which time chlorophyll fluorescence under light ( $F_s$ ) was followed by measuring  
1252 flashes given once in 2 minutes. Then the actinic light was turned off to allow for 20-  
1253 min dark adaptation, after which  $F_o$  and  $F_m$  were measured. Following the  $F_m$   
1254 measurement, the next light cycle was initiated. Saturating light pulses to measure  
1255  $F_m$  are depicted by blue arrows, actinic light periods by blue boxes, and dark  
1256 adaptation by black boxes. PSII photochemical yield was calculated as  $F_v/F_m =$   
1257  $(F_m - F_o)/F_m$ . To study different levels of MV tolerance, different concentrations of  
1258 MV were employed throughout the study, as indicated in the figures or figure  
1259 legends.

1260 **Figure 1 – figure supplement 3. Production rate of hydrogen peroxide in Col-0 and**  
1261 ***rcd1* during illumination of MV-pre-treated rosettes.** Col-0 and *rcd1* rosettes  
1262 were pre-treated with  $1 \mu\text{M}$  MV overnight in the darkness. Then they were exposed  
1263 to light for indicated time. After this, the rosettes were infiltrated with DAB staining  
1264 solution and exposed to 20 minutes of light ( $180 \mu\text{mol m}^{-2} \text{s}^{-1}$ ). Similar initial  
1265 increase in  $\text{H}_2\text{O}_2$  production rate was observed in MV-pre-treated dark-adapted Col-  
1266 0 and *rcd1*. During longer incubation under light, the production rate of  $\text{H}_2\text{O}_2$  further  
1267 increased in Col-0, but decreased in *rcd1*. The experiment was performed three  
1268 times with similar results.

1269 **Figure 1 – figure supplement 4. Altered resistance of *rcd1* photosynthetic**  
1270 **apparatus to chloroplastic ROS.**

1271 (A) Protein extracts from Col-0 and *rcd1* leaves pre-treated with  $1 \mu\text{M}$  MV and exposed  
1272 to light for indicated time, were separated by SDS-PAGE followed by  
1273 immunoblotting with antibodies against the PSII subunit D1 and the PSI subunit  
1274 PsaB. No significant differences in stoichiometry of photosystems were detected.  
1275 (B) Thylakoid protein complexes isolated from leaves treated as above were separated  
1276 by native PAGE. Immunoblotting with  $\alpha\text{D1}$  antibody revealed PSII species of  
1277 diverse molecular weights that were annotated as in (Järvi *et al.*, 2011). The largest  
1278 of the complexes corresponds to PSII associated with its light-harvesting antennae

1279 complex (LHCII) while the smallest are the PSII monomers (top panel). Incubation  
 1280 under light in presence of MV led to destabilization of PSII-LHCII complexes in Col-  
 1281 0, but not in *rcd1*. At the same time, immunoblotting with  $\alpha$ PsaB antibody showed  
 1282 no changes in PSI complex (bottom panel).

1283 **Figure 1 – figure supplement 5. Components of photosynthetic electron transfer**  
 1284 **and chloroplast ROS scavenging; abundance and distribution of NAD<sup>+</sup>/ NADH**  
 1285 **and NADP<sup>+</sup>/ NADPH redox couples in Col-0 and *rcd1*.**

1286 (A) Abundance of proteins related to photosynthetic electron transfer or chloroplast  
 1287 ROS scavenging was assessed by separating Col-0 and *rcd1* protein extracts (in  
 1288 dilution series) by SDS-PAGE and immunoblotting with specific antibodies, as  
 1289 indicated. 100 % corresponds to 20  $\mu$ g of thylakoid protein. No difference was  
 1290 observed between Col-0 and *rcd1*.

1291 (B) Abundance of nucleotides NAD<sup>+</sup>, NADP<sup>+</sup>, NADH and NADPH in total leaf extracts  
 1292 isolated from Col-0 and *rcd1* (mean  $\pm$  SE). No difference was observed between the  
 1293 genotypes. Source data and statistics are presented in *Figure 1 – source data 1*.

1294 (C) Distribution of NAD<sup>+</sup>/ NADH and NADP<sup>+</sup>/ NADPH redox couples in various cellular  
 1295 compartments of Col-0 and *rcd1* was assessed by non-aqueous fractionation  
 1296 metabolomics (mean  $\pm$  SE, an asterisk indicates the value significantly different  
 1297 from that in the corresponding wild type, \*P value < 0.05, Student's t-test). In brief,  
 1298 the light-adapted rosettes were harvested in the middle of the light period, freeze-  
 1299 dried, homogenated and separated on non-aqueous density gradient, which allowed  
 1300 for enrichment in specific membrane compartments. No major difference was  
 1301 detected between Col-0 and *rcd1*. Note that the method does not allow for  
 1302 separation of apoplastic and vacuolar compartments or reliable definition of the  
 1303 mitochondria (*Fettke et al., 2005*). Source data and statistics are presented in  
 1304 *Figure 1 – source data 1*.

1305 **Figure 2 – figure supplement 1. Characterization of the *rcd1*: RCD1 $\Delta$ 7Cys-HA**  
 1306 **lines.**

1307 (A) Domain structure of RCD1 with the positions of cysteine residues shown with  
 1308 circles. Interdomain cysteines mutated in the RCD1 $\Delta$ 7Cys-HA lines (RCD1 $\Delta$ 7Cys =  
 1309 RCD1 C14A-C37A-C50A-C175A-C179A-C212A-C243A) are shown in yellow.

1310 (B) The *rcd1* complementation line expressing the RCD1 $\Delta$ 7Cys-HA variant under the  
 1311 control of the native *RCD1* promoter was treated with high light, MV or H<sub>2</sub>O<sub>2</sub> as

- 1312 described in *Figure 2*. In this line accumulation of high-molecular-weight RCD1  
 1313 aggregates observed in RCD1-HA line (*Figure 2B*) was largely abolished. Reduced  
 1314 (red) and oxidized (ox) forms of the protein are labeled. To ascertain that all HA-  
 1315 tagged protein including that forming high-molecular-weight aggregates has been  
 1316 detected by immunoblotting, the transfer to a membrane was performed using the  
 1317 entire SDS-PAGE gel including the stacking gel and the well pockets. The  
 1318 experiment was performed three times with similar results.
- 1319 (C) Independent single-insertion homozygous *rcd1* complementation lines expressing  
 1320 RCD1 $\Delta$ 7Cys-HA were compared to those expressing RCD1-HA as described in  
 1321 *Figure 1 – figure supplement 1D*. In all the tested lines, RCD1 $\Delta$ 7Cys-HA  
 1322 accumulated to higher amounts than the wild-type RCD1-HA as revealed by  
 1323 immunoblotting with  $\alpha$ HA antibody. MV tolerance of the RCD1 $\Delta$ 7Cys-HA lines was  
 1324 not different from that of the RCD1-HA lines or Col-0. Source data and statistics are  
 1325 presented in *Figure 2 – source data 1*.
- 1326 (D) Expression of RCD1-regulated genes was measured by real time quantitative PCR  
 1327 in Col-0, *rcd1*, two *rcd1*: RCD1-HA lines expressing high levels of RCD1-HA and  
 1328 two lines expressing RCD1 $\Delta$ 7Cys-HA. No difference in expression of the selected  
 1329 RCD1-regulated genes *AOX1a* (AT3G22370), *UPOX* (AT2G21640), or the stress-  
 1330 induced gene *ZAT12* (AT5G59820) was detected in the *rcd1*: RCD1 $\Delta$ 7Cys-HA line  
 1331 as compared to *rcd1*: RCD1-HA or Col-0. For MV treatment detached rosettes were  
 1332 soaked in 1  $\mu$ M MV overnight in the darkness and then exposed to 1 hour of white  
 1333 luminescent light of 220-250  $\mu$ mol m<sup>-2</sup> s<sup>-1</sup>. Note that inactivation of *RCD1* prevented  
 1334 induction of a general stress marker gene *ZAT12* in response to MV. Five rosettes  
 1335 were pooled together for each sample. The experiment was repeated twice with  
 1336 similar results. Source data and statistics are presented in *Figure 2 – source data 1*.

1337 **Figure 4 – figure supplement 1. Effect of mitochondrial complex III inhibitors on**  
 1338 **expression of AOXs in Col-0 and *rcd1*.**

- 1339 (A) Changes in AOX abundance after overnight pre-treatment of leaf discs with 2.5  $\mu$ M  
 1340 AA or 2.5  $\mu$ M myx (C – control treatment with no inhibitor). Notably, *rcd1 aox1a*  
 1341 double mutant accumulated AOXs other than AOX1a, including putative AOX1d  
 1342 (*Konert et al., 2015*) (labeled with asterisk).
- 1343 (B) Quantification of  $\alpha$ AOX immunoblotting signal after pre-treatment with 2.5  $\mu$ M AA or  
 1344 myx. To avoid saturation of  $\alpha$ AOX signal in *rcd1*, a dilution series of protein extracts

1345 was made. Quantification was performed using ImageJ. Mean  $\pm$  SD are shown,  
1346 asterisks denote selected values that are significantly different (P value < 0.001,  
1347 Bonferroni post hoc correction, for source data and statistics see *Figure 4 – source*  
1348 *data 1*).

1349 **Figure 4 – figure supplement 2. Effect of mitochondrial complex III inhibitors on**  
1350 **abundance and redox state of the RCD1 protein.**

1351 (A) Chemical induction of mitochondrial dysfunction signaling did not alter abundance of  
1352 the RCD1 protein. Leaf discs were treated with 2.5  $\mu$ M AA or 2.5  $\mu$ M myx overnight.  
1353 Then total protein extracts were isolated and separated in SDS-PAGE. Levels of  
1354 RCD1-HA and of AOXs were assessed by immunoblotting with the specific  
1355 antibodies as indicated.

1356 (B) Redox state of RCD1 protein was only very mildly altered by mitochondrial complex  
1357 III inhibitors or by MV in the darkness. Treatment with AA or myx was performed as  
1358 in panel (A). MV, D – leaf discs after overnight pre-treatment with 1  $\mu$ M MV in the  
1359 darkness; MV, L – leaf discs after overnight pre-treatment with MV followed by 30  
1360 min of illumination; H<sub>2</sub>O<sub>2</sub> – leaf discs after 30 min of incubation in presence of 100  
1361 mM H<sub>2</sub>O<sub>2</sub> under light. Reduced (red) and oxidized (ox) forms of the protein are  
1362 labelled.

1363 **Figure 4 – figure supplement 3. Specificity of inhibitor treatments.** All chlorophyll  
1364 fluorescence analyses are presented as mean  $\pm$  SD, for source data and statistics  
1365 see *Figure 4 – source data 1*.

1366 (A) Interaction of AA with cyclic electron flow through binding to chloroplastic protein  
1367 PGR5 (*Sugimoto et al., 2013*) is not the reason of AA-induced ROS tolerance.  
1368 Possible off-target effect of AA was assessed by using the *pgr5* mutant. Pre-  
1369 treatment with 2.5  $\mu$ M AA made both *pgr5* and its background wild type *gl1* equally  
1370 more tolerant to chloroplastic ROS. For each experiment leaf discs from at least  
1371 four individual rosettes were used. The experiment was performed three times with  
1372 similar results.

1373 (B) SHAM treatment results in only slight PSII inhibition both in Col-0 and *rcd1*. Fv/Fm  
1374 was monitored under light after 1-hour pre-treatment with 2 mM SHAM. No  
1375 significant difference was detected between Col-0 and *rcd1*. SHAM stock solution  
1376 was prepared in DMSO, thus pure DMSO was added in the SHAM-minus controls.

1377 For each experiment leaf discs from at least four individual rosettes were used. The  
 1378 experiment was performed three times with similar results.

1379 (C) PTOX, plastid terminal oxidase analogous to AOX, is not involved in the SHAM-  
 1380 induced decrease of ROS tolerance. To exclude possible involvement of PTOX in  
 1381 MV-induced PSII inhibition, green sectors of the *ptox* mutant leaves were treated  
 1382 with 2 mM SHAM, 1  $\mu$ M MV, or both chemicals together. *ptox* mutant was  
 1383 responsive to SHAM treatment similarly to Col-0. For each experiment leaf discs  
 1384 from at least four individual rosettes were used. The experiment was performed  
 1385 twice with similar results.

1386 **Figure 4 – figure supplement 4. Irrelevance of AOX1a isoform for MV tolerance.** All  
 1387 chlorophyll fluorescence analyses are presented as mean  $\pm$  SD, for source data and  
 1388 statistics see *Figure 4 – source data 1*.

1389 (A) Abundance of total AOX in the *AOX1a*-overexpressor line (*AOX1a*-OE) as assessed  
 1390 by immunoblotting was comparable to that in *rcd1* (m – molecular weight marker;  
 1391 AA – overnight treatment with 2.5  $\mu$ M AA).

1392 (B) Increased expression of AOX1a isoform is not sufficient to provide ROS tolerance.  
 1393 MV-induced PSII inhibition in the *AOX1a*-OE and *aox1a* lines was monitored by  
 1394 Fv/Fm. No significant difference was observed between *AOX1a*-OE and *aox1a* at  
 1395 any time point of the experiment.

1396 (C) AOX1a isoform is not necessary for chloroplastic ROS tolerance. MV-induced PSII  
 1397 inhibition in *rcd1 aox1a* double mutant was monitored by Fv/Fm. No significant  
 1398 difference was detected between *rcd1 aox1a* and *rcd1*.

1399 **Figure 5 – figure supplement 1. Alternations in chloroplast electron transfer**  
 1400 **induced by MV and SHAM.** During the first 20 minutes of light exposure, MV-pre-  
 1401 treated Col-0 and *rcd1* experienced transient decrease in PSII photochemical  
 1402 quenching (qP). Within the next hour, photosynthesis recovered in *rcd1* to the level  
 1403 observed in the non-treated control, while only very mild recovery was observed in  
 1404 Col-0. In *rcd1*, the recovery was significantly inhibited by co-application of SHAM  
 1405 together with MV. Leaf discs were pre-treated with MV and SHAM for 1 hour in the  
 1406 darkness. SHAM stock solution was prepared in DMSO, thus pure DMSO was  
 1407 added in the SHAM-minus controls. To calculate qP, Fs was recorded as in *Figure*  
 1408 *5A*; saturating pulses were introduced every 10 minutes to measure Fm'. Data is

1409 presented as mean  $\pm$  SD, for source data and statistics, see *Figure 5 – source data*  
 1410 *1*.

1411 **Figure 5 – figure supplement 2. Distribution of malate in subcellular**  
 1412 **compartments of Col-0 and *rcd1*.** Distribution of malate was assessed by non-  
 1413 aqueous fractionation metabolomics as described in *Figure 1 – figure supplement*  
 1414 *5C*. Mean values  $\pm$  SE are presented. For source data and statistics, see *Figure 5 –*  
 1415 *source data 1*.

1416 **Figure 6 – figure supplement 1. Clustering analysis of genes mis-regulated in**  
 1417 ***rcd1* (with cutoff of  $\log_{2}FC < 0.5$ ) in published gene expression data sets**  
 1418 **acquired after perturbations of chloroplasts or mitochondria.** Mitochondrial  
 1419 dysfunction stimulon (MDS) genes are labeled green. Enrichment of the ANAC013/  
 1420 ANAC017 *cis*-element CTTGNNNNNCA[AC]G (*De Clercq et al., 2013*) in promoter  
 1421 regions is shown by shaded boxes next to the gene names. Notably, MDS genes  
 1422 represent only a subclass of all genes whose expression is affected by RCD1. For  
 1423 example, a cluster of genes that have lower expression in both *rcd1* and *sal1*  
 1424 mutants and are mostly associated with defense against pathogens did not have  
 1425 enrichment of ANAC motif in their promoters. This is likely a consequence of  
 1426 interaction of RCD1 with about forty different transcription factors belonging to  
 1427 several families (*Jaspers et al., 2009*).

1428 **Figure 6 – figure supplement 2. Induction of MDS genes in *rcd1*, and *rcd1***  
 1429 **complementation lines.** To address the role of RCD1 in transcriptional response to  
 1430 AA, plant rosettes were sprayed with water solution of 50  $\mu$ M AA (or of DMSO as  
 1431 the control). This concentration of AA has been commonly used in the studies (*De*  
 1432 *Clercq et al., 2013; Ng et al., 2013a; Ng et al., 2013b; Ivanova et al., 2014*).  
 1433 However, in addition to mitochondria, AA is known to inhibit chloroplast cyclic  
 1434 electron flow (*Labs et al., 2016*). *In vivo*, this side effect is pronounced at a 20- $\mu$ M,  
 1435 but not at a 2- $\mu$ M AA concentration (*Watanabe et al., 2016*). After 3-hour incubation  
 1436 under growth light, relative expression of the selected MDS genes was measured  
 1437 by real time quantitative PCR. Similar induction of *AOX1a* or *ANAC013* was  
 1438 observed in *rcd1*, Col-0, *rcd1*: RCD1-HA, and *rcd1*: RCD1 $\Delta$ 7Cys-HA lines.  
 1439 Interestingly, induction of another tested MDS gene, *UPOX*, was suppressed in the  
 1440 *rcd1*: RCD1-HA lines expressing high levels of RCD1 and in the *rcd1*: RCD1 $\Delta$ 7Cys-



1441 HA lines (see *Figure 1 – figure supplement 1C* for the expression of *RCD1* in these  
 1442 lines). Analogous effect was observed for the MDS gene *At5G24640*, although with  
 1443 low statistical power (*Figure 6 - source data 1. Source data and statistics*).  
 1444 Suppressed MDS induction in the lines with high levels of *RCD1* was in line with the  
 1445 observation that *RCD1* abundance *in vivo* inversely correlated with different  
 1446 tolerance of plants to MV (*Figure 1 – figure supplement 1*). Four rosettes were  
 1447 pooled together for each sample. Relative expression was calculated from three  
 1448 biological repeats and the data was scaled relative to control Col-0. Asterisks  
 1449 indicate significant difference between the selected genotypes (\*\*P value < 0.01,  
 1450 Bonferroni post hoc correction). Source data and statistics are presented in *Figure 6*  
 1451 – *source data 1*.

1452 **Figure 6 – figure supplement 3. Tolerance of PSII to chloroplastic ROS in *sal1***  
 1453 **mutants.** MV-induced PSII inhibition was tested in 2.5-week rosettes. The single  
 1454 *sal1* mutant was more tolerant to MV than the wild type (left panel). The double *rcd1*  
 1455 *sal1* mutant was more tolerant to MV than *rcd1* (right panel). Note different  
 1456 concentrations of MV used in the two panels. For source data and statistics, see  
 1457 *Figure 6 – source data 1*.

1458 **Figure 7 – figure supplement 1. Biochemical interaction of RCD1 with ANAC013/  
 1459 ANAC017 transcription factors in human embryonic kidney (HEK293) cells.**

1460 HA-RCD1 was co-expressed with ANAC013-myc (A) or ANAC017-myc (B) (IP –  
 1461 eluate after immunoprecipitation).

1462 (A) Co-immunoprecipitation of HA-RCD1 with  $\alpha$ myc antibody (top) and of ANAC013-  
 1463 myc with  $\alpha$ HA antibody (bottom) indicated complex formation between HA-RCD1  
 1464 and ANAC013-myc.

1465 (B) Co-immunoprecipitation of HA-RCD1 with  $\alpha$ myc antibody (top) and of ANAC017-  
 1466 myc with  $\alpha$ HA antibody (bottom) indicated complex formation between HA-RCD1  
 1467 and ANAC017-myc.

1468 **Figure 7 – figure supplement 2. Structure of the RST domain of RCD1.** Structure of  
 1469 the C-terminal domain of RCD1 (residues G468-L589) was determined by NMR  
 1470 spectroscopy. The first 38 N-terminal and the last 20 C-terminal residues are devoid  
 1471 of any persistent structure, hence only the structure of the folded part (residues  
 1472 P506-P570) is shown. The ensemble of 15 lowest-energy structures is on the left

1473 and a ribbon representation of the lowest-energy structure is on the right. The  
 1474 folded part represented by the RST domain is entirely  $\alpha$ -helical and consists of four  
 1475  $\alpha$ -helices, F510-I517, E523-R537, R543-V554 and D556-L566. The structured  
 1476 region ends at position N568, which corresponds to the necessary C-terminal part  
 1477 for the interaction with transcription factors (*Jaspers et al., 2010b*). The structure of  
 1478 the beginning of the first helix is dispersed in the ensemble due to sparseness of  
 1479 distance restraints. This arises from several missing amide chemical shift  
 1480 assignments (*Tossavainen et al., 2017*) as well as the presence of four proline  
 1481 residues in this region (P503, P506, P509 and P511), which severely hindered  
 1482 distance restraint generation. The many conserved hydrophobic residues (*Jaspers*  
 1483 *et al., 2010a*), shown in stick representation, form the domain's hydrophobic core.  
 1484 Mutagenesis experiments identified hydrophobic residues L528/I529 and I563 as  
 1485 critical for RCD1 interaction with DREB2A (*Vainonen et al., 2012*). I529 and I563  
 1486 are constituents of the hydrophobic core, and substitution of these residues  
 1487 probably disrupts the core of the RST domain thus abolishing the interaction. The  
 1488 atomic coordinates and structural restraints for the C-terminal domain of RCD1<sup>468-</sup>  
 1489 <sup>589</sup> have been deposited in the Protein Data Bank with the accession code 5N9Q.

1490 **Figure 7 – figure supplement 3. Analysis of interaction of the ANAC013-derived**  
 1491 **peptides with the RST domain of RCD1.**

- 1492 (A) According to yeast two-hybrid data (*O'Shea et al., 2017*), ANAC013 residues 205-  
 1493 299 are responsible for interaction with RCD1. To narrow down the RCD1-  
 1494 interacting domain, three overlapping peptides ANAC013<sup>205-258</sup>, ANAC013<sup>235-284</sup>,  
 1495 ANAC013<sup>251-299</sup> were designed and tested for their binding to RCD1 by surface  
 1496 plasmon resonance.
- 1497 (B) Surface plasmon resonance interaction analysis of three ANAC013-derived peptides  
 1498 with the C-terminal domain of RCD1. The strongest binding was detected for  
 1499 ANAC013 peptide 235-284 (red in panel A), which was further used for the NMR  
 1500 titration experiment with the purified C-terminal domain of RCD1 (RCD1<sup>468-589</sup>).
- 1501 (C) Histogram depicting the changes in <sup>1</sup>H and <sup>15</sup>N chemical shifts in RCD1<sup>468-589</sup> upon  
 1502 addition of the ANAC013<sup>235-284</sup> peptide. Changes were quantified according to the  
 1503 “minimum chemical shift procedure”. That is, each peak in the free form spectrum  
 1504 was linked to the nearest peak in the bound form spectrum. An arbitrary value -  
 1505 0.005 ppm was assigned to residues for which no data could be retrieved. The

1506 largest changes ( $\Delta\delta \geq 0.10$  ppm) were found for residues located on one face of the  
1507 domain, formed by the first and last helices and loops between the first and the  
1508 second, and the third and the fourth helices. These residues probably representing  
1509 the peptide interaction site are highlighted on the RST<sub>RCD1</sub> structure in *Figure 7A*  
1510 *inset*. In addition, relatively large perturbations were observed throughout the RST  
1511 domain, and notably, in the unstructured C-terminal tail, which might originate from  
1512 a conformational rearrangement in the domain induced by ligand binding.

1513 **Figure 8 – figure supplement 1. Induction of MDS genes in *anac017* and *rcd1***  
1514 ***anac017* mutants.** Expression of the selected MDS genes was assessed in  
1515 rosettes 3 hours after spraying them with 50  $\mu$ M AA, as described in *Figure 6 –*  
1516 *figure supplement 2*. The *anac017* mutation strongly suppressed induction of MDS  
1517 genes in *rcd1* both under control conditions and after AA treatment. Relative  
1518 expression was calculated from three biological repeats and the data was scaled  
1519 relative to control Col-0. Source data is presented in *Figure 6 – source data 1*.

1520 **References**

- 1521 **Ahlfors R**, Lång S, Overmyer K, Jaspers P, Brosché M, Tauriainen A, Kollist H,  
 1522 Tuominen H, Belles-Boix E, Piippo M, Inzé D, Palva ET, Kangasjärvi J. 2004.  
 1523 Arabidopsis RADICAL-INDUCED CELL DEATH1 belongs to the WWE protein-protein  
 1524 interaction domain protein family and modulates abscisic acid, ethylene, and methyl  
 1525 jasmonate responses. *Plant Cell* **16**:1925-1937.
- 1526  
 1527 **Allahverdiyeva Y**, Suorsa M, Tikkanen M, Aro EM. 2015. Photoprotection of  
 1528 photosystems in fluctuating light intensities. *Journal of Experimental Botany* **66**:2427-  
 1529 2436.
- 1530  
 1531 **Ap Rees T**. 1978. Assessment of the contribution of metabolic pathways to plant  
 1532 respiration. *Metabolism and Respiration. A Comprehensive Treatise*. Edited by David  
 1533 D. Davies. Academic Press Inc. San Diego, 1-27.
- 1534  
 1535 **Arrivault S**, Guenther M, Florian A, Encke B, Feil R, Vosloh D, Lunn JE, Sulpice R,  
 1536 Fernie AR, Stitt M, Schulze WX. 2014. Dissecting the subcellular compartmentation of  
 1537 proteins and metabolites in Arabidopsis leaves using non-aqueous fractionation.  
 1538 *Molecular and Cellular Proteomics* **13**:2246-2259.
- 1539  
 1540 **Asada K**. 2006. Production and scavenging of reactive oxygen species in chloroplasts  
 1541 and their functions. *Plant Physiology* **141**:391-396.
- 1542  
 1543 **Awad J**, Stotz HU, Fekete A, Krischke M, Engert C, Havaux M, Berger S, Mueller MJ.  
 1544 2015. 2-cysteine peroxiredoxins and thylakoid ascorbate peroxidase create a water-  
 1545 water cycle that is essential to protect the photosynthetic apparatus under high light  
 1546 stress conditions. *Plant Physiology* **167**:1592-1603.
- 1547  
 1548 **Bailleul B**, Berne N, Murik O, Petroutsos D, Prihoda J, Tanaka A, Villanova V, Bligny R,  
 1549 Flori S, Falconet D, Krieger-Liszkay A, Santabarbara S, Rappaport F, Joliot P, Tirichine  
 1550 L, Falkowski PG, Cardol P, Bowler C, Finazzi G. 2015. Energetic coupling between  
 1551 plastids and mitochondria drives CO<sub>2</sub> assimilation in diatoms. *Nature* **524**:366-369.
- 1552  
 1553 **Belles-Boix E**, Babiychuk E, Van Montagu M, Inzé D, Kushnir S. 2000. CEO1, a new  
 1554 protein from *Arabidopsis thaliana*, protects yeast against oxidative damage. *FEBS*  
 1555 *Letters* **482**:19-24.
- 1556  
 1557 **Blanco NE**, Guinea-Diaz M, Whelan J, Strand, Å. 2014. Interaction between plastid and  
 1558 mitochondrial retrograde signalling pathways during changes to plastid redox status.  
 1559 *Philosophical Transactions of the Royal Society B* **369**:20130231.
- 1560  
 1561 **Brosché M**, Blomster T, Salojärvi J, Cui F, Sipari N, Leppälä J, Lamminmäki A, Tomai  
 1562 G, Narayanasamy S, Reddy RA, Keinänen M, Overmyer K, Kangasjärvi J. 2014.  
 1563 Transcriptomics and functional genomics of ROS-induced cell death regulation by  
 1564 *RADICAL-INDUCED CELL DEATH1*. *PLoS Genetics* **10**:e1004112.
- 1565  
 1566 **Bugge K**, Staby L, Kemplen KR, O'Shea C, Bendtsen SK, Jensen MK, Olsen JG,  
 1567 Skriver K, Kragelund BB. 2018. Structure of Radical-Induced Cell Death1 hub domain

- 1568 reveals a common  $\alpha$ -scaffold for disorder in transcriptional networks. *Structure* **26**:734-  
1569 746.
- 1570
- 1571 **Caplan JL**, Kumar AS, Park E, Padmanabhan MS, Hoban K, Modla S, Czymmek K,  
1572 Dinesh-Kumar SP. 2015. Chloroplast stromules function during innate immunity.  
1573 *Developmental Cell* **34**:45-57.
- 1574
- 1575 **Cardol P**, Alric J, Girard-Bascou J, Franck F, Wollman FA, Finazzi G. 2009. Impaired  
1576 respiration discloses the physiological significance of state transitions in  
1577 *Chlamydomonas*. *PNAS* **106**:15979-15984.
- 1578
- 1579 **Carrari F**, Baxter C, Usadel B, Urbanczyk-Wochniak E, Zanol MI, Nunes-Nesi A,  
1580 Nikiforova V, Centero D, Ratzka A, Pauly M, Sweetlove LJ, Fernie AR. 2006. Integrated  
1581 analysis of metabolite and transcript levels reveals the metabolic shifts that underlie  
1582 tomato fruit development and highlight regulatory aspects of metabolic network  
1583 behavior. *Plant Physiology* **142**:1380-1396.
- 1584
- 1585 **Case DA**, Cheatham III TE, Darden T, Gohlke H, Luo R, Merz JR KM, Onufriev A,  
1586 Simmerling C, Wang B, Woods RJ. 2005. The Amber biomolecular simulation  
1587 programs. *Journal of Computational Chemistry* **26**:1668-1688.
- 1588
- 1589 **Chan KX**, Mabbitt PD, Phua SY, Mueller JW, Nisar N, Gigolashvili T, Stroehrer E, Grassl  
1590 J, Arlt W, Estavillo GM, Jackson CJ, Pogson BJ. 2016. Sensing and signaling of  
1591 oxidative stress in chloroplasts by inactivation of the SAL1 phosphoadenosine  
1592 phosphatase. *PNAS* **113**:E4567-4576.
- 1593
- 1594 **Clifton R**, Millar AH, Whelan J. 2006. Alternative oxidases in Arabidopsis: A  
1595 comparative analysis of differential expression in the gene family provides new insights  
1596 into function of non-phosphorylating bypasses. *Biochimica et Biophysica Acta*  
1597 **1757**:730-741.
- 1598
- 1599 **Crisp PA**, Smith AB, Ganguly DR, Murray KD, Eichten SR, Millar AA, Pogson BJ. 2018.  
1600 RNA Polymerase II read-through promotes expression of neighboring genes in SAL1-  
1601 PAP-XRN retrograde signaling. *Plant Physiology* **178**:1614-1630.
- 1602
- 1603 **Cross JM**, von Korff M, Altmann T, Bartzetko L, Sulpice R, Gibon Y, Palacios N, Stitt M.  
1604 2006. Variation of enzyme activities and metabolite levels in 24 Arabidopsis accessions  
1605 growing in carbon-limited conditions. *Plant Physiology* **142**:1574-1588.
- 1606
- 1607 **Cui, F**, Brosché, M, Shapiguzov A, He, X-Q, Vainonen, JP, Leppälä, J, Trotta, A,  
1608 Kangasjärvi, S, Salojärvi, J, . Kangasjärvi J, Overmyer K. 2019. Interaction of methyl  
1609 viologen-induced chloroplast and mitochondrial signalling in *Arabidopsis*. *Free Radical*  
1610 *Biology and Medicine* doi: 10.1016/j.freeradbiomed.2019.02.006
- 1611
- 1612 **Cvetkovska M**, Alber NA, Vanlerberghe GC. 2013. The signaling role of a mitochondrial  
1613 superoxide burst during stress. *Plant Signaling and Behavior* **8**:e22749.
- 1614
- 1615 **Daudi A**, Cheng Z, O'Brien JA, Mammarella N, Khan S, Ausubel FM, Bolwell GP. 2012.  
1616 The apoplasmic oxidative burst peroxidase in *Arabidopsis* is a major component of  
1617 pattern-triggered immunity. *Plant Cell* **24**:275-287.

- 1618  
 1619 **De Clercq I**, Vermeirssen V, Van Aken O, Vandepoele K, Murcha MW, Law SR, Inzé A,  
 1620 Ng S, Ivanova A, Rombaut D, van de Cotte B, Jaspers P, Van de Peer Y, Kangasjärvi J,  
 1621 Whelan J, Van Breusegem F. 2013. The membrane-bound NAC transcription factor  
 1622 ANAC013 functions in mitochondrial retrograde regulation of the oxidative stress  
 1623 response in *Arabidopsis*. *Plant Cell* **25**:3472-3490.  
 1624
- 1625 **De Rybel B**, Möller B, Yoshida S, Grabowicz I, Barbier de Reuille P, Boeren S, Smith  
 1626 RS, Borst JW, Weijers D. 2013. A bHLH complex controls embryonic vascular tissue  
 1627 establishment and indeterminate growth in *Arabidopsis*. *Developmental Cell* **24**:426-  
 1628 437.  
 1629
- 1630 **de Souza A**, Wang JZ, Dehesh K. 2017. Retrograde signals: integrators of  
 1631 interorganellar communication and orchestrators of plant development. *Annual Review*  
 1632 *of Plant Biology* **68**:85-108.  
 1633
- 1634 **Dietz KJ**, Mittler R, Noctor G. 2016. Recent progress in understanding the role of  
 1635 reactive oxygen species in plant cell signaling. *Plant Physiology* **171**:1535-1539.  
 1636
- 1637 **Estavillo GM**, Crisp PA, Pornsiriwong W, Wirtz M, Collinge D, Carrie C, Giraud E,  
 1638 Whelan J, David P, Javot H, Brearley C, Hell R, Marin E, Pogson BJ. 2011. Evidence  
 1639 for a SAL1-PAP chloroplast retrograde pathway that functions in drought and high light  
 1640 signaling in *Arabidopsis*. *Plant Cell* **23**:3992-4012.  
 1641
- 1642 **Exposito-Rodriguez M**, Laissue PP, Yvon-Durocher G, Smirnoff N, Mullineaux PM.  
 1643 2017. Photosynthesis-dependent H<sub>2</sub>O<sub>2</sub> transfer from chloroplasts to nuclei provides a  
 1644 high-light signalling mechanism. *Nature Communications* **8**:49.  
 1645
- 1646 **Farrington JA**, Ebert M, Land EJ, Fletcher K. 1973. Bipyridylum quaternary salts and  
 1647 related compounds. V. Pulse radiolysis studies of the reaction of paraquat radical with  
 1648 oxygen. Implications for the mode of action of bipyridyl herbicides. *Biochimica et*  
 1649 *Biophysica Acta* **314**:372-381.  
 1650
- 1651 **Fernie AR**, Roscher A, Ratcliffe RG, Kruger NJ. 2001. Fructose 2,6-bisphosphate  
 1652 activates pyrophosphate: fructose-6-phosphate 1-phosphotransferase and increases  
 1653 triose phosphate to hexose phosphate cycling in heterotrophic cells. *Planta* **212**:250-  
 1654 263.  
 1655
- 1656 **Fettke J**, Eckermann N, Tiessen A, Geigenberger P, Steup M. 2005. Identification,  
 1657 subcellular localization and biochemical characterization of water-soluble heteroglycans  
 1658 (SHG) in leaves of *Arabidopsis thaliana* L.: distinct SHG reside in the cytosol and in the  
 1659 apoplast. *Plant Journal* **43**:568-585.  
 1660
- 1661 **Fu A**, Liu H, Yu F, Kambakam S, Luan S, Rodermeil S. 2012. Alternative Oxidases  
 1662 (AOX1a and AOX2) can functionally substitute for Plastid Terminal Oxidase in  
 1663 *Arabidopsis* chloroplasts. *Plant Cell* **24**:1579-1595.  
 1664
- 1665 **Fujibe T**, Saji H, Arakawa K, Yabe N, Takeuchi Y, Yamamoto KT. 2004. A methyl  
 1666 viologen-resistant mutant of *Arabidopsis*, which is allelic to ozone-sensitive *rcd1*, is  
 1667 tolerant to supplemental ultraviolet-B irradiation. *Plant Physiology* **134**:275-285.

- 1668  
1669 **Garmier M**, Carroll AJ, Delannoy E, Vallet C, Day DA, Small ID, Millar AH. 2008.  
1670 Complex I dysfunction redirects cellular and mitochondrial metabolism in Arabidopsis.  
1671 *Plant Physiology* **148**:1324-1341.  
1672
- 1673 **Geigenberger P**, Fernie AR, Gibon Y, Christ M, Stitt M. 2000. Metabolic activity  
1674 decreases as an adaptive response to low internal oxygen in growing potato tubers.  
1675 *Biological Chemistry* **381**:723-740.  
1676
- 1677 **Geigenberger P**, Reimholz R, Geiger M, Merlo L, Canale V Stitt, M. 1997. Regulation  
1678 of sucrose and starch metabolism in potato tubers in response to short-term water  
1679 deficit. *Planta* **201**:502-518.  
1680
- 1681 **Geisler DA**, Pöpke C, Obata T, Nunes-Nesi A, Matthes A, Schneitz K, Maximova E,  
1682 Araujo WL, Fernie AR, Persson S. 2012. Downregulation of the  $\delta$ -subunit reduces  
1683 mitochondrial ATP synthase levels, alters respiration, and restricts growth and  
1684 gametophyte development in *Arabidopsis*. *Plant Cell* **24**:2792-2811.  
1685
- 1686 **Gibon Y**, Blaesing OE, Hannemann J, Carillo P, Höhne M, Hendriks JH, Palacios N,  
1687 Cross J, Selbig J, Stitt M. 2004. A robot-based platform to measure multiple enzyme  
1688 activities in Arabidopsis using a set of cycling assays: comparison of changes of  
1689 enzyme activities and transcript levels during diurnal cycles and in prolonged darkness.  
1690 *Plant Cell* **16**:3304-3325.  
1691
- 1692 **Giraud E**, Van Aken O, Ho LH, Whelan J. 2009. The transcription factor ABI4 is a  
1693 regulator of mitochondrial retrograde expression of *ALTERNATIVE OXIDASE1a*. *Plant*  
1694 *Physiology* **150**:1286-1296.  
1695
- 1696 **González-Pérez S**, Gutiérrez J, García-García F, Osuna D, Dopazo J, Lorenzo Ó,  
1697 Revuelta JL, Arellano JB. 2011. Early transcriptional defense responses in Arabidopsis  
1698 cell suspension culture under high-light conditions. *Plant Physiology* **156**:1439-1456.  
1699
- 1700 **Gutiérrez J**, González-Pérez S, García-García F, Daly CT, Lorenzo Ó, Revuelta JL,  
1701 McCabe PF, Arellano, JB. 2014. Programmed cell death activated by Rose Bengal in  
1702 *Arabidopsis thaliana* cell suspension cultures requires functional chloroplasts. *Journal of*  
1703 *Experimental Botany* **65**:3081-3095.  
1704
- 1705 **Hawkes TR**. 2014. Mechanisms of resistance to paraquat in plants. *Pest Management*  
1706 *Science* **70**:1316-1323.  
1707
- 1708 **Heiber I**, Ströher E, Raatz B, Busse I, Kahmann U, Bevan MW, Dietz KJ, Baier M.  
1709 2007. The *redox imbalanced* mutants of Arabidopsis differentiate signaling pathways for  
1710 redox regulation of chloroplast antioxidant enzymes. *Plant Physiology* **143**:1774-1788.  
1711
- 1712 **Hiller K**, Hangebrauk J, Jager C, Spura J, Schreiber K, Schomburg D. 2009.  
1713 MetaboliteDetector: comprehensive analysis tool for targeted and nontargeted GC/MS  
1714 based metabolome analysis. *Analytical Chemistry* **81**:3429-3439.  
1715
- 1716 **Hiltscher H**, Rudnik R, Shaikhali J, Heiber I, Mellenthin M, Meirelles Duarte I, Schuster  
1717 G, Kahmann U, Baier M. 2014. The *radical induced cell death* protein 1 (RCD1)

- 1718 supports transcriptional activation of genes for chloroplast antioxidant enzymes.  
1719 *Frontiers in Plant Science* **5**:475.
- 1720
- 1721 **Huang S**, Van Aken O, Schwarzländer M, Belt K, Millar AH. 2016. The roles of  
1722 mitochondrial reactive oxygen species in cellular signaling and stress response in  
1723 plants. *Plant Physiology* **171**:1551-1559.
- 1724
- 1725 **Ivanova A**, Law SR, Narsai R, Duncan O, Lee JH, Zhang B, Van Aken O, Radomiljac  
1726 JD, van der Merwe M, Yi K, Whelan, J. 2014. A functional antagonistic relationship  
1727 between auxin and mitochondrial retrograde signaling regulates *Alternative Oxidase1a*  
1728 expression in Arabidopsis. *Plant Physiology* **165**:1233-1254.
- 1729
- 1730 **Järvi S**, Suorsa M, Paakkarinen V, Aro EM. 2011. Optimized native gel systems for  
1731 separation of thylakoid protein complexes: novel super- and mega-complexes.  
1732 *Biochemical Journal* **439**:207-214.
- 1733
- 1734 **Järvi S**, Suorsa M, Tadini L, Ivanauskaite A, Rantala S, Allahverdiyeva Y, Leister D, Aro  
1735 EM. 2016. Thylakoid-bound FtsH proteins facilitate proper biosynthesis of Photosystem  
1736 I. *Plant Physiology* **171**:1333-1343.
- 1737
- 1738 **Jaspers P**, Blomster T, Brosché M, Salojärvi J, Ahlfors R, Vainonen JP, Reddy RA,  
1739 Immink R, Angenent G, Turck F, Overmyer K, Kangasjärvi J. 2009. Unequally  
1740 redundant RCD1 and SRO1 mediate stress and developmental responses and interact  
1741 with transcription factors. *Plant Journal* **60**:268-279.
- 1742
- 1743 **Jaspers P**, Brosché M, Overmyer K, Kangasjärvi J. 2010. The transcription factor  
1744 interacting protein RCD1 contains a novel conserved domain. *Plant Signaling and*  
1745 *Behavior* **5**:78-80.
- 1746
- 1747 **Jaspers P**, Overmyer K, Wrzaczek M, Vainonen JP, Blomster T, Salojärvi J, Reddy RA,  
1748 Kangasjärvi J. 2010. The RST and PARP-like domain containing SRO protein family:  
1749 analysis of protein structure, function and conservation in land plants. *BMC Genomics*  
1750 **11**:170.
- 1751
- 1752 **Joo JH**, Wang S, Chen JG, Jones AM, Fedoroff NV. 2005. Different signaling and cell  
1753 death roles of heterotrimeric G protein  $\alpha$  and  $\beta$  subunits in the Arabidopsis oxidative  
1754 stress response to ozone. *Plant Cell* **17**:957-970.
- 1755
- 1756 **Kacprzak SM**, Mochizuki N, Naranjo B, Xu D, Leister D, Kleine T, Okamoto H, Terry  
1757 MJ. 2019. Plastid-to-nucleus retrograde signalling during chloroplast biogenesis does  
1758 not require ABL4. *Plant Physiology* **179**:18-23.
- 1759
- 1760 **Katiyar-Agarwal S**, Zhu J, Kim K, Agarwal M, Fu X, Huang A, Zhu J K. 2006. The  
1761 plasma membrane Na<sup>+</sup>/H<sup>+</sup> antiporter SOS1 interacts with RCD1 and functions in  
1762 oxidative stress tolerance in *Arabidopsis*. *PNAS* **103**:18816-18821.
- 1763
- 1764 **Keech O**, Dizengremel P, Gardeström P. 2005. Preparation of leaf mitochondria from  
1765 *Arabidopsis thaliana*. *Physiologia Plantarum* **124**:403-409.
- 1766



- 1767 **Kinkema M**, Fan W, Dong X. 2000. Nuclear localization of NPR1 is required for  
1768 activation of *PR* gene expression. *Plant Cell* **12**:2339-2350.  
1769
- 1770 **Klein M**, Papenbrock J. 2004. The multi-protein family of *Arabidopsis*  
1771 sulphotransferases and their relatives in other plant species. *Journal of Experimental*  
1772 *Botany* **55**:1809-1820.  
1773
- 1774 **Kleine T**, Kindgren P, Benedict C, Hendrickson L, Strand Å. 2007. Genome-wide gene  
1775 expression analysis reveals a critical role for CRYPTOCHROME1 in the response of  
1776 *Arabidopsis* to high irradiance. *Plant Physiology* **144**:1391-1406.  
1777
- 1778 **Konert G**, Trotta A, Kouvonon P, Rahikainen M, Durian G, Blokhina O, Fagerstedt K,  
1779 Muth D, Corthals GL, Kangasjärvi S. 2015. Protein phosphatase 2A (PP2A) regulatory  
1780 subunit B'γ interacts with cytoplasmic ACONITASE 3 and modulates the abundance of  
1781 AOX1A and AOX1D in *Arabidopsis thaliana*. *New Phytologist* **205**:1250-1263.  
1782
- 1783 **König J**, Baier M, Horling F, Kahmann U, Harris G, Schürmann P, Dietz, KJ. 2002. The  
1784 plant-specific function of 2-Cys peroxiredoxin-mediated detoxification of peroxides in the  
1785 redox-hierarchy of photosynthetic electron flux. *PNAS* **99**:5738-5743.  
1786
- 1787 **Koussevitzky, S., Nott, A., Mockler, T.C., Hong, F., Sabetto-Martins, G., Surpin,**  
1788 **M., Lim, J., Mittler, R., and Chory, J.** 2007. Signals from chloroplasts converge to  
1789 regulate nuclear gene expression. *Science* **316**:715-719.  
1790
- 1791 **Kragelund BB**, Jensen MK, Skriver K. 2012. Order by disorder in plant signaling.  
1792 *Trends in Plant Science* **17**:625-632.  
1793
- 1794 **Krueger S**, Giavalisco P, Krall L, Steinhauser MC, Büssis D, Usadel B, Flügge UI,  
1795 Fernie AR, Willmitzer L, and Steinhauser D. 2011. A topological map of the  
1796 compartmentalized *Arabidopsis thaliana* leaf metabolome. *PLoS One* **6**:e17806.  
1797
- 1798 **Krueger S**, Steinhauser D, Lisec J, Giavalisco P. 2014. Analysis of subcellular  
1799 metabolite distributions within *Arabidopsis thaliana* leaf tissue: a primer for subcellular  
1800 metabolomics. *Methods in Molecular Biology* **1062**:575-596.  
1801
- 1802 **Labs M**, Rühle T, Leister D. 2016. The antimycin A-sensitive pathway of cyclic electron  
1803 flow: from 1963 to 2015. *Photosynthesis Research* **129**:231-238.  
1804
- 1805 **Laemmli UK**. 1970. Cleavage of structural proteins during the assembly of the head of  
1806 bacteriophage T4. *Nature* **227**:680-685.  
1807
- 1808 **Leister D**. 2017. Piecing the puzzle together: the central role of reactive oxygen species  
1809 and redox hubs in chloroplast retrograde signaling. *Antioxidants and Redox Signaling*  
1810 doi: 10.1089/ars.2017.7392.  
1811
- 1812 **Leister D**, Kleine T. 2016. Definition of a core module for the nuclear retrograde  
1813 response to altered organellar gene expression identifies GLK overexpressors as *gun*  
1814 mutants. *Physiologia Plantarum* **157**:297-309.  
1815

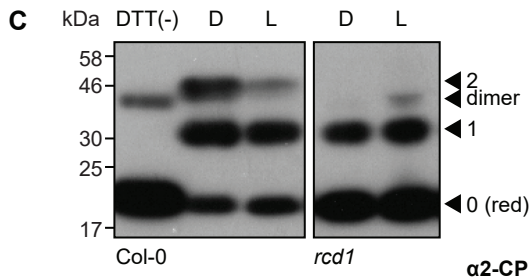
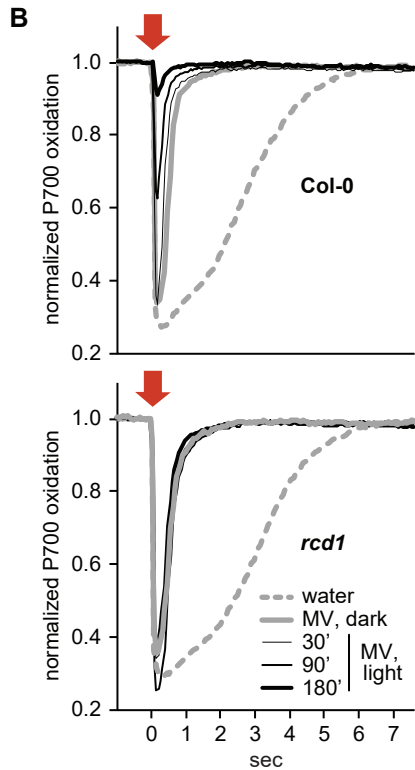
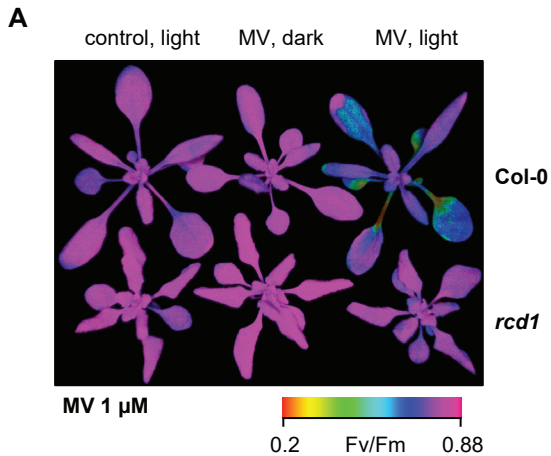
- 1816 **Leister D**, Romani I, Mittermayr L, Paieri F, Fenino E, Kleine T. 2014. Identification of  
1817 target genes and transcription factors implicated in translation-dependent retrograde  
1818 signaling in *Arabidopsis*. *Molecular Plant* **7**:1228-1247.  
1819
- 1820 **Liebthal M**, Maynard D, Dietz KJ. 2018. Peroxiredoxins and redox signaling in plants.  
1821 *Antioxidants and Redox Signaling*. **28**:609-624.  
1822
- 1823 **Lopez-Mendez B**, Guntert P. 2006. Automated protein structure determination from  
1824 NMR spectra. *Journal of the American Chemical Society* **128**:13112-13122.  
1825
- 1826 **Lowry OH**, Rosebrough NJ, Farr AL, Randall RJ. 1951. Protein measurement with the  
1827 folin phenol reagent. *Journal of Biological Chemistry* **193**:265-275.  
1828
- 1829 **Meyer EH**, Tomaz T, Carroll AJ, Estavillo G, Delannoy E, Tanz SK, Small ID, Pogson  
1830 BJ, Millar AH. 2009. Remodeled respiration in *ndufs4* with low phosphorylation  
1831 efficiency suppresses *Arabidopsis* germination and growth and alters control of  
1832 metabolism at night. *Plant Physiology* **151**, 603-619.  
1833
- 1834 **Møller IM**, Kristensen BK. 2004. Protein oxidation in plant mitochondria as a stress  
1835 indicator. *Photochemical and Photobiological Sciences* **3**:730-735.  
1836
- 1837 **Mou Z**, Fan W, Dong X. 2003. Inducers of plant systemic acquired resistance regulate  
1838 NPR1 function through redox changes. *Cell* **113**:935-944.  
1839
- 1840 **Mullineaux PM**, Exposito-Rodriguez M, Laissue PP, Smirnoff N. 2018. ROS-dependent  
1841 signalling pathways in plants and algae exposed to high light: Comparisons with other  
1842 eukaryotes. *Free Radical Biology and Medicine* **122**:52-64.  
1843
- 1844 **Munekage Y**, Hojo M, Meurer J, Endo T, Tasaka M, Shikanai T. 2002. PGR5 is  
1845 involved in cyclic electron flow around Photosystem I and is essential for  
1846 photoprotection in *Arabidopsis*. *Cell* **110**:361-371.  
1847
- 1848 **Ng S**, De Clercq I, Van Aken O, Law SR, Ivanova A, Willems P, Giraud E, Van  
1849 Breusegem F, Whelan, J. 2014. Anterograde and retrograde regulation of nuclear  
1850 genes encoding mitochondrial proteins during growth, development, and stress.  
1851 *Molecular Plant* **7**:1075-1093.  
1852
- 1853 **Ng S**, Giraud E, Duncan O, Law SR, Wang Y, Xu L, Narsai R, Carrie C, Walker H, Day  
1854 DA, Blanco NE, Strand Å, Whelan J, Ivanova A. 2013. Cyclin-dependent kinase E1  
1855 (CDKE1) provides a cellular switch in plants between growth and stress responses.  
1856 *Journal of Biological Chemistry* **288**:3449-3459.  
1857
- 1858 **Ng S**, Ivanova A, Duncan O, Law SR, Van Aken O, De Clercq I, Wang Y, Carrie C, Xu  
1859 L, Kmiec B, Walker H, Van Breusegem F, Whelan J, Giraud E. 2013. A membrane-  
1860 bound NAC transcription factor, ANAC017, mediates mitochondrial retrograde signaling  
1861 in *Arabidopsis*. *Plant Cell* **25**:3450-3471.  
1862
- 1863 **Nietzel T**, Mostertz J, Hochgrafe F, Schwarzländer M. 2017. Redox regulation of  
1864 mitochondrial proteins and proteomes by cysteine thiol switches. *Mitochondrion* **33**:72-  
1865 83.

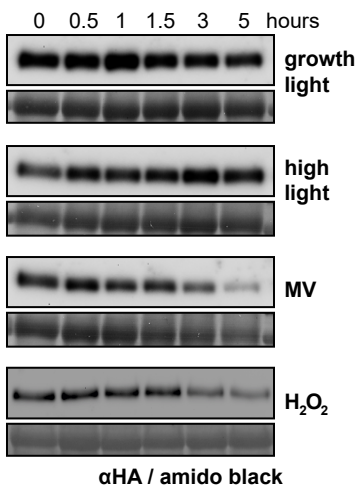
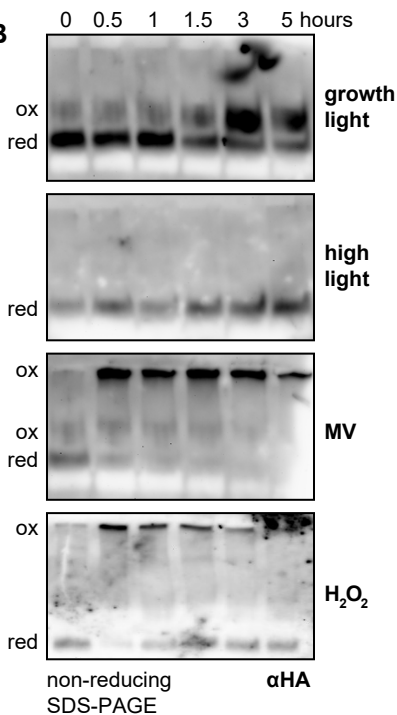
- 1866  
1867 **Nikkanen L**, Toivola J, Rintamäki E. 2016. Crosstalk between chloroplast thioredoxin  
1868 systems in regulation of photosynthesis. *Plant, Cell and Environment* **39**:1691-1705.  
1869
- 1870 **Nishiyama Y**, Allakhverdiev SI, Murata N. 2011. Protein synthesis is the primary target  
1871 of reactive oxygen species in the photoinhibition of photosystem II. *Physiologia*  
1872 *Plantarum* **142**:35-46.  
1873
- 1874 **Noctor G**, Reichheld JP, Foyer CH. 2017. ROS-related redox regulation and signaling  
1875 in plants. *Seminars in Cell & Developmental Biology* **80**:3-12.  
1876
- 1877 **Noguchi K**, Yoshida K. 2008. Interaction between photosynthesis and respiration in  
1878 illuminated leaves. *Mitochondrion* **8**:87-99.  
1879
- 1880 **O'Shea C**, Staby L, Bendtsen SK, Tidemand FG, Redsted A, Willemoës M, Kragelund  
1881 BB, Skriver K. 2017. Structures and short linear motif of disordered transcription factor  
1882 regions provide clues to the interactome of the cellular hub protein Radical-induced Cell  
1883 Death1. *Journal of Biological Chemistry* **292**:512-527.  
1884
- 1885 **Obata T**, Rosado-Souza L, Fernie AR. 2017. Coupling radiotracer experiments with  
1886 chemical fractionation for the estimation of respiratory fluxes. *Methods in Molecular*  
1887 *Biology* **1670**:17-30.  
1888
- 1889 **Ojeda V**, Pérez-Ruiz JM, Cejudo FJ. 2018. 2-Cys Peroxiredoxins participate in the  
1890 oxidation of chloroplast enzymes in the dark. *Molecular Plant* **11**:1377-1388.  
1891
- 1892 **Overmyer K**, Tuominen H, Kettunen R, Betz C, Langebartels C, Sandermann Jr H,  
1893 Kangasjärvi J. 2000. Ozone-sensitive Arabidopsis *rcd1* mutant reveals opposite roles  
1894 for ethylene and jasmonate signaling pathways in regulating superoxide-dependent cell  
1895 death. *Plant Cell* **12**:1849-1862.  
1896
- 1897 **Oxborough K**, Baker NR. 1997. Resolving chlorophyll a fluorescence images of  
1898 photosynthetic efficiency into photochemical and non-photochemical components -  
1899 calculation of  $qP$  and  $Fv'/Fm'$  without measuring  $Fo'$ . *Photosynthesis Research*  
1900 **54**:135-142.  
1901
- 1902 **Peltier JB**, Cai Y, Sun Q, Zabrouskov V, Giacomelli L, Rudella A, Ytterberg AJ,  
1903 Rutschow H, van Wijk KJ. 2006. The oligomeric stromal proteome of *Arabidopsis*  
1904 *thaliana* chloroplasts. *Molecular and Cellular Proteomics* **5**:114-133.  
1905
- 1906 **Petrov V**, Hille J, Mueller-Roeber B, Gechev TS. 2015. ROS-mediated abiotic stress-  
1907 induced programmed cell death in plants. *Frontiers in Plant Science* **6**:69.  
1908
- 1909 **Porra RJ**, Thompson WA, Kriedemann PE. 1989. Determination of accurate extinction  
1910 coefficients and simultaneous-equations for assaying chlorophyll-A and chlorophyll-B  
1911 extracted with 4 different solvents - verification of the concentration of chlorophyll  
1912 standards by atomic-absorption spectroscopy. *Biochimica et Biophysica Acta* **975**:384-  
1913 394.  
1914

- 1915 **Quintero FJ**, Garcíadeblás B, Rodríguez-Navarro A. 1996. The *SAL1* gene of  
1916 *Arabidopsis*, encoding an enzyme with 3'(2'),5'-bisphosphate nucleotidase and inositol  
1917 polyphosphate 1-phosphatase activities, increases salt tolerance in yeast. *Plant Cell*  
1918 **8**:529-537.
- 1919  
1920 **Roessner U**, Wagner C, Kopka J, Trethewey RN, Willmitzer L. 2000. Technical  
1921 advance: simultaneous analysis of metabolites in potato tuber by gas chromatography-  
1922 mass spectrometry. *Plant Journal* **23**:131-142.
- 1923  
1924 **Scheibe R**. 2004. Malate valves to balance cellular energy supply. *Physiologia*  
1925 *Plantarum* **120**:21-26.
- 1926  
1927 **Schwarzländer M**, Fricker MD, Sweetlove, LJ. 2009. Monitoring the *in vivo* redox state  
1928 of plant mitochondria: effect of respiratory inhibitors, abiotic stress and assessment of  
1929 recovery from oxidative challenge. *Biochimica et Biophysica Acta* **1787**:468-475.
- 1930  
1931 **Shapiguzov A**, Vainonen JP, Wrzaczek M, Kangasjärvi J. 2012. ROS-talk - how the  
1932 apoplast, the chloroplast, and the nucleus get the message through. *Frontiers in Plant*  
1933 *Science* **3**:292.
- 1934  
1935 **Sharma R**, Priya P, Jain M. 2013. Modified expression of an auxin-responsive rice CC-  
1936 type glutaredoxin gene affects multiple abiotic stress responses. *Planta* **238**:871-884.
- 1937  
1938 **Shedge V**, Davila J, Arrieta-Montiel MP, Mohammed S, Mackenzie SA. 2010. Extensive  
1939 rearrangement of the *Arabidopsis* mitochondrial genome elicits cellular conditions for  
1940 thermotolerance. *Plant Physiology* **152**:1960-1970.
- 1941  
1942 **Siligato R**, Wang X, Yadav SR, Lehesranta S, Ma G, Ursache R, Sevilem I, Zhang J,  
1943 Gorte M, Prasad K, Wrzaczek M, Heidstra R, Murphy A, Scheres B, Mähönen AP.  
1944 2016. Multisite Gateway-compatible cell type-specific gene-inducible system for plants.  
1945 *Plant Physiology* **170**:627-641.
- 1946  
1947 **Sowden RG**, Watson SJ, Jarvis P. 2017. The role of chloroplasts in plant pathology.  
1948 *Essays in Biochemistry* **62**:21-39.
- 1949  
1950 **Sugimoto K**, Okegawa Y, Tohri A, Long TA, Covert SF, Hisabori T, Shikanai T. 2013. A  
1951 single amino acid alteration in PGR5 confers resistance to antimycin A in cyclic electron  
1952 transport around PSI. *Plant and Cell Physiology* **54**:1525-1534.
- 1953  
1954 **Tiwari A**, Mamedov F, Grieco M, Suorsa M, Jajoo A, Styring S, Tikkanen M, Aro EM.  
1955 2016. Photodamage of iron-sulphur clusters in photosystem I induces non-  
1956 photochemical energy dissipation. *Nature Plants* **2**:16035.
- 1957  
1958 **Tossavainen H**, Hellman M, Vainonen JP, Kangasjärvi J, Permi P. 2017. <sup>1</sup>H, <sup>13</sup>C and  
1959 <sup>15</sup>N NMR chemical shift assignments of *A. thaliana* RCD1 RST. *Biomolecular NMR*  
1960 *Assignments* **11**:207-210.
- 1961  
1962 **Trotta A**, Rahikainen M, Konert G, Finazzi G, Kangasjärvi S. 2014. Signalling crosstalk  
1963 in light stress and immune reactions in plants. *Philosophical Transactions of the Royal*  
1964 *Society B* **369**:20130235.

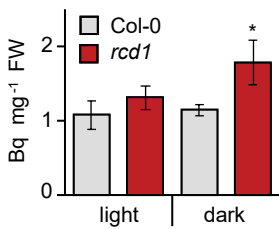
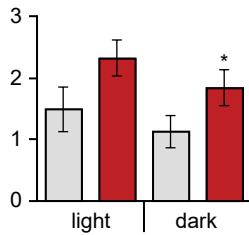
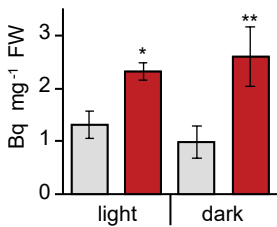
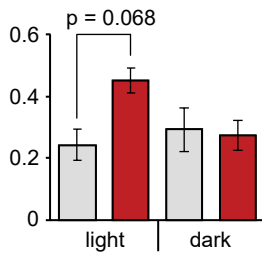
- 1965  
 1966 **Umbach AL**, Fiorani F, Siedow JN. 2005. Characterization of transformed Arabidopsis  
 1967 with altered alternative oxidase levels and analysis of effects on reactive oxygen  
 1968 species in tissue. *Plant Physiology* **139**:1806-1820.  
 1969  
 1970 **Vainonen JP**, Jaspers P, Wrzaczek M, Lamminmäki A, Reddy RA, Vaahtera L,  
 1971 Brosché M, Kangasjärvi J. 2012. RCD1-DREB2A interaction in leaf senescence and  
 1972 stress responses in *Arabidopsis thaliana*. *Biochemical Journal* **442**:573-581.  
 1973  
 1974 **Vainonen JP**, Kangasjärvi J. 2015. Plant signalling in acute ozone exposure. *Plant, Cell*  
 1975 *and Environment* **38**:240-252.  
 1976  
 1977 **Van Aken O**, De Clercq I, Ivanova A, Law SR, Van Breusegem F, Millar AH, Whelan J.  
 1978 2016a. Mitochondrial and chloroplast stress responses are modulated in distinct touch  
 1979 and chemical inhibition phases. *Plant Physiology* **171**:2150-2165.  
 1980  
 1981 **Van Aken O**, Ford E, Lister R, Huang S, Millar AH. 2016b. Retrograde signalling  
 1982 caused by heritable mitochondrial dysfunction is partially mediated by ANAC017 and  
 1983 improves plant performance. *Plant Journal* **88**:542-558.  
 1984  
 1985 **Van Aken O**, Pogson BJ. 2017. Convergence of mitochondrial and chloroplastic  
 1986 ANAC017/PAP-dependent retrograde signalling pathways and suppression of  
 1987 programmed cell death. *Cell Death and Differentiation* **24**:955-960  
 1988  
 1989 **Van Aken O**, Zhang B, Law S, Narsai R, Whelan J. 2013. AtWRKY40 and AtWRKY63  
 1990 modulate the expression of stress-responsive nuclear genes encoding mitochondrial  
 1991 and chloroplast proteins. *Plant Physiology* **162**:254-271.  
 1992  
 1993 **van Leeuwen LAG**, Hinchey EC, Murphy MP, Robb EL, Cochemé HM. 2017. Click-  
 1994 PEGylation - A mobility shift approach to assess the redox state of cysteines in  
 1995 candidate proteins. *Free Radical Biology and Medicine* **108**:374-382.  
 1996  
 1997 **Vaseghi MJ**, Chibani K, Telman W, Liebthal MF, Gerken M, Schnitzer H, Müller SM,  
 1998 Dietz KJ. 2018. The chloroplast 2-cysteine peroxiredoxin functions as thioredoxin  
 1999 oxidase in redox regulation of chloroplast metabolism. *Elife* **7**:e38194 doi:  
 2000 10.7554/eLife.38194.  
 2001  
 2002 **Wang Y**, Berkowitz O, Selinski J, Xu Y, Hartmann A, Whelan J. 2018. Stress  
 2003 responsive mitochondrial proteins in *Arabidopsis thaliana*. *Free Radical Biology and*  
 2004 *Medicine* **122**:28-39.  
 2005  
 2006 **Waszczak C**, Carmody M, Kangasjärvi J. 2018. Reactive oxygen species in plant  
 2007 signaling. *Annual Review of Plant Biology* **69**:209-236.  
 2008  
 2009 **Watanabe CK**, Yamori W, Takahashi S, Terashima I, Noguchi K. 2016. Mitochondrial  
 2010 alternative pathway-associated photoprotection of Photosystem II is related to the  
 2011 photorespiratory pathway. *Plant and Cell Physiology* **57**:1426-1431.  
 2012

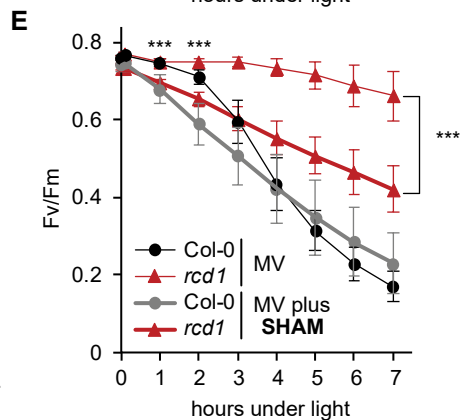
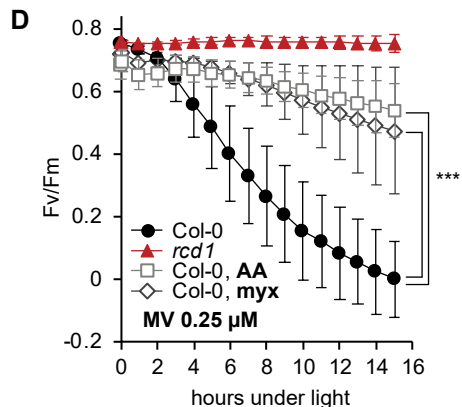
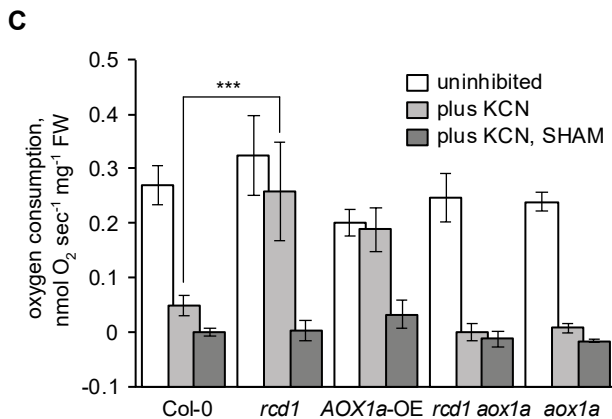
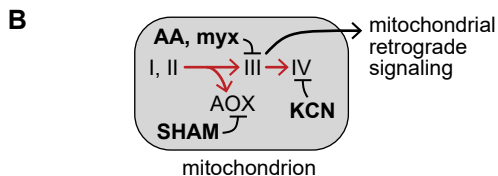
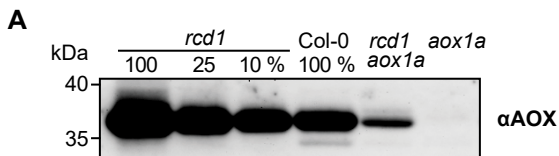
- 2013 **Wendrich JR**, Boeren S, Möller BK, Weijers D, De Rybel B. 2017. In vivo identification  
 2014 of plant protein complexes using IP-MS/MS. *Methods in Molecular Biology* **1497**:147-  
 2015 158.
- 2016
- 2017 **Wetzel CM**, Jiang CZ, Meehan LJ, Voytas DF, Rodermel SR. 1994. Nuclear—organelle  
 2018 interactions: the *immutans* variegation mutant of *Arabidopsis* is plastid autonomous and  
 2019 impaired in carotenoid biosynthesis. *Plant Journal* **6**:161-175.
- 2020
- 2021 **Wilson PB**, Estavillo GM, Field KJ, Pornsiriwong W, Carroll AJ, Howell KA, Woo NS,  
 2022 Lake JA, Smith SM, Millar HA, von Caemmerer S, Pogson BJ. 2009. The  
 2023 nucleotidase/phosphatase SAL1 is a negative regulator of drought tolerance in  
 2024 *Arabidopsis*. *Plant Journal* **58**:299-317.
- 2025
- 2026 **Wirthmueller L**, Asai S, Rallapalli G, Sklenar J, Fabro G, Kim DS, Lintermann R,  
 2027 Jaspers P, Wrzaczek M, Kangasjärvi J, MacLean D, Menke FLH, Banfield MJ, Jones  
 2028 JDG. 2018. *Arabidopsis* downy mildew effector HaRxL106 suppresses plant immunity  
 2029 by binding to RADICAL-INDUCED CELL DEATH1. *New Phytologist* **220**:232-248.
- 2030
- 2031 **Withers J**, Dong X. 2016. Posttranslational modifications of NPR1: a single protein  
 2032 playing multiple roles in plant immunity and physiology. *PLoS Pathogens* **12**:e1005707.
- 2033
- 2034 **Wrzaczek M**, Brosché M, Salojärvi J, Kangasjärvi S, Idänheimo N, Mersmann S,  
 2035 Robatzek S, Karpiński S, Karpińska B, Kangasjärvi J. 2010. Transcriptional regulation of  
 2036 the CRK/DUF26 group of receptor-like protein kinases by ozone and plant hormones in  
 2037 *Arabidopsis*. *BMC Plant Biology* **10**:95.
- 2038
- 2039 **Wu J**, Sun Y, Zhao Y, Zhang J, Luo L, Li M, Wang J, Yu H, Liu G, Yang L, Xiong G,  
 2040 Zhou J M, Zuo J, Wang Y, Li J. 2015. Deficient plastidic fatty acid synthesis triggers cell  
 2041 death by modulating mitochondrial reactive oxygen species. *Cell Research* **25**:621-633.
- 2042
- 2043 **Yoshida K**, Hara A, Sugiura K, Fukaya Y, Hisabori T. 2018. Thioredoxin-like2/2-Cys  
 2044 peroxiredoxin redox cascade supports oxidative thiol modulation in chloroplasts. *PNAS*  
 2045 **115**:E8296-E8304.
- 2046
- 2047 **Zhao Y**, Luo L, Xu J, Xin P, Guo H, Wu J, Bai L, Wang G, Chu J, Zuo J, Yu H, Huang X,  
 2048 Li J. 2018. Malate transported from chloroplast to mitochondrion triggers production of  
 2049 ROS and PCD in *Arabidopsis thaliana*. *Cell Research* **28**:448-461.

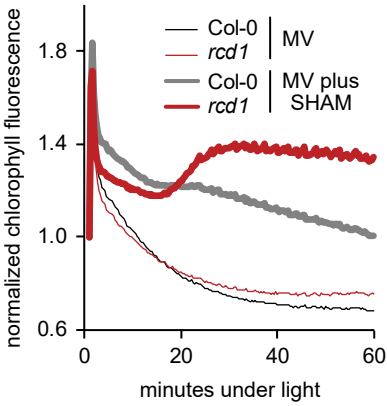
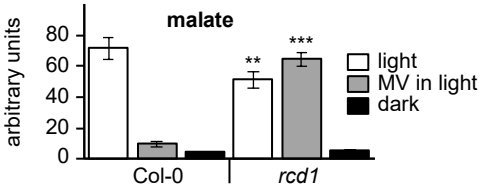
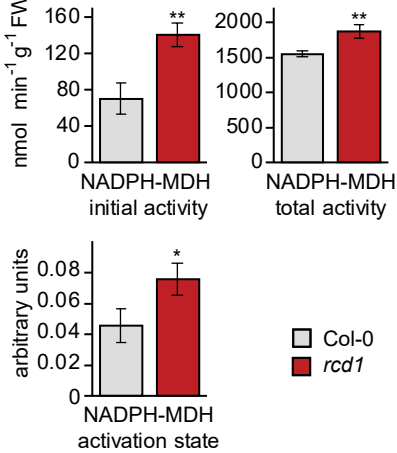


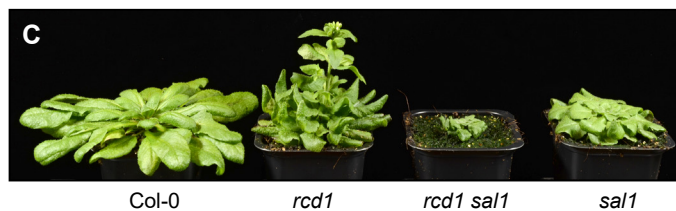
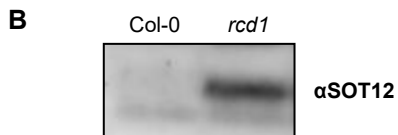
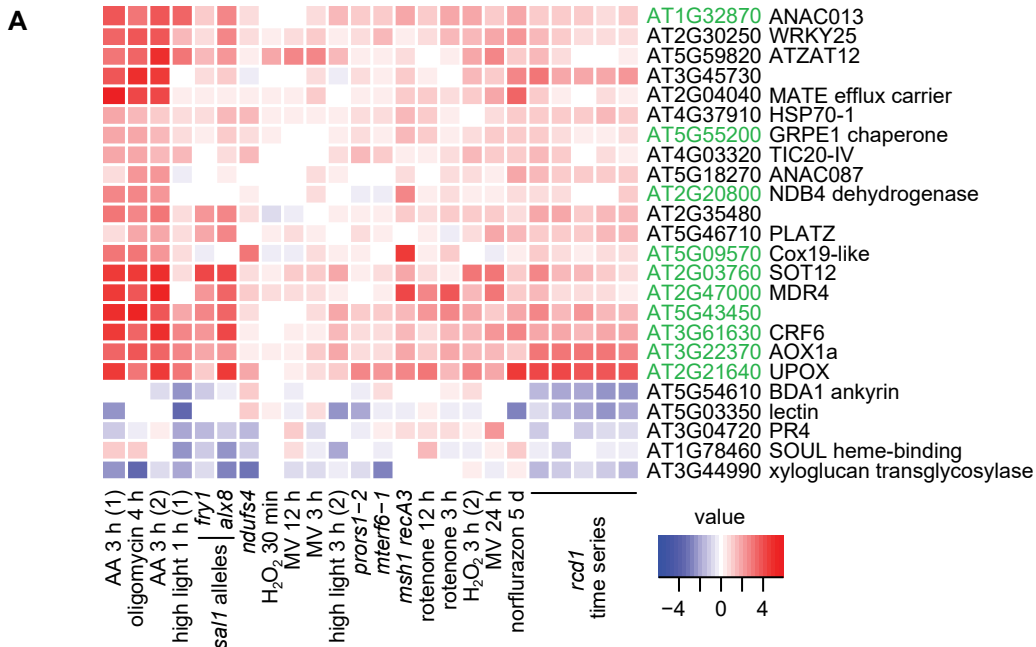
**A****B**

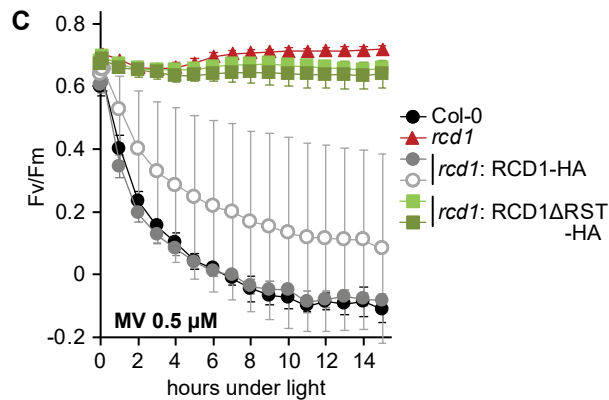
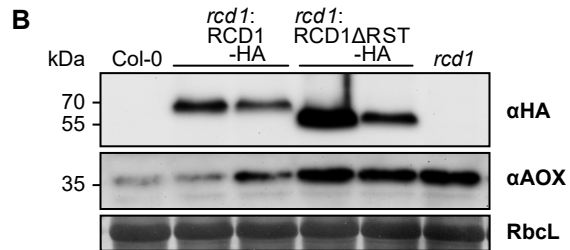
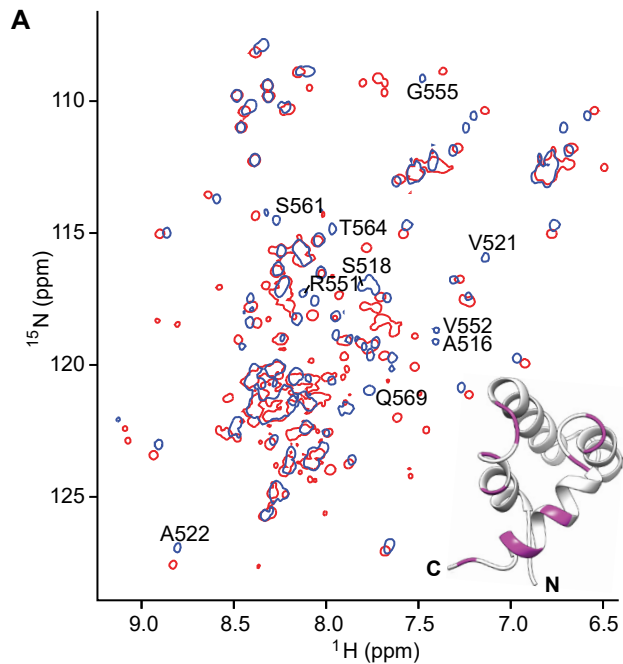


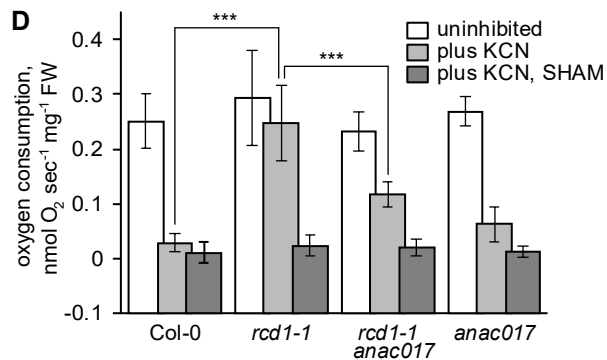
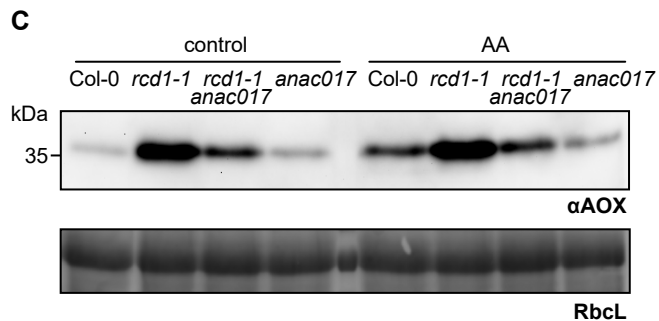
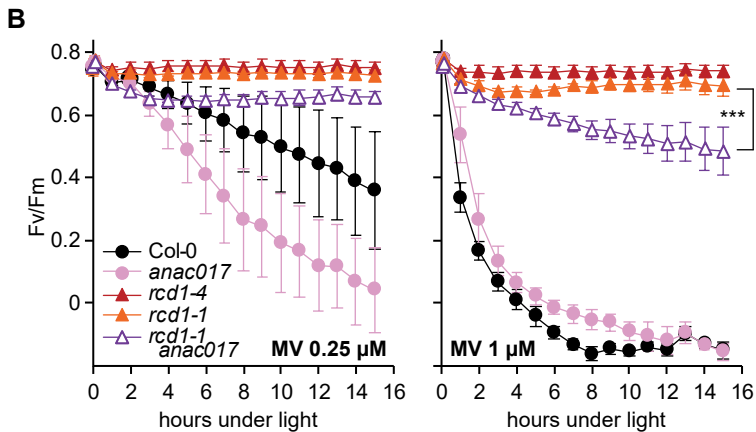
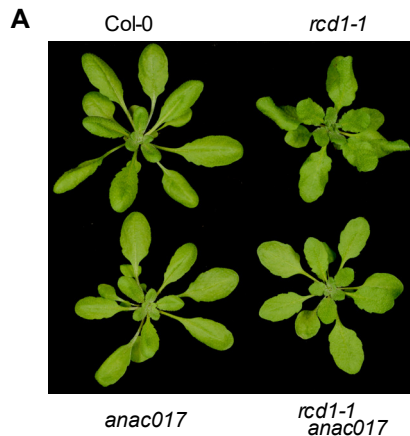
**respiration flux****sucrose flux****starch flux****cell wall flux**

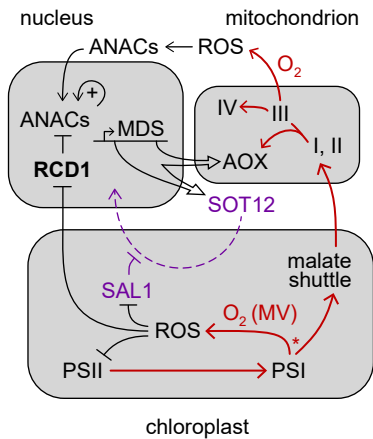


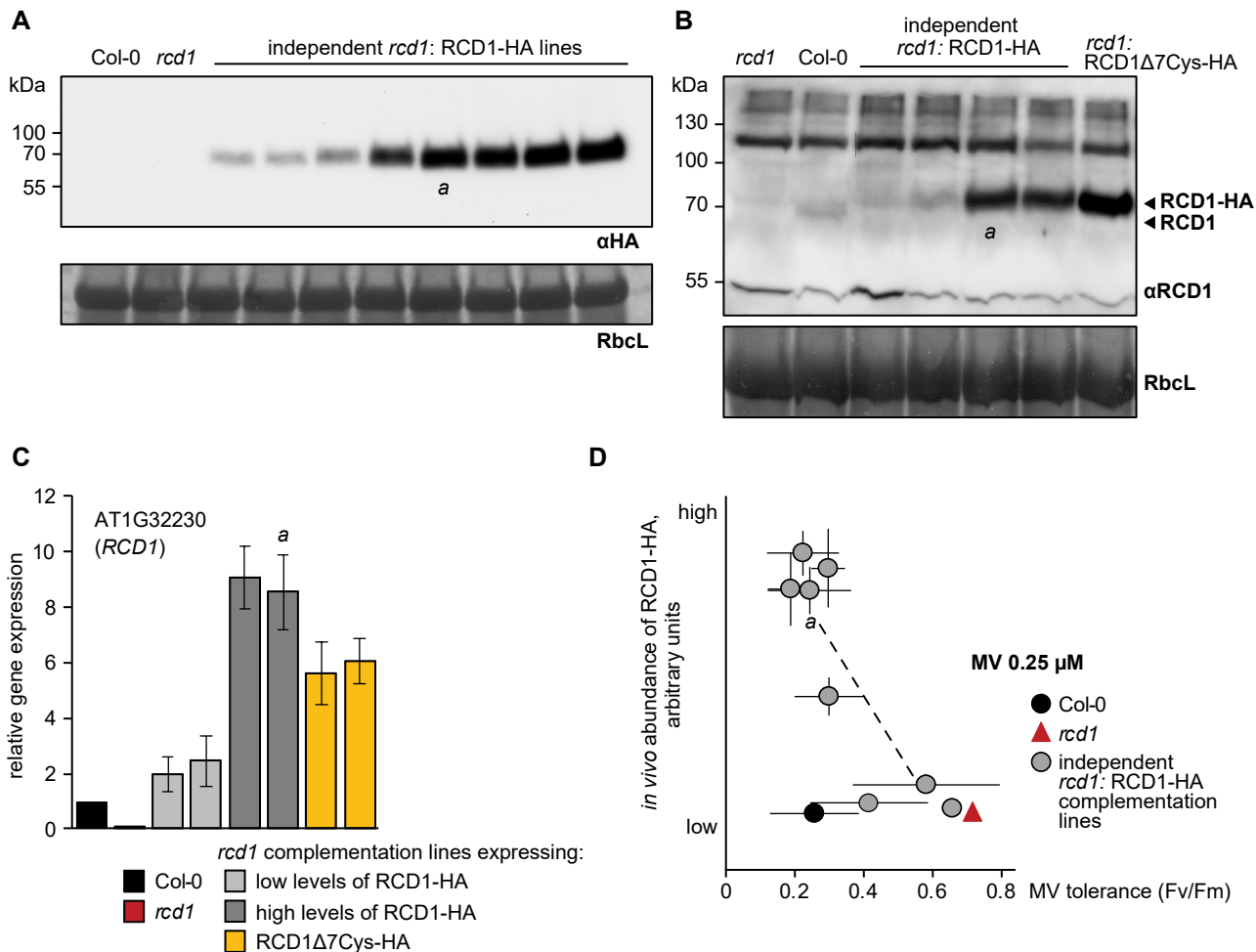
**A****B****C**





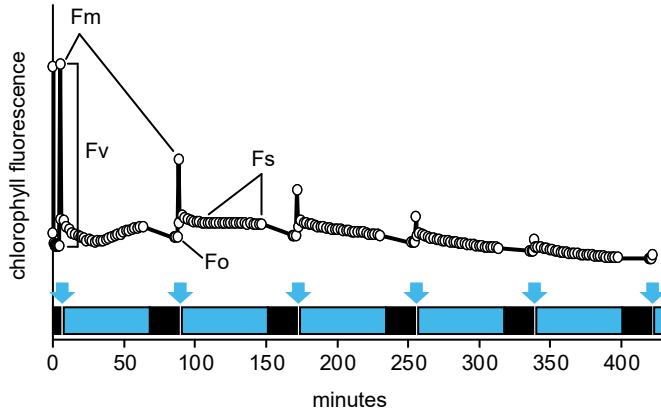




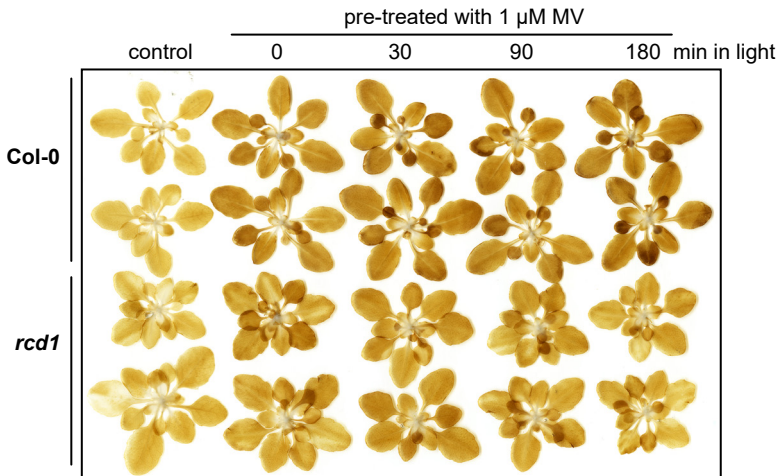


**Figure 1 – figure supplement 1. Inverse correlation of RCD1 abundance with tolerance to chloroplastic ROS.**

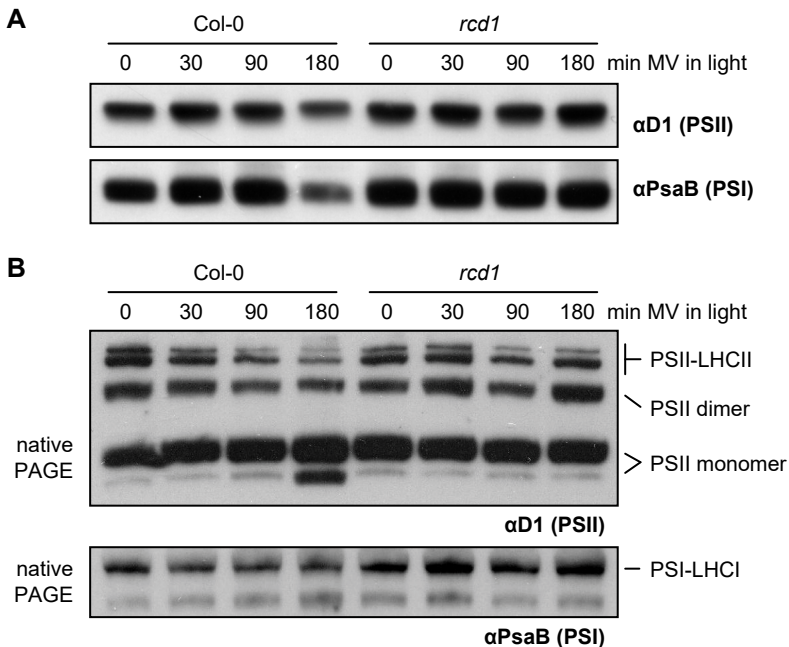




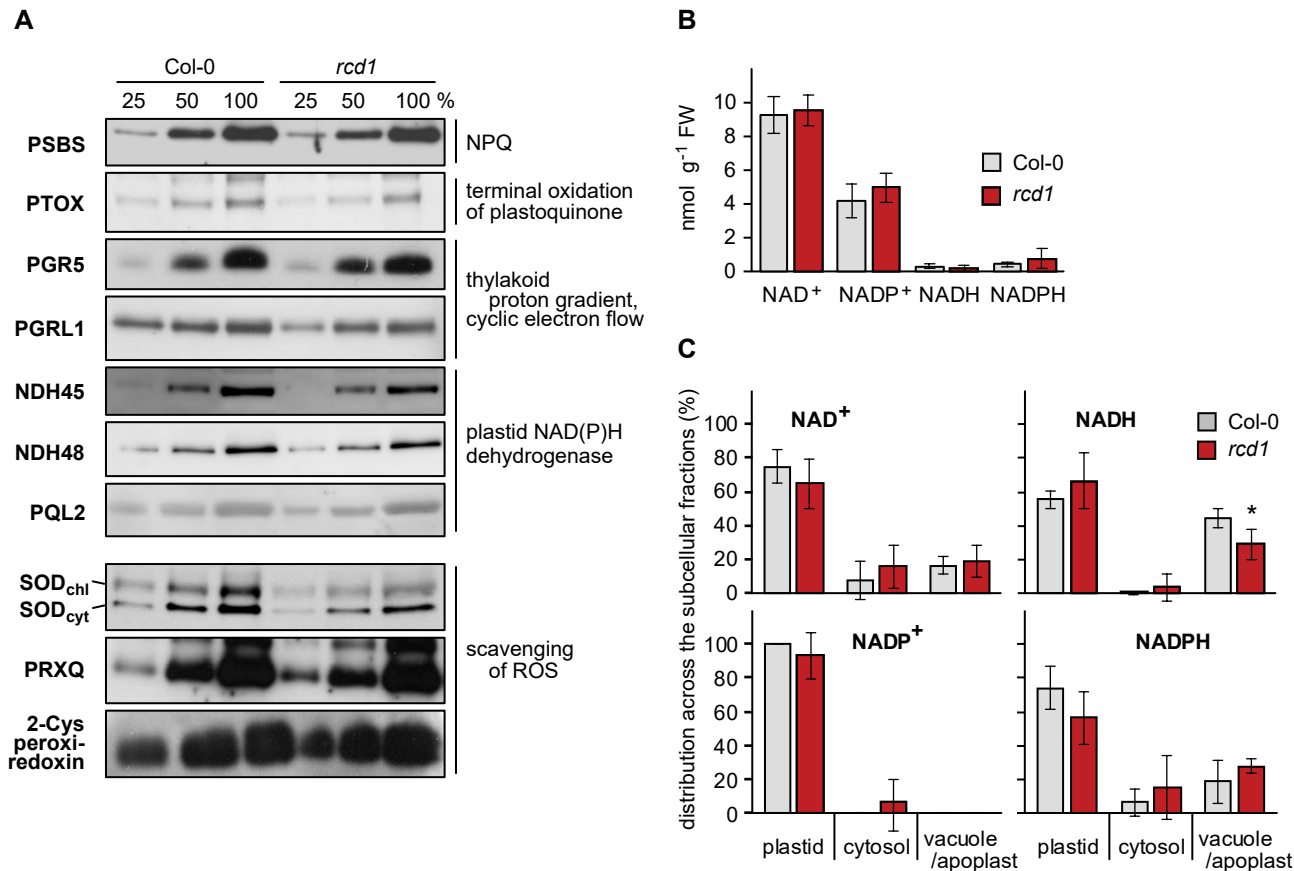
**Figure 1 – figure supplement 2. The Imaging PAM protocol developed to monitor kinetics of PSII inhibition by repetitive 1-hour light cycles.**



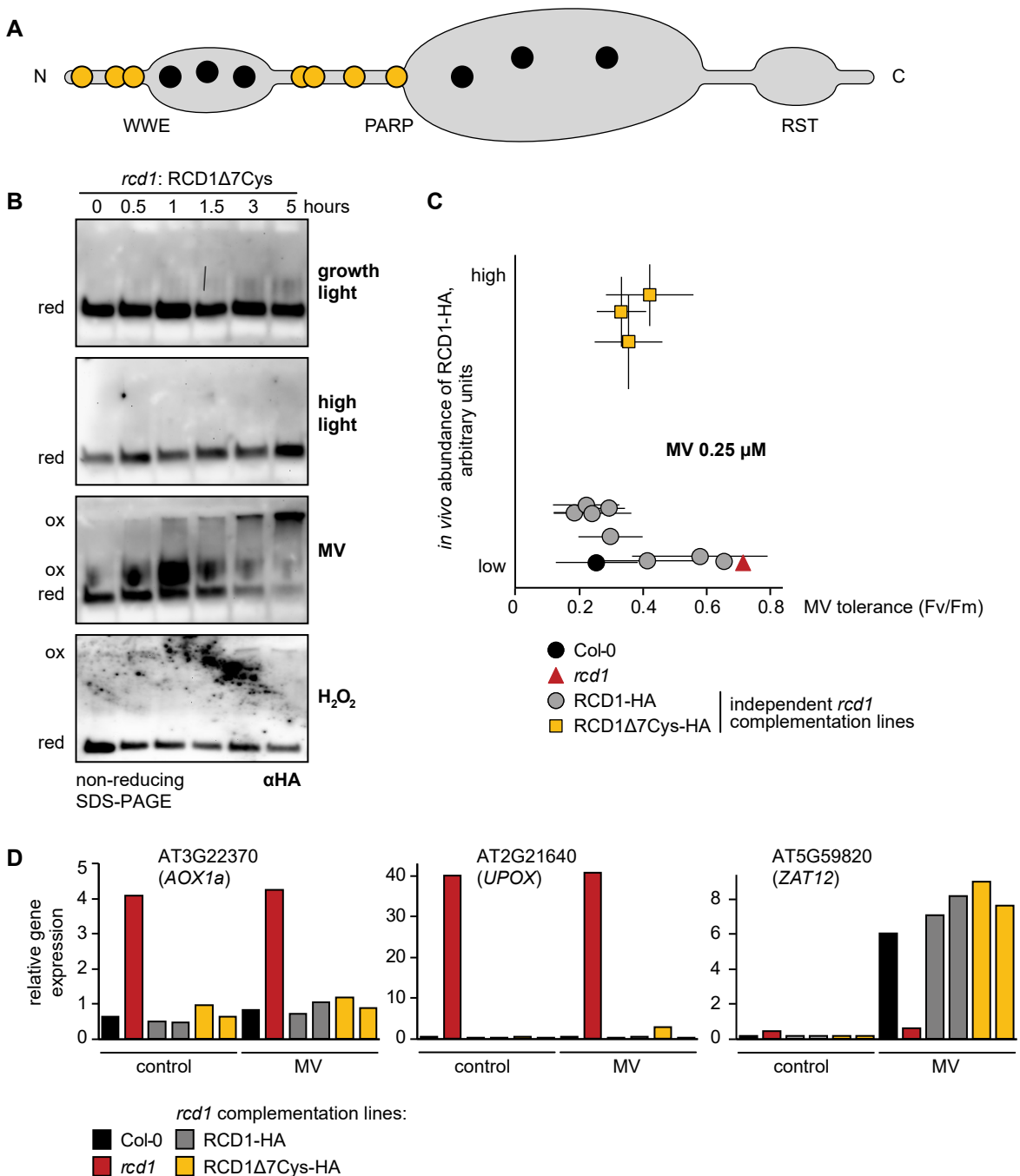
**Figure 1 – figure supplement 3. Production rate of hydrogen peroxide in Col-0 and *rcd1* during illumination of MV-pre-treated rosettes.**



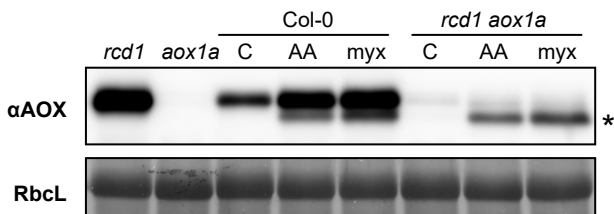
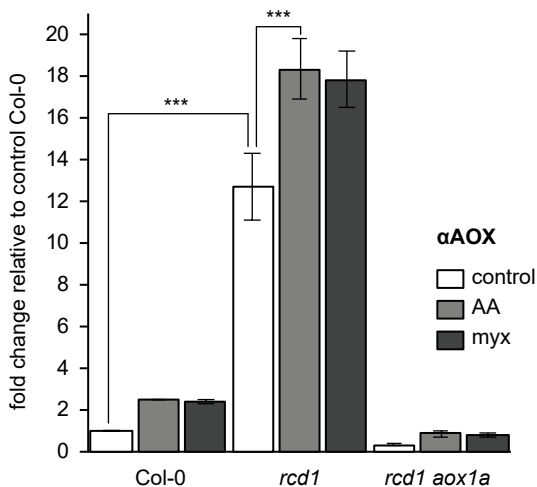
**Figure 1 – figure supplement 4. Altered resistance of *rcd1* photosynthetic apparatus to chloroplastic ROS.**



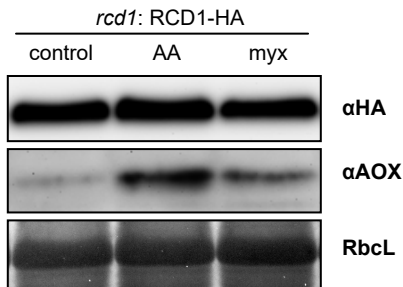
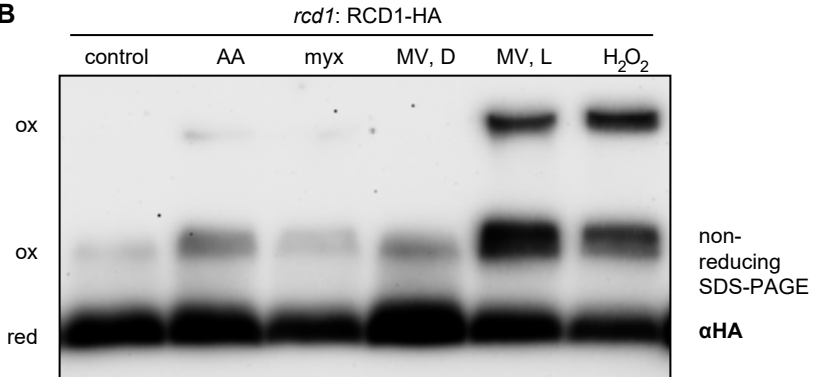
**Figure 1 – figure supplement 5. Components of photosynthetic electron transfer and chloroplast ROS scavenging; abundance and distribution of NAD<sup>+</sup>/ NADH and NADP<sup>+</sup>/ NADPH redox couples in Col-0 and *rcd1*.**



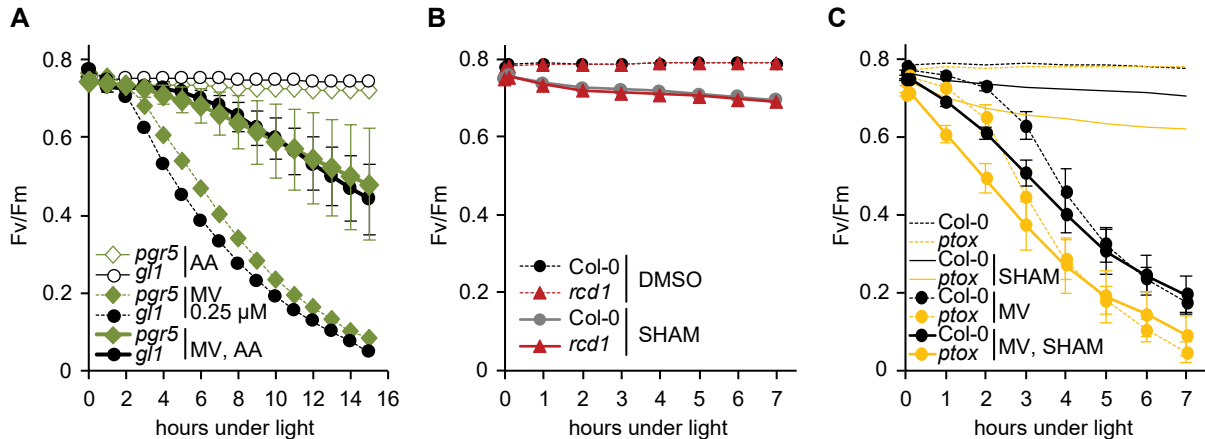
**Figure 2 – figure supplement 1. Characterization of the *rcd1: RCD1Δ7Cys*-HA lines.**

**A****B**

**Figure 4 – figure supplement 1. Effect of mitochondrial complex III inhibitors on expression of AOXs in Col-0 and *rcd1*.**

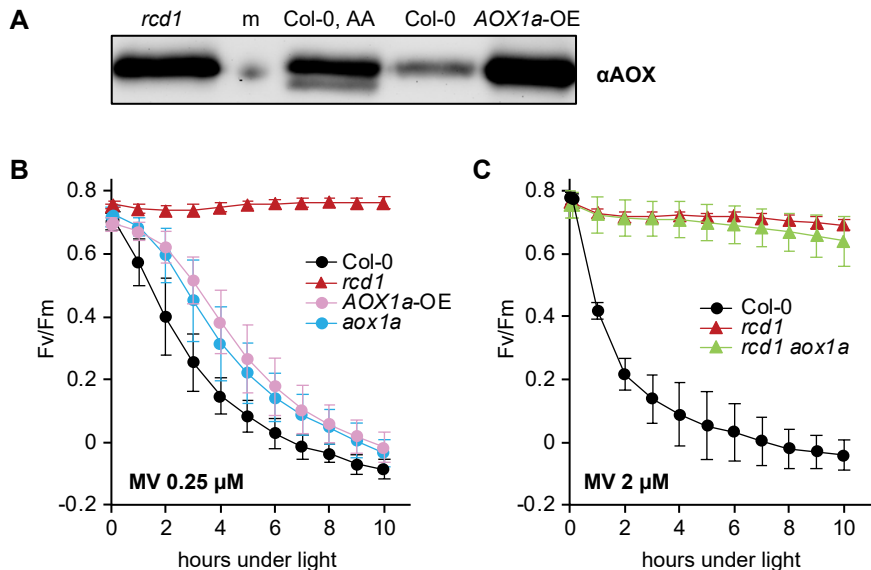
**A****B**

**Figure 4 – figure supplement 2. Effect of mitochondrial complex III inhibitors on abundance and redox state of the RCD1 protein.**

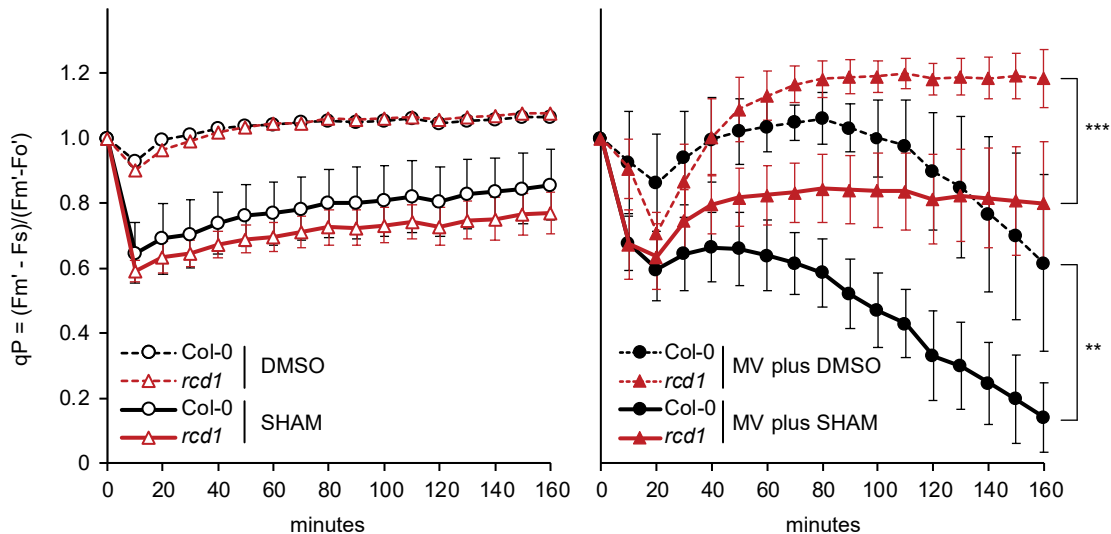


**Figure 4 – figure supplement 3. Specificity of inhibitor treatments.**

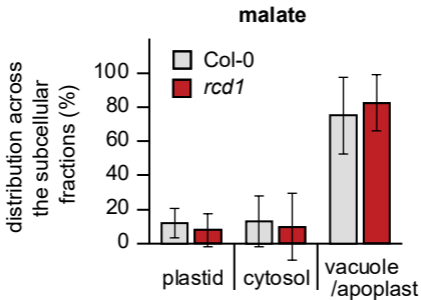




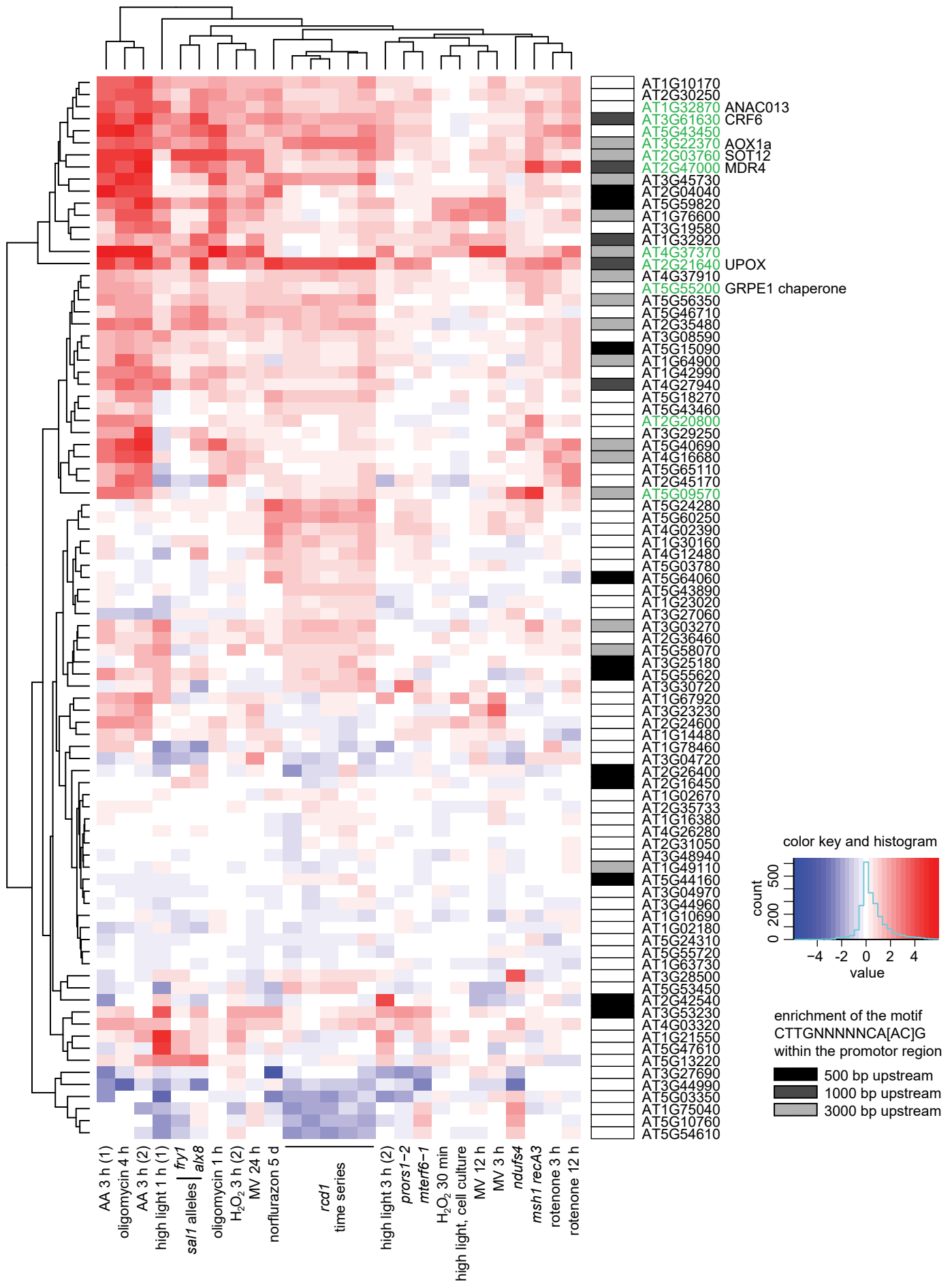
**Figure 4 – figure supplement 4. Irrelevance of AOX1a isoform for MV tolerance.**



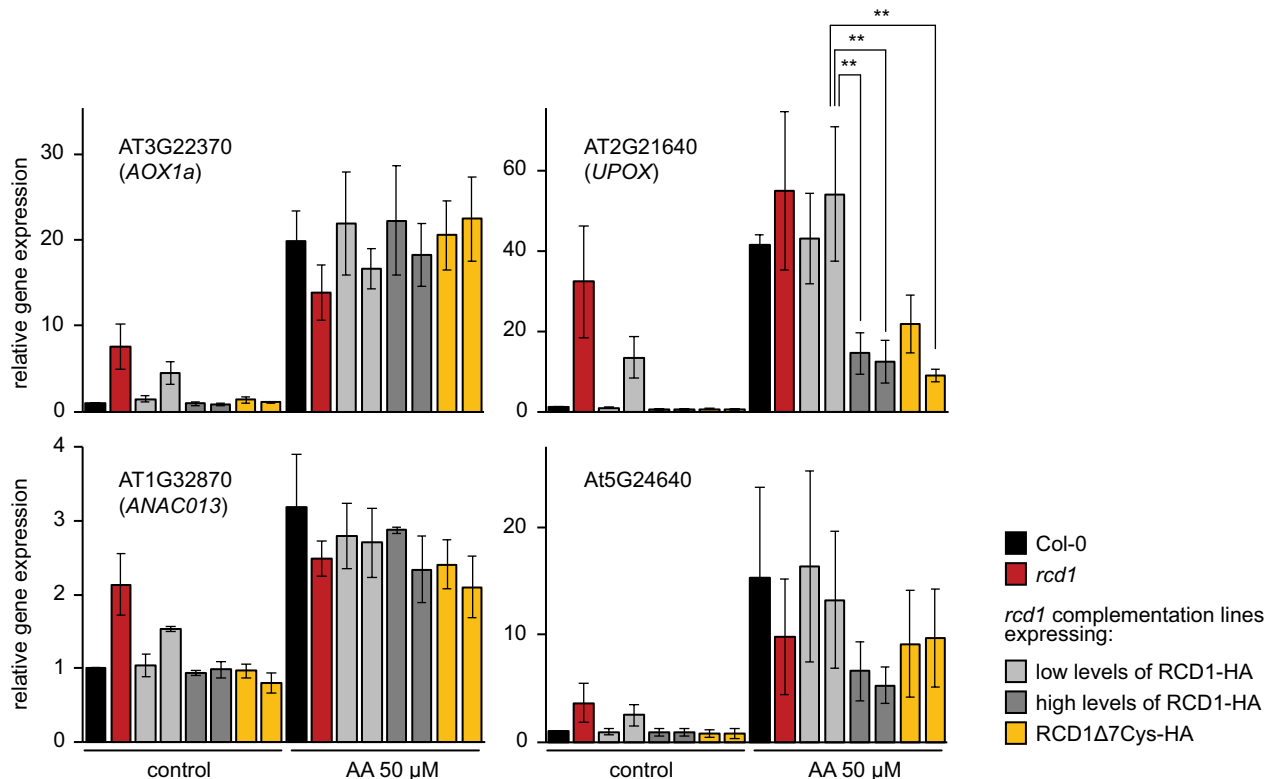
**Figure 5 – figure supplement 1. Alternations in chloroplast electron transfer induced by MV and SHAM.**



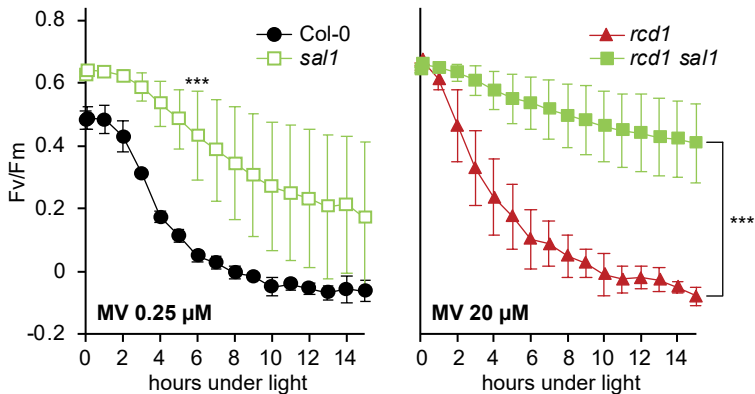
**Figure 5 – figure supplement 2.**  
**Distribution of malate**  
**in subcellular compartments**  
**of Col-0 and *rcd1*.**



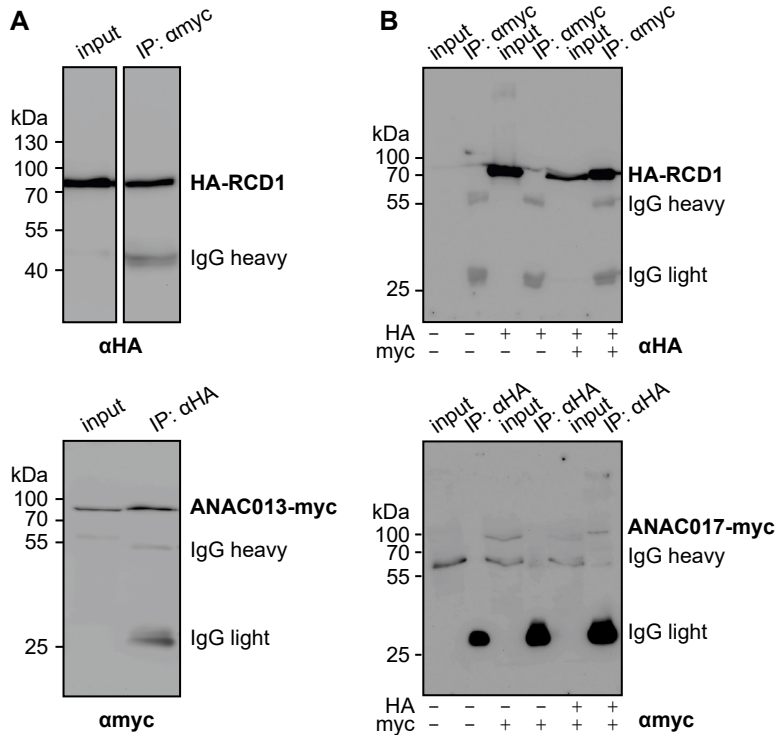
**Figure 6 – figure supplement 1. Clustering analysis of genes mis-regulated in *rcd1* (with cutoff of  $\log_{FC} < 0.5$ ) in published gene expression data sets acquired after perturbations of chloroplasts or mitochondria.**



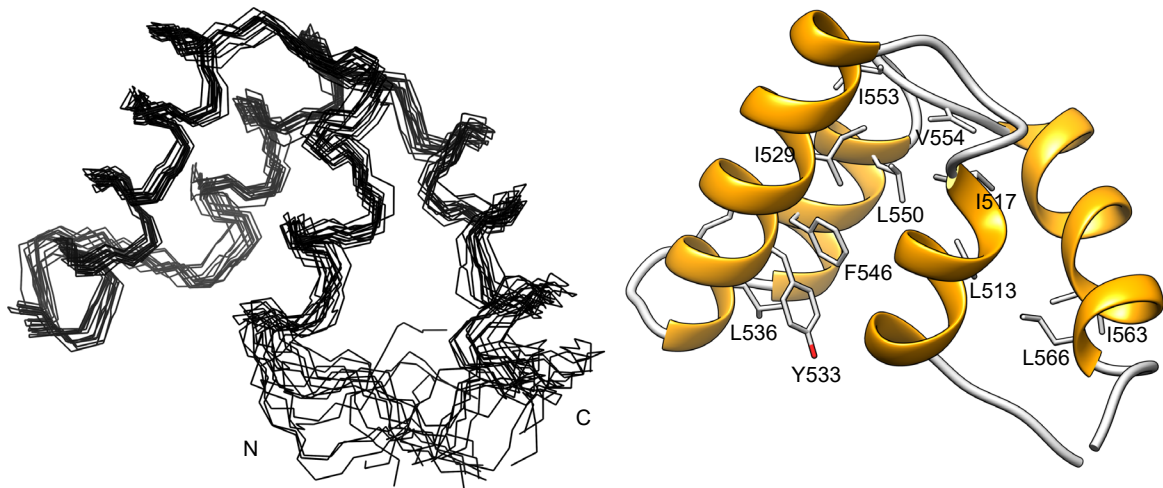
**Figure 6 – figure supplement 2. Induction of MDS genes in *rcd1*, and *rcd1* complementation lines.**



**Figure 6 – figure supplement 3. Tolerance of PSII to chloroplastic ROS in *sal1* mutants.**



**Figure 7 – figure supplement 1. Biochemical interaction of RCD1 with ANAC013/ ANAC017 transcription factors in human embryonic kidney (HEK293) cells.**

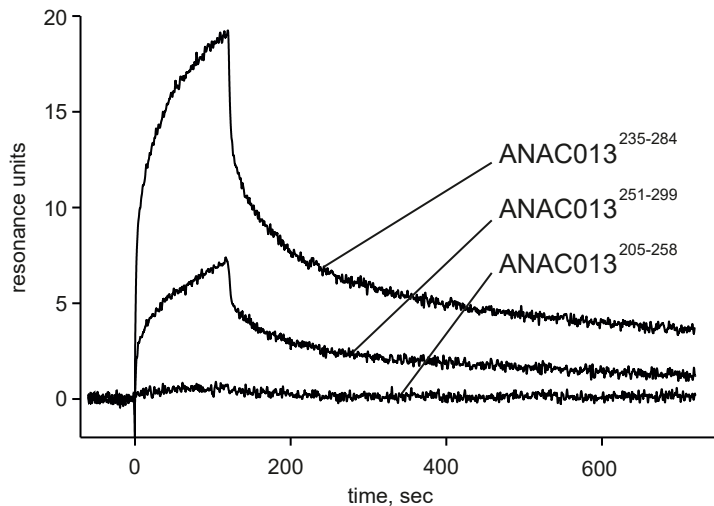
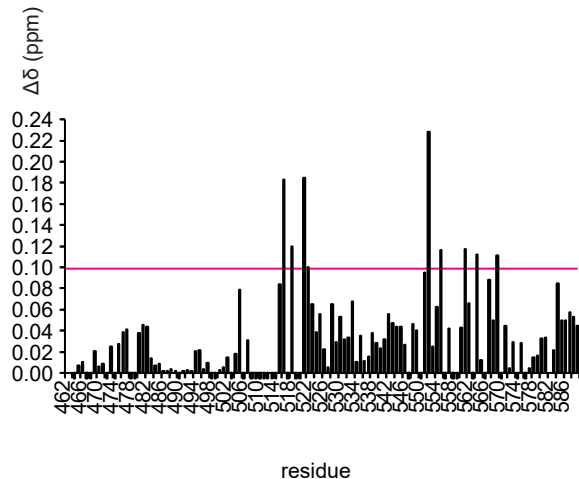


**Figure 7 – figure supplement 2. Structure of the RST domain of RCD1.**



**A**

205 LWGKGLNQSELDDNDIEELMSQVRDQSGPTLQQNGVSGLNSHVDTYNLENLEEDMYLEINDLMEPEPEPTSVEVMENNWNEDGSGLLNDDDFVGA 299  
 205 LWGKGLNQSELDDNDIEELMSQVRDQSGPTLQQNGVSGLNSHVDTYNLENLEED 258  
 235 LQQNGVSGLNSHVDTYNLENLEEDMYLEINDLMEPEPEPTSVEVMENNWN 284  
 251 NLENLEEDMYLEINDLMEPEPEPTSVEVMENNWNEDGSGLLNDDDFVGA 299

**B****C**

**Figure 7 – figure supplement 3. Analysis of interaction of the ANAC013-derived peptides with the RST domain of RCD1.**

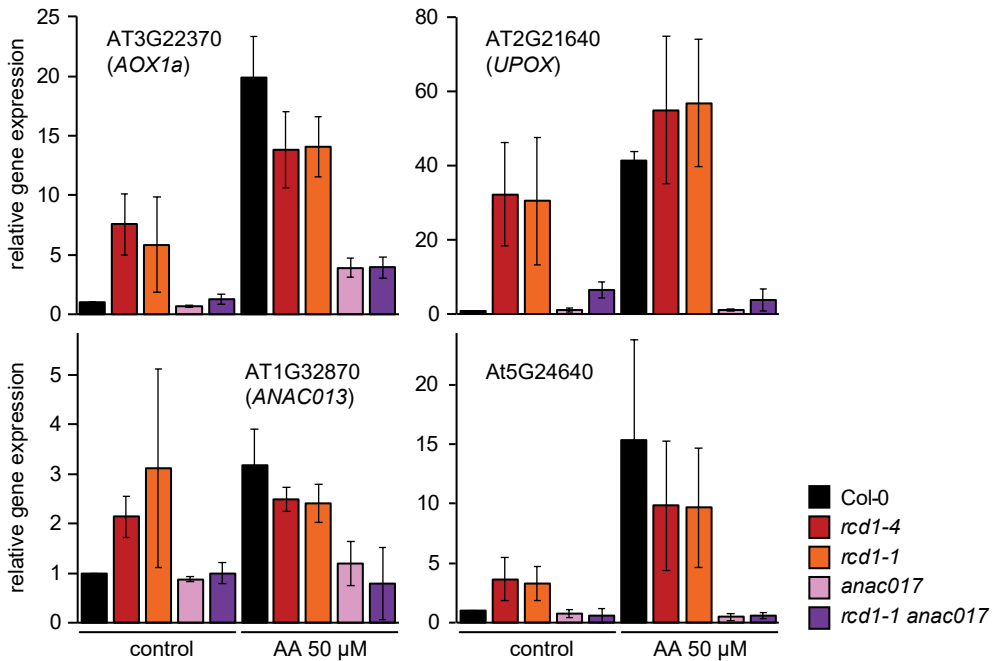


**Figure 8 – figure supplement 1. Induction of MDS genes in *anac017* and *rcd1 anac017* mutants.**